UNIVERSITÀ DELLA CALABRIA

Università della Calabria

Dottorato di Ricerca in "Scienze e Tecnologie Fisiche, Chimiche e dei Materiali"
in convenzione con il CNR
XXXI Ciclo

Tesi di dottorato

Dynamic Methods for Monitoring Structural Health: analytical and experimental aspects

S.S.D. Scienza delle costruzioni ICAR/08

Supervisore
Prof. Raffaele Zinno

Coordinatore
Prof. Vincenzo Carbone

Dottoranda
Ing. Angela Miceli

Novembre 2018

It's not enough to exist, I want to live.

Contents

Introduction

The aim of this work is the study of the dynamic characterization of road and civil structures.

The basis of this study is the structural monitoring through environmental vibrations but above all the idea of being able to test road infrastructures in situ and not in the laboratory, through the use of adequate machinery to induce artificial forcing. All this in order to simplify the process of dynamic identification and structural monitoring by means of tests that can be performed on site, easy and immediate.

Actually, the most common practice for simulations on structures subject to seismic actions is to realize the relevant prototype in a suitable scale, almost always not real but of reduced dimensions, and test it on a shaking table bringing it to destruction.

The idea of making tests with induced forcing easier was born from the thought of not scaling down the structure and testing the prototype but of inducing appropriate artificial forcing, so to speak reduced, and testing in-situ structures.

And here together all the others members of SmartLab[1] coordinated by Prof. Raffaele Zinno it was decided to create a portable kit to induce artificial sinusoidal forcing in situ. In particular, together with DRC Srl, a company already collaborating with SmartLab, and with Engine Lab Srl, the portable vibrodina prototype was designed and built.

The thesis is divided into five chapters.

In the **1st chapter** an introduction of Structural Health Monitoring based on vibrations is provided and the implementation of a software type tool for the study of dynamic behavior is reported.

In the **2nd chapter** the dynamic characterization is faced defining the nature and the measure of the vibrations, the techniques of detention of the vibrations and the techniques to induce vibrations and excitations in general. This chapter also describes the implementation of a kit for in situ dynamic identification test.

In the **3rd chapter** the analysis of the signal that the experimental instrumentation acquires in situ and transfers it to a PC to be interpreted is tackled.

[1] F.Ansioso, S.Artese, G.Clausi, A.Grano, F.Magarò, S.Meduri, C.Miceli, M.Perrelli, A.Venneri, G.Zagari, G.Zucco

The various types of signal and the problems of acquisition and interpretation of the signals themselves are also taken into consideration.

The last two chapters are purely experimental as they show the monitoring and dynamic identification tests performed in situ.

The **4th chapter** shows the tests carried out on some calabrian road infrastructures with the aid of a modest single-axial cabled accelerometric network and a tromograph in order to verify the differences occurring with the theoretical modal analysis conducted with commercial solver.

Finally, in the **5th chapter** the experiment carried out on a school building in Cosenza is reported with the use, in addition to the accelerometric network and the tromograph, of the portable experimental vibrodina (VIBRO9001) made ad hoc for the monitoring of the structures.

Chapter 1

Vibration-based SHM

1.1 Introduction

Non-destructive damage identification techniques is one of the important parts of health monitoring of civil infrastructure, and a permanent and automatic observation of the dynamic behavior of structures is known as *Structural Health Monitoring*. Structural damage is defined as the change in the structural parameters that may affect its present or future performances. Damage is defined as the deviation in original material or geometric properties of a structure due to cracks, corrosion, loosen bolts, fatigue or broken welds causing displacements, vibrations or undesirable stresses. Most nondestructive damage identification methods can be categorized as either local or global damage identification techniques [1]. Local damage identification techniques, such as ultrasonic methods and X-ray methods, require that the proximity of damage is known a priori and readily accessible for testing, which cannot be guaranteed for most cases in civil or aerospace engineering. Structural Health Monitoring is an innovative method for monitoring the structural status and performance without affecting the structure itself. It involves understanding the behavior of structure under different hazardous conditions, reducing the vulnerability to damage by taking precautions and assisting in the maintenance and repair work of structure. An approach is to choose the parameters that are sensitive to the damage occurring in the structure but not sensitive to operational or environmental damages. So, out of all the various monitoring methodologies, the *vibration-based* structural health monitoring system is preferred as it deals with the change in modal curvatures and natural frequencies to define the damage probability functions.

Hence, the vibration-based damage identification method as a global damage identification technique is developed to overcome the difficulties of unknown and/or inaccessible damage. The fundamental idea for vibration-based damage identification is that the damage induced changes in the physical properties (mass, damping, and stiffness) will cause detectable changes in modal properties (natu-

ral frequencies, modal damping, and mode shapes). For instance, reductions in stiffness result from the onset of cracks. Therefore, the damage can be identified by analyzing the changes in vibration features of the structure. The vibration-based damage detection techniques used for health monitoring of structures are: modal-based method, local diagnostic method, non-parametric method and times series analysis. The modal-based method and the local diagnostic method use a system model to study the responses. Whereas the non-parametric method and times series analysis identify the damage by comparing the mode shapes and natural frequency data between the healthy and damaged structural model. In all four methods, damage assessment is based on the changes in the dynamic characteristics that include a number of signal features: mode shape and its derivatives, frequencies, strain energy, frequency response functions, wave propagation parameters, modal damping ratio and autoregressive coefficients using time history method [2]. The detection of damage of a structure by vibration analysis is based on the changes in structural properties: stiffness, mass and damping. These changes occurring due to alterations in the structure and lead to changes in the structural dynamic characteristics: mode shapes, natural frequency, etc. The change in the structural dynamic characteristics are measured with the help of sensors. These sensors detect the damage without interfering with the structure and without high costs.

1.2 Civil buildings monitoring

The need to monitor buildings is motivated by the need to understand their performance during earthquakes and storms. Ambient Vibration Tests [3, 4] have been carried out since the 1980s in order to understand the dynamic response of the structures. Knowledge of the dynamic response of the structure during serious events, such as earthquakes, has led to the implementation of monitoring systems permanent. In California, the mandatory structural monitoring is managed by the CSMIP, California Strong Motion Instrumentation Program[1], which performs the installation of accelerometers on buildings and other types of structures. While these data provide knowledge of the structure, the goal is to obtain information in order to improve the design of structures subject to earthquakes. There is, therefore, the need to identify a large scale of structural performance to better operate in the field of seismic engineering.

Many of the monitoring activities on buildings (for example the Bank of Commerce in Toronto [5]) were carried out to increase the understanding of the loads and the mechanical response against earthquakes, while the monitoring of towers (for example the Hume Point in London [6]) also for wind loads. The skyscrapers of Dubai, for example, have been equipped with monitoring systems and modern technologies such as the use of TMD, Tuned Mass Damper. This approach is part

[1] California Geological Survey 2003

of the idea of creating smart structures [7] capable of reducing human intervention to a minimum, self-heading systems [8].

The seismic events of Kobe in Japan in 1995 and of Northridge in California in 1994 offered opportunities for the birth of some organizations that provide accurate data after major seismic events and support citizens during emergency management, such as the ANSS, Advanced National Seismic and the FEMA, Federal Emergency Management Agency in the United States or the RAN[2], Rete Accelerometrica Nazionale, in Italy, and the development of an integrated approach to SHM that involved the use of automatic sensors, embedded systems, communications and data management, [9, 10]. In Italy the OSS[3] is active, a Seismic Observatory of Structures, a national network of permanent monitoring of the seismic response of buildings, designed, built and managed by the Department of Civil Protection (DPC), with both cognitive and control purposes. The OSS allows the assessment of the damage caused by an earthquake to the monitored structures and to buildings with characteristics similar to those monitored in the same seismic conditions, providing useful information for planning Civil Protection activities in the post-seismic emergency.

The data collected by the acquisition unit of the Department of Civil Protection are interpreted and disseminated via the internet. The OSS is formed by the subnet of the fundamental sample 105 schools, hospitals, municipalities, 10 bridges and various dams, subject to sophisticated monitoring systems, equipped with dynamic identification equipment, based on a layout of 16 to 32 accelerometers and from the subnetwork of the supplementary sample 300 strategic buildings for the management of emergency activities, equipped with simple systems of monitoring, consisting of 7 accelerometers.

The merits of the legislative aspects connected to the application of SHM systems on civil engineering constructions, despite the growth of interest in Europe on this topic, is present only a brief mention of Eurocode 8, Design guidelines for seismic resistance of the structures, in Appendix B, for information: *For the evaluation of the structures, besides to collect general historical information and data during the inspection, experimental tests and in-situ measurements can be conducted by studying the evolution over time of the dimensions, alignments, eccentricities, opening of cracks or gaps and deformations, especially due to aftershocks (with the possible installation of monitoring equipment).* We also recall the ISO 16587 Standard mechanical vibration and shock - Performance parameters for condition monitoring of structures in 2004 which only mentions the topic.

[2]http://ran.protezionecivile.it/IT/index.php
[3]http://www.protezionecivile.gov.it/home

1.3 Modal-based methods

The identification of the damage through the analysis of the changes in the dynamic properties is based on the fact that the frequently measured modal parameters (main frequencies, modal forms and damping factor) are a function of the physical properties of the structure (mass, stiffness and damping). Therefore, variations in these physical properties, such as the reductions in stiffness resulting from the onset of cracks, will cause appreciable changes in the modal characteristics. These changes in modal characteristics, used as indicators of damage, lead the process of vibrational identification of damage to a model identification problem.

In vibration test the excitation and response are always measured and recorded in the form of time history because it is usually difficult to examine the time domain data for damage identification. A more popular method is to examine the modal domain data through modal analysis technique, in which the time domain data is transformed into the frequency domain, and then the modal domain data can be further extracted from the frequency domain data. The modal domain methods attract more attention and play a dominant role in the *state of the art* of structural damage identification. The modal domain methods evolve along with the rapid development of experimental modal analysis technique, and they gain their popularity because the modal properties (i.e., natural frequencies, modal damping, modal shapes, etc.) have their physical meanings and are thus easier to be interpreted or interrogated than those abstract mathematical features extracted from the time or frequency domain.

In this context the modal properties will be defined as: *natural frequencies*, *modal damping coefficient*, *modal shapes* and *curvature of the modal shapes*.

1.3.1 Changes in natural frequencies

It is possible to determine the presence of damage in a structure through the analysis of variations in its natural frequencies on the basis of the observation that changes in the structural properties cause variations in the vibration frequencies. It must be said, however, that frequency changes may not be sufficient for the location of the damage as there may be cases of uncertainty [11]. For example, the presence of similar defects at different points of a structure causes virtually identical frequency changes. Likewise, in symmetrical structures, damage located at symmetrical points gives rise to the same changes in frequency. However, in large structures it can happen that considerable damage causes very small changes in the natural frequencies, so much so that they can be confused with a measurement error.

The changes in natural frequency occur due to change in mass, stiffness and other structural parameters [12]. The frequency changes in a structure are measured with the use of sensors, placed at specific points, which can detect the

decrease or increase in natural frequencies caused due to the change in stiffness. The only disadvantage is the determination of the number of sensors to be used. For effective damage detection, sensors should be uniformly placed throughout the structure. The main positions for sensors placement are the points where the summation of mode shape vector magnitudes is zero [13]. The frequency response is obtained from the second order differential equation of motion:

$$M\ \ddot{x}\ (t) + C\ \dot{x}\ (t) + Kx(t) = f(t) \tag{1.1}$$

where $\ddot{x}$, $\dot{x}$ and x are the vectors of size n respectively of acceleration, speed and displacement of each degree of freedom; M, C and K are the matrices with dimensions n x n respectively of mass, damping and stiffness and $f(t)$ is the vector of dimension n of the loads applied as a function of time [14]. Replacing in the (1.1) the external force

$$f(t) = F(\omega)e^{i\omega t} \tag{1.2}$$

and the dislpacement

$$x(t) = x(\omega)e^{i\omega t} \tag{1.3}$$

we obtain

$$\frac{-\omega^2 M + \jmath\omega C + K}{-\omega^2}\ \ddot{x}\ (\omega)e^{i\omega t} = F(\omega)e^{i\omega t} \tag{1.4}$$

$$\frac{-\omega^2 M + \jmath\omega C + K}{-\omega^2}\ \ddot{x}\ (\omega) = F(\omega) \tag{1.5}$$

Indicating with $H(\omega)$ the FRF (Frequency Response Function) acceleration matrix, we can write that:

$$H(\omega) = \frac{-\omega^2}{-\omega^2 M + \jmath\omega C + K} \tag{1.6}$$

and we obtain:

$$\frac{\ddot{x}\ (\omega)}{H(\omega)} = F(\omega)$$

$$\ddot{x}\ (\omega) = H(\omega)F(\omega) \tag{1.7}$$

where $\ddot{x}\ (\omega)$ is acceleration response amplitude vector in frequency domain and $F(\omega)$ is force amplitude vector in frequency domain. In the presence of damage in a structure there is a change in stiffness and the $H(\omega)$ for original and damaged matrix will be different [12]. Therefore, the damage location is obtained by iteration of the $H(\omega)$ matrix for the damaged and undamaged structure. By introducing the damping coefficients of the first and second order defined by Rayleigh, α and β, the C matrix becomes

$$C = \alpha M + \beta K \tag{1.8}$$

Introducing the Rayleigh damping (1.8) in the FRF acceleration matrix (1.6)

$$H(\omega) = \frac{-\omega^2}{-\omega^2 M + \jmath\omega\alpha M + \jmath\omega\beta K + K}$$

$$H(\omega) = \frac{-\omega^2}{(-\omega^2 + \jmath\omega\alpha)M + (\jmath\omega\beta + 1)K} \tag{1.9}$$

The damage in a structure can be measured distinctly only if the frequency change is above 5%. However, it is difficult to excite a high natural frequency out of a structure, because such vibration would require higher energy. Also the selection of exact natural frequencies is highly inadvisable due structural resonance. So, a range of frequencies nearer to the natural frequency is chosen, which helps to detect frequency change. Noise interference in the calculation of change in frequency can be a great nuisance. The damaged frequency can be measured even if the noise level is between 0% and 10%. However, there may be a chance of error amounting to less than 2%. Therefore, for accurate measurement, noise level is kept within 5% [12].

For the determination of structural damage, methods based on frequency changes are divided into two categories: *direct problem* and *inverse problem*.

The direct problem is the calculation of frequency changes knowing the damage *a priori*. Thus, once the damage has been mathematically modeled, the frequencies obtained from the theoretical model are compared to the frequencies experimentally measured to confirm the variations due to the damage. In order to localize the damage, a set of possible damage localizations is considered and an error term is constructed that correlates the frequency values measured for each mode considered with those (called theoretical ones) taken from a model based on the reduction of stiffness local in the points considered. Then, for each potential location of the damage, a certain number of pairs of vibrating modes are considered and where the error has the lowest value the damage is identified. Obviously, this does not take into account multiple localizations of structural damage. In this case we proceed with the comparison of the resonance frequencies or with the simulations of possible damage states. Choy, Hu and Liang [15] addressed the issue of determining frequency sensitivity for simply supported or cantilevered beam with one crack and developed analytical relationships between the first-order changes in the eigenfrequencies and the location and severity of the damage. This method requires symbolic computation of the characteristic equation. Morassi [16] showed that the frequency sensitivity of a cracked beam-type structure can be explicitly evaluated by using a general perturbation approach. Frequency sensitivity turns to be proportional to the potential energy stored at the cracked cross section of the undamaged beam. Moreover, the ratio of the frequency changes of two different modes turns to be a function of damage location only. Both methods were based on Euler–Bernoulli beam theory and modeled crack as a massless, infinitesimal rotational spring. All of the above mentioned expressions are valid only for small defects.

The inverse problem calculates the position and size of the damage of a given structure based on the measurement of the natural frequency. The inverse problem was studied for the first time in 1978 [17]. Subsequent publications [18] have suggested that variations in natural frequency alone may not be sufficient for a univocal identification of the position of structural damage because the cracks associated with similar cracks lengths but in different positions may cause the same amount of variation of frequency and therefore create confusion. The use of a correlation coefficient defined as the Multiple Damage Localization Assurance Criterion, MDLAC, was then introduced to estimate the size of defects in a structure. The method is based on the sensitivity of the frequency of each mode to damage in each position. MDLAC is a statistical correlation between the analytical predictions of the frequency variations δf and the measured frequency changes Δf. The change in analytical frequency δf can be written as a function of vector δD. The damage status required is obtained by looking for the damage extension vector δD which maximizes the value of MDLAC:

$$MDLAC(\delta D) = \frac{[\Delta f^T \delta f(\delta D)]^2}{(\Delta f^T \Delta f)(\delta f(\delta D))^T(\delta f(\delta D))} \tag{1.10}$$

The results of the numerical and experimental tests show that the MDLAC approach requires only measurements of changes in some of the natural frequencies of the structure between the undamaged and damaged states and provides good predictions of both the position and the absolute size of the damage in one or more sites.

1.3.2 Changes in mode shapes

The changes in mode shape by undamaged and damaged structures are used as a basic feature for damage identification. The baseline data from undamaged structure can be obtained from either an experimental test on the undamaged structure or an accurate numerical model of the undamaged structure. When experimental data on the undamaged structure is not available, a finite element model is usually adopted to generate the baseline data.

In the early 1990s [19] a method was developed to counteract the drawbacks of the frequency response (FRF) method through changes in the mode shapes. A damage in a structure alters its dynamic characteristics. The change is characterized by changes in the eigenparameters [11]: natural frequency, damping values and the mode shapes associated with each natural frequency. Considerable effort has been spent in obtaining a relationship between the changes in eigenparameters, the damage location and the damage size.

In [11] the parameter curvature mode shape is investigated as a possible candidate for identifying and locating damage in a structure. By using a cantilever and a simply supported analytical beam model, it is shown here that the absolute changes in the curvature modal are localized in the region of damage and hence

can be used to detect damage in a structure. The changes in the curvature mode shapes increase with increasing size of damage. This information can be used to obtain the amount of damage in the structure. Finite element analysis was used to obtain the displacement mode shapes of the two models. By using a central difference approximation, curvature mode shapes were then calculated from the displacement mode shapes. It has been observed that changes in the derivatives of the higher order mode shape, such as the curvature modal, the third order derivative and the fourth order derivative are more accurate damage indicators than the mode shapes. But a structure does not excite the higher modes to environmental conditions because it requires a high energy to be excited [20]. Therefore, the fundamental modality [21] is taken into account for the analysis of the damage.

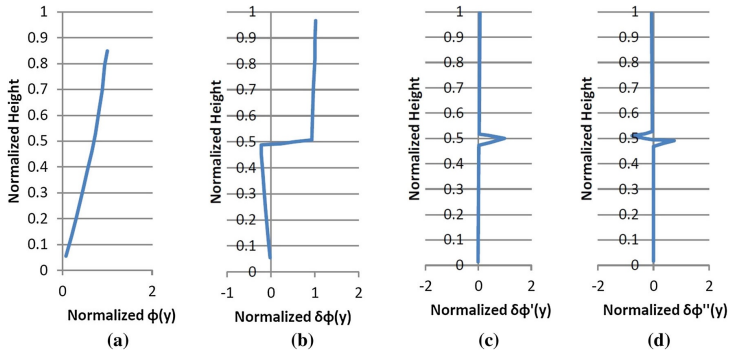

Figure 1.1: normalized (a) mode shape and changes in (b) mode shape, (c) slope of mode shape and (d) curvature of mode shape for a beam

The basic equation for mode shapes for beam [22] is plotted in fig. 1.1 for a beam with 100 elements and damage at the $50th$ element. We obtain a steep slope at the point of damage (a), a discontinuity in the slope (c) and changes the sign in the curvature (d) that clearly indicate the damage location. The same analysis was performed with a 12 storeyed building, fig. 1.2, with damage induced at the $6th$ storey. Were obtained similar curves.

From 2000s the damage localization method with the use of MDLAC, Multiple Damage Location Assurance Criterion [23], was extended to using by incomplete mode shapes [24]. The damage detection procedure is divided in two−step: preliminarily localize the damage sites by using measured mode shapes and then detect the damage site and its extent again by using measured natural frequencies. In this method, the use of mode shape is only for preliminary damage localization, and the accurate localization and quantification of damage still rely on measured frequency changes.

For the model-based method, the credibility of a numerical model must be established through careful model verification and validation, fig. 1.3.

For real-time structure damage detection is to developing a response-based method that depends only on experimental data from damaged structures. The

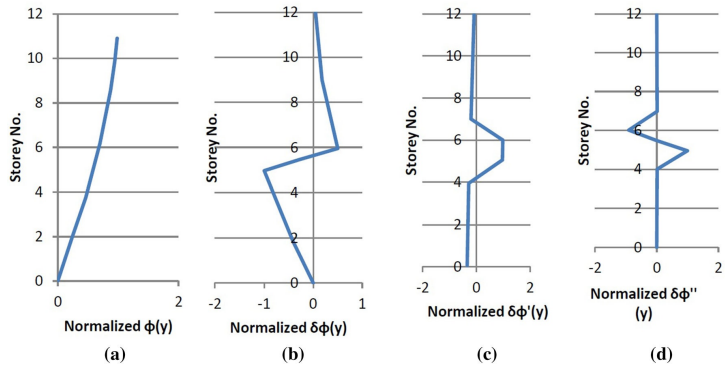

Figure 1.2: normalized (a) mode shape and changes in (b) mode shape, (c) slope of mode shape and (d) curvature of mode shape for a building

basic assumption is that the mode shape data from a healthy structure contains only low-frequency signal in spatial domain compared to the damage-induced high-frequency signal change.

1.3.3 Changes in modal strain energy

The strain energy method [25][26] takes into account all the vibrating elements of the structure and is based only on the modal forms and on the matrix of elemental stiffness. It does not take into account any external and environmental influences. This method is able to locate the damage in the area where a rigidity reduction of even 10% occurs [27]. The strain energy method is pratically applicable for the detection of damage in beam and plate type structures. The modal strain energy can be directly related to mode shape curvatures by derivating it. Hence, the modal strain energy-based method can also be considered as a special case of mode shape curvature-based method. The mode shape curvatures is obtain from the second derivatives of mode shape and are highly sensitive to damage and can be used to localize it. The curvature mode shapes are derivated using a central difference approximation as follows

$$k_i = \frac{(w_{i+1} + w_{i-1} - 2w_i)}{h^2} \tag{1.11}$$

where w is the modal displacement at i-th point and h is the sensor spacing.

The mode shape is given by [28, 29] Euler-Bernoulli's equation:

$$U_i = \frac{1}{2}\int_0^1 EI\left(\frac{d^2\phi_i}{dx^2}\right)^2 dx \tag{1.12}$$

$$U_{ij} = \frac{1}{2}\int_{a_i}^{a_{j+1}} EI\left(\frac{d^2\phi_i}{dx^2}\right)^2 dx \tag{1.13}$$

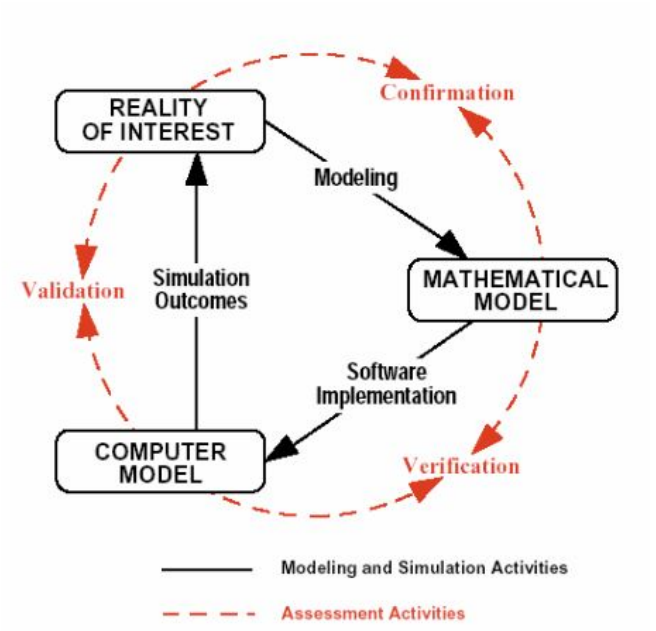

Figure 1.3: verification and validation method

$$U_{ij}^{*} = \frac{1}{2}\int_{a_i}^{a_{j+1}} EI^{*}\left(\frac{d^2\phi_i^{*}}{dx^2}\right)^2 dx \tag{1.14}$$

For beam-type structures, the bending stiffness EI is assumed to be essentially constant over the length of the beam for both the undamaged and damaged modes. The fractional strain energy of undamaged F_{ij} and damaged F_{ij}^{*} beam for the i-th mode at sub-region j are

$$F_{ij} = \frac{U_{ij}}{U_i} \tag{1.15}$$

$$F_{ij}^{*} = \frac{U_{ij}^{*}}{U_i} \tag{1.16}$$

The Damage Index, β_{ij}, for several modes is

$$\beta_{ij} = \frac{1}{2}\frac{\sum_{i=1}^{m} F_{ij}^{*} + 1}{\sum_{i=1}^{m} F_{ij} + 1} + 1 \tag{1.17}$$

where m is the number of measured bending modes.

Then, assuming that the Damage Indices β_{ij} at different sub-regions is a normally distributed random variable, a normalized Damage Index Z at sub-region j can be obtained using

$$Z_j = \frac{\beta_{ij} - \bar{\beta}}{\sigma_\beta} \tag{1.18}$$

where $\bar{\beta}$ represents the mean of the Damage Indices β_{ij} and σ_β is the standard deviation of the Damage Indices β_{ij}. Usually, a damage detection criterion can be set as $Z_j > 2$.

1.4 Linear structural dynamics analysis

Any structure can be discretized into a more or less elevated number of parts either by analytical-descriptive procedures or by more sophisticated techniques such as finite elements. The number of degrees of freedom that we are going to consider depends on both the degree of approximation we want to obtain, and on the intrinsic characteristics of the structure. For example, a regular multi-storey building can be approximated by means of a shear-type model assuming a degree of freedom per floor, with masses concentrated at the floor and inter-floor stiffness and damping. Instead, for a more complex building it is necessary to resort to a more refined modeling. In both cases, once the structure is discretized, we arrive at an expression of the type as the (1.1). The (1.1) is a system of n equations from which it is possible to obtain the structural response in terms of displacements, velocities and accelerations of the various degrees of freedom for a certain forcing. On the other hand, the intrinsic properties of the structure, the system's proper frequencies and the modal forms (eigenvectors) relative to each individual mode can be calculated independently from the type of forcing. In order to simplify the calculations and evaluate the dynamic properties of the system (1.1), damping is neglected, which is generally around 1% for steel and 5% for concrete, and the forcing equals zero, since the properties of the system, in hypothesis of linearity, do not depend on the type of excitation. Setting the zero damping greatly simplifies the calculations and does not introduce big errors since when it is small it does not influence both the eigenfrequencies and the associated modal shapes.

So, if $C = 0$ and $f(t) = 0$ we obtain:

$$M\,\ddot{x} + Kx = 0 \tag{1.19}$$

The solutions for free vibration of the structure will be a harmonic function of the type

$$a_i = \sin(\omega_i t - \alpha)$$

So, the associated system (1.19) is reduced to:

$$(K - \omega_i^2 M)a_i = 0 \tag{1.20}$$

where ω is the natural frequency of the system (eigenvalue) and a is the modal shape associated with it (eigenvector). Necessary condition is:

$$det(K - \omega^2 M) = 0 \tag{1.21}$$

you get non-trivial solutions of the problem (all the a_i equal to zero). Equation (1.21), known as a characteristic equation, admits n solutions. The solutions ω_i

turn out to be the frequencies proper to the structural system, while the vector a consists of the modal shapes associated with them. The knowledge of these proper frequencies is very useful because in correspondence with them the structure will be more easily excitable. In theory, in the absence of damping, a forcing with a frequency equal to a frequency of the system would lead to oscillations gradually increasing until the collapse. In practice, however, the damping related to each mode means that at a certain point it is possible to reach a regime situation with amplitudes smaller and smaller as the value of the damping is greater. By ordering the natural frequencies of a system in increasing order, it can be seen that at higher frequencies there are associated ways of vibrating more and more disordered. For example, given a four-storey building, regular and with very rigid floor slabs with respect to the columns, one wants to analyze it in a single direction by modeling it as a concentrated mass structure by means of a shear-type schematization. The building taken as an example has floor masses of $m = 10ton$ and stiffnesses of $k = 1000kN/m$.

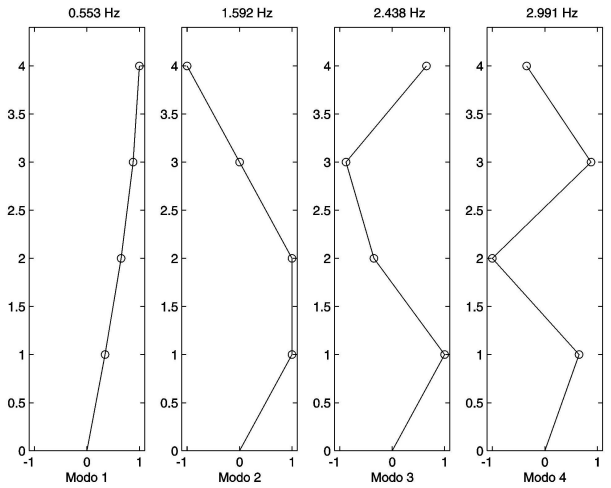

Figure 1.4: Frequency and vibration modes with shear-type modeling

In the common practice, a building is modeled to the finite elements and the vibrating modes are certainly greater than the example of the sheare-type frame, fig. 1.4, even if the most significant modes are the first and associated with the larger eigenvalues. In particular, the Italian legislation requires the choice of the main modes according to the percentage of participant mass that must reach 85%.

1.4.1 Laplace transforms

The study of the behavior of a structure in elastic linear field immediately leads to the solution of a system of differential equations with a number of equations and unknowns equal to the number of degrees of freedom that are to be considered.

This problem, formulated in matrix form, is the (1.1). To achieve the solution of this system, are used the functional transformation, known as the Laplace transformer, and the inverse transformer, known as the Laplace anti-transformer. Through this transformations it is possible to solve the system in an indirect way. The procedure consists in solving an image problem, a simpler solution than the object problem, and then the solution is transformed to obtain the solution of the original problem.

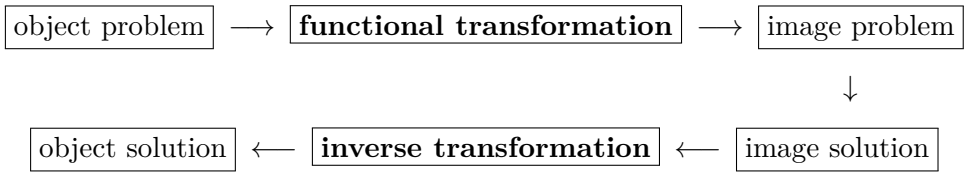

Where, the functional (or Laplace) transformation is given by the expression:

$$F(s) = \int_0^\infty f(t)e^{-st}dt \tag{1.22}$$

While, the inverse transformation (or Laplace antitransformation) is given by this expression:

$$f(t) = \frac{1}{2\pi\jmath}\int_{\sigma_0-j\infty}^{\sigma_0+j\infty} F(s)e^{st}ds \tag{1.23}$$

Thus, the system of ordinary differential equations (1.1) is transformed into a system of algebraic equations

$$(Ms^2 + Cs + K)X(s) = F(s) \tag{1.24}$$

much simpler to solve, with solution:

$$X(s) = \frac{F(s)}{Ms^2 + Cs + K} \tag{1.25}$$

where, all the dynamics of the system is concentrated in the denominator.

1.4.2 Fourier transform

Imposing

$$\frac{1}{(Ms^2 + Cs + K)} = H(s) \tag{1.26}$$

we indicate with $H(s)$ the function of transferring a forcing date to the structural parameters of a building defined as the ratio between the Fourier transform of the structural response and the input transform:

$$H(s) = \frac{X(s)}{F(s)} \tag{1.27}$$

and we introduce the frequency response function $H(\jmath\omega)$ defined as the restriction of the transfer function to the imaginary axis only. So, the (1.26) becomes:

$$H(\jmath\omega) = \frac{1}{-M\omega^2 + C\jmath\omega + K} \tag{1.28}$$

This mathematical artifact actually has a very precise physical meaning. In fact, similarly to what was done with the Laplace transformation for the transfer functions, the Fourier transformation is used for the frequency response functions. The Fourier transform is defined by:

$$F(\omega(t)) = \int_{-\infty}^{+\infty} \omega(t) e^{-\jmath\omega t} dt \tag{1.29}$$

Given that, to be able to talk about the width of the input and output, it is fundamental the hypothesis that the system is in regime[4]. Thus, the frequency response function is nothing other than that function of ω which allows to know the value of the output, note the amplitude of the input and its pulsation ω. At each ω the transfer function provides the factor by which the amplitude of the input is measured to obtain the amplitude of the output. A methodology for obtaining this answer is the following: given the known forcing in both amplitude and pulsation, the amplitude of the system's response is measured and a comparison is made. The ratio between amplitude and output is called gain. Also the phase of the output will generally be different from that of the input and therefore it is necessary to measure both and make the difference in order to have the phase shift between the two curves. Then, the output phase will be equal to that of the input plus the phase shift.

1.5 Implementation of software tool, data-driven, study of dynamic behavior

From the simple carrying out of didactic projects, models of typical structures have been realized through the use of finite element modeling software. The behavior of these structures was then simulated using seismological data in the literature and the data concerning the dynamic response were used for analysis using experimental techniques. For this purpose, commercial software, ARTEMIS, has been used, with an interface that is quite user-friendly but costly enough. In order to optimize costs, the work group decided to implement an economic and effective software tool for the dynamic analysis of real structures. The data-driven dynamic identification techniques used are F.D.D. (Frequency Domain Decomposition) and S.S.I. (Stochastic Subspace Identification - Time domain), which essentially translate into the following operational procedural process:

[4] the transfer function between two transient signals does not make sense

- Drawing geometry structure;
- Indication of sensor positions;
- Data analysis;
- Validation of results.

The term *data-driven* identifies the dynamic response analysis procedures based exclusively on the analysis of data recorded by sensors directly placed on the structure to be characterized. The use of such techniques has the extreme advantage of being able to analyze the structures of interest without making any preliminary hypothesis, and, in the best of situations, without using any artificial forcing (OMA analysis). Therefore, in addition to economic efficiency, these procedures are characterized by the fact that the surveys are performed in the real operating conditions of the structure. The analysis of the data-driven dynamic response performed by the SmartLab work-group focused on the identification of frequencies and modal shapes, as shown for example in fig. 1.5.

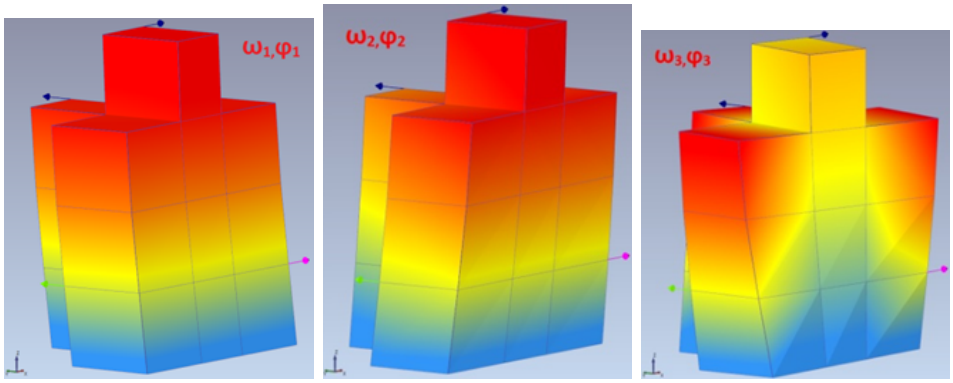

Figure 1.5: Modal Shapes: the first three modes of vibration

The techniques commonly used for the dynamic analysis of structures can be distinguished according to the domain in which they operate, be it of time or frequency; in the present work we will refer to the latter, generally less onerous from the computational point of view. In particular, reference will be made to the so-called FDD (Frequency Domain Decomposition) method, which operates in the frequency domain; the technique provides, first of all, to calculate the Power Spectral Density, PSD, of the measured data.

The Power Spectral Density (PSD) is the magnitude squared of the Fourier Transform of a continuos time and finite power signal. It is the quantity of power for each frequency component: therefore, PSD integral (in frequency domain) is the total signal power.

Power spectral density function (PSD) shows the strength of the variations (energy) as a function of frequency. In other words, it shows at which frequencies

variations are strong and at which frequencies variations are weak. The unit of PSD is energy (variance) per frequency(width) and you can obtain energy within a specific frequency range by integrating PSD within that frequency range.

PSD is a very useful tool if you want to know frequencies and amplitudes of oscillatory signals in your time series data. Looking at PSD is like looking at simple time series plot except that we look at time series as a function of frequency instead of a function of time. Frequency is a transformation of time and looking at variations in frequency domain is just another way to look at variations of time series data.

PSD tells us at which frequency ranges variations are strong.

When we have two sets of time series data at hand and we want to know the relationships between them, we compute coherency function and some other functions computed from cross spectral density function (CSD) of two time series data and power spectral density functions of both time series data. If we have more than two sets of time series data, we might compute frequency domain complex empirical orthogonal functions from cross spectral density function to know the relationships among those data. The cross spectral density function is a Fourier transform of cross correlation function but we can compute CSD directly using a method called FFT.

Chapter 2

Dynamic Characterization

2.1 Introduction

The dynamic characterization is the phase of the dynamic analysis in which the dynamic properties of the structure are determined through the use of experimental tests. In this phase the experimental test planning is essential:

- number and position of the measuring instruments;
- type, intensity, duration and frequency range of the excitation;
- length and sampling step of the data acquisition.

2.2 Vibration's nature

A body vibrates when an oscillatory motion is described around a reference position whose parameters, such as amplitude and frequency, are not generally constant over time. The nature of a vibration can be predictable starting from the knowledge of previous recurrences, the phenomenon is in this case deterministic, or can be considered from having only some properties that follow statistical laws, in this case we speak of stochastic motion or vibrations random.

Among the periodic deterministic oscillatory motions are, for example, the vibrations generated by the machines, in relation to the type, are characterized by harmonic components with multiple pulsations of the rotation speed of the rotating shafts inside the machine. The random motions with stationary characteristics include, for example, wave motion and wind. Among the noperiodic phenomena are the shocks in the various forms or the vibrations that occur in the transients of starting or stopping the machines. Usually deterministic vibrations usually overlap with random vibrations, which can be considered as disturbances or noise. Summing up, the nature of vibration or motion can be deterministic or stocastic (random). The deterministic motion can be periodic, such as armonic

and multiharmonic, or not periodic, such as transient and shock. The stocastic motion can be stationary and non-stationary.

Vibration signals, deterministic or random, usually have multiple harmonic components of different frequency and phase; the representation of a vibration in the time domain allows only to estimate some parameters of synthesis (peak, peak-peak, RMS, etc.) and the analysis in frequency is essential to be able to estimate the contribution provided by each harmonic.

2.3 Vibration's measurement

Vibration measurements can be made in different ways depending on what you want to achieve. They are usually divided into three macro-areas: measurement of the vibration level, measure of excitation and measurement of the response to a known excitation. The measurement of the vibration level is carried out for a mechanical system or to determine the level of vibration transmitted to the human body and then compare it with the value admitted by safety or hygiene rules, or to evaluate the mechanical stresses induced. The measure of excitation consists in the measurement of forcing (forces or moments) that are nothing more than the actions that applied to a vibrating system put it into vibration. The measurement of a system's response to a known excitation is carried out to identify experimentally the frequency response function of a body or a system of bodies and to estimate its own frequencies and modes of vibration: *Experimental Modal Analysis*, EMA.

2.4 Excitation techniques

2.4.1 Noise environmental

It is produced by vehicular traffic and wind and is characterized by limited energy but by a wide spectrum. The advantages are: no load additional, practically no cost and does not require additional sources of excitement. However, there is difficulty in identifying the transfer function between input and output and the signal/noise ratio is low.

2.4.2 Vibrodyne

It can be counter-rotating masses or rotating masses and consequently it changes the direction of the forcing while the trend is always sinusoidal. In any case, the frequency of the forcing is always linked to the speed of rotation, instead the intensity can vary, adding mass. In the case of counter-rotating masses, the stress induced to the structure occurs in one direction, while in the second case the stress is in all directions. The advantages of vibrodin are that the transmitted energy can be of some importance with beneficial consequences on the signal-to-noise

ratio and that the forcing frequency can be accurately controlled. On the other hand, there are objective difficulties: to identify the most convenient location and to excite coupled ways. Obviously, we must not exceed the intensity so as not to damage the structure. The mechanical shaker, like the vibrodina used for school tests, is a device able to generate vibrations of appropriate intensity and frequency. In particular, it is a machine that, firmly anchored to the structure, allows the application of variable forces over time with sinusoidal law. The functionaling principle consists in the fact that an eccentric mass m rotating around an axis with constant angular velocity ω generates a centrifugal force F, which can be represented by a rotating vector in the plane orthogonal to the rotation axis, whose width is

$$F = me\omega^2 \tag{2.1}$$

where e represents eccentricity. Indicating with f the frequency the (2.1) become

$$F = me(2\pi f)^2 \tag{2.2}$$

The eccentric mass of the vibrodin is obtained by means of two equal masses constrained on the peripheral crown of each individual disk. By moving along the circumference of the peripheral crown one of the two masses (moving mass) with respect to the other (fixed mass), it is possible to adjust the eccentricity value.

The main limit of the vibrodina is constituted by the dependence between generated force and rotation speed, as well as by the power of the electric motor. In theory, the vibrodina is suitable for all types of structures, even if its use is strongly conditioned by the search for the first harmonics. At low frequencies, the excitation force is determinable only with very high masses, to the detriment of ease and speed of use. Therefore, its weight can weigh on the structure, influencing its behavior, especially in the case of light structures.

2.4.3 Electrodynamic exciter

The forcing takes place in one direction. As for the vibrodina, to vary the intensity of the forcing one can add mass or vary the acceleration of the mass itself. Forcing can be obtained with frequencies between a few tenths of a Hz and 50 Hz and the excitation is of a random type. It has limited power and if you exceed the intensity you risk damaging the structure.

2.4.4 Hydraulic exciter

Also in this case the forcing can have a single direction. As for the electrodynamic exciter, one can obtain forcing with frequencies between a few tenths of Hz and 50 Hz, random excitation. Limitations on the use of this excitation technique are the need to have a pumping station and the high cost.

2.4.5 Instrumented hammer

The instrumental apparatus consists of a force transducer on the head protected by rubber and according to the hardness of this one can analyze different parts of the spectrum. Basically, once the accelerometers are set, you can go directly to the test. However, if a two-channel analyzer is used, this instrumentation loses its practicality and the performance of the test is cumbersome. However, it is an instrumentation that is easy to transport and not expensive. The only disadvantage is the signal/noise ratio which is not always good.

2.5 Measurement's chain

Vibration measurements require an instrumentation that includes at least one transducer, an amplifier and an indicator. The transducer is an instrument sensitive to displacement, velocity or acceleration, able to output a voltage, or other electrical quantity, proportional to the instantaneous value of the input quantity. The electrical quantity output from the transducer is first amplified and then sent to an instrument that indicates its value, or rather, being appropriately calibrated, it directly indicates the value of the quantity (displacement, velocity, acceleration) detected by the transducer. A complete measurement chain usually consists of the following components: Transducer, Pre-Amplifier, Signal Conditioner, Analogue/Digital Converter, Signal Analyzer, other devices (Display, Printer, Plotter, etc).

The signal, that is the electrical quantity whose value is proportional to that of the detected quantity, coming from the Transducer is amplified by the Pre-Amplifier and then sent to an Equipment, Signal Conditioner that amplifies it further and filters it in frequency. Frequency filtering can be performed either with analog filters, in which the input signal is continuous, or with digital filters placed downstream of the A/D converter and inside the Signal Analyzer. The operation of filtering in frequency on the input signal allows the passage of only specific harmonics in the output signal, usually a low-pass filter is used that allows the passage of only the components at a frequency lower than an imposed value Fmax cutting frequency of the filter. A band-pass filter allows you to filter all harmonics outside of an assigned frequency band. The analog band-pass filters are used to perform broadband frequency analysis by calculating a signal parameter, the RMS value, for each band in frequency and providing the typical representation of the signal through octave band histograms or 1/3 of an octave band. The narrow-band frequency analysis with the Fast Fourier Transform is performed downstream of the A/D converter after the signal has been quantized.

The presence of an integrating apparatus allows the transition from acceleration to speed or from speed to displacement. The conditioned signal is usually sent to an A/D Converter, which samples it at a frequency chosen by the user, sampling rate, detecting its numerical value at regular intervals of time. The sig-

nal coming from the Transducer is a continuous analogic signal, whose trend is similar to that of the measured quantity. The A/D Converter detects the instantaneous value of the signal at regular intervals of time, transforming it into the digital signal and then into a discrete set of numbers that can be managed and processed by a computer. Finally, the signal reaches the Signal Analyzer, which can operate on the analog signal by means of electronic circuits (filters, derivators, integrators); if instead the signal has been digitized by the A/D Converter, the Analyzer is directly a Calculator, which analyzes the sampled signal treating it as a set of numerical input data, performing on it the most varied mathematical operations.

2.6 Vibration detection techniques

To measure the vibrations of a structure that is the object of dynamic identification, the first step is to choose the technique to be used for their detection. These techniques are subdivided into speed transducers and accelerometers transducers.

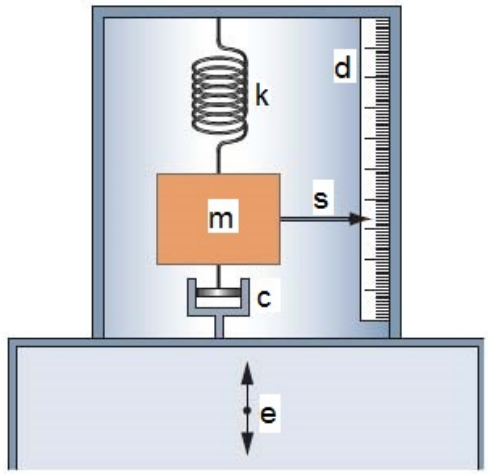

Figure 2.1: Basic element of a transducer for the measurement of vibrations.

We assume z the displacement of the internal mass to the transducer, y the displacement of the constraint and x the overall displacement of the transducer-vibrating element system. Consider the equation of motion (1.1) rewritten, however, in relative [1] y and z

$$m\,\ddot{z} + c\,\dot{z} + kz = -m\,\ddot{y} \tag{2.3}$$

[1] $x = z + y$

Considering that the displacement y of the constraint is of the harmonic type

$$y = Ye^{i\Omega t} \tag{2.4}$$

we obtain a solution of (2.3) always of the harmonic type

$$z = Z\cos(\Omega t - \phi) \tag{2.5}$$

with Z/Y displacement amplitude or amplification ratio, a frequency ratio, ω_0 own pulsation, ξ damping ratio and ϕ phase angle

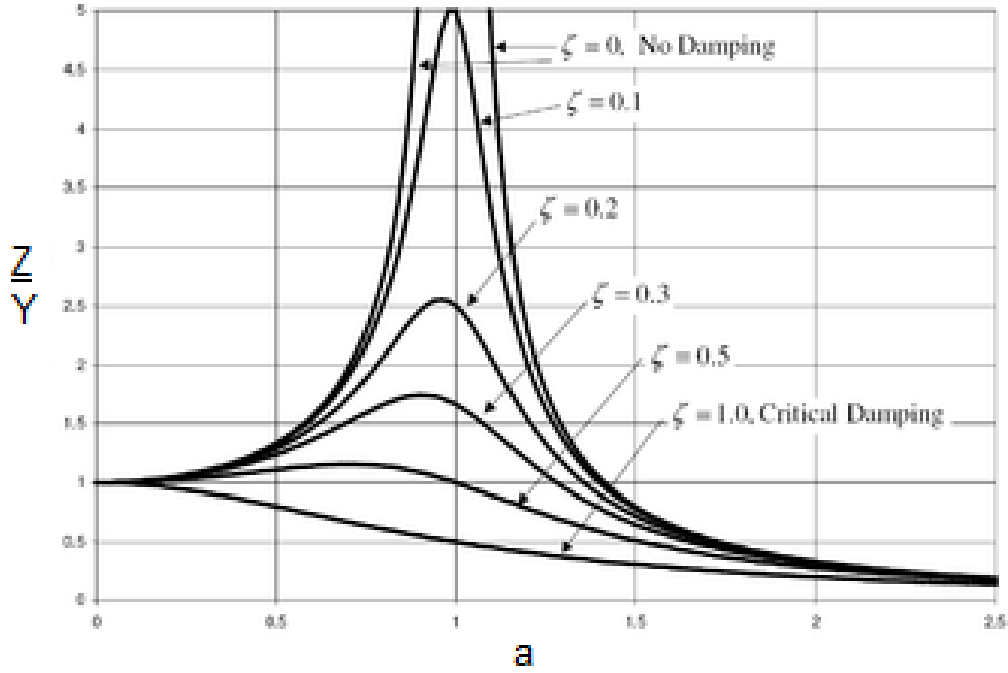

Figure 2.2: Damping ratio, ξ, as a function of amplitude: a frequency ratio and Z/Y amplification ratio

$$\frac{Z}{Y} = \frac{m\Omega^2}{\sqrt{(k - m\Omega^2)^2 + (c\Omega)^2}}$$

$$a = \frac{\Omega}{\omega_0}; \quad \omega_0 = \sqrt{\frac{k}{m}}$$

$$\frac{Z}{Y} = \frac{a^2}{\sqrt{(1 - a^2)^2 + (2a\xi)^2}}$$

$$\xi = \frac{c}{c_{crit}}; \quad c_{crit} = 2m\omega_0; \quad \xi = \frac{c}{2m\omega_0}$$

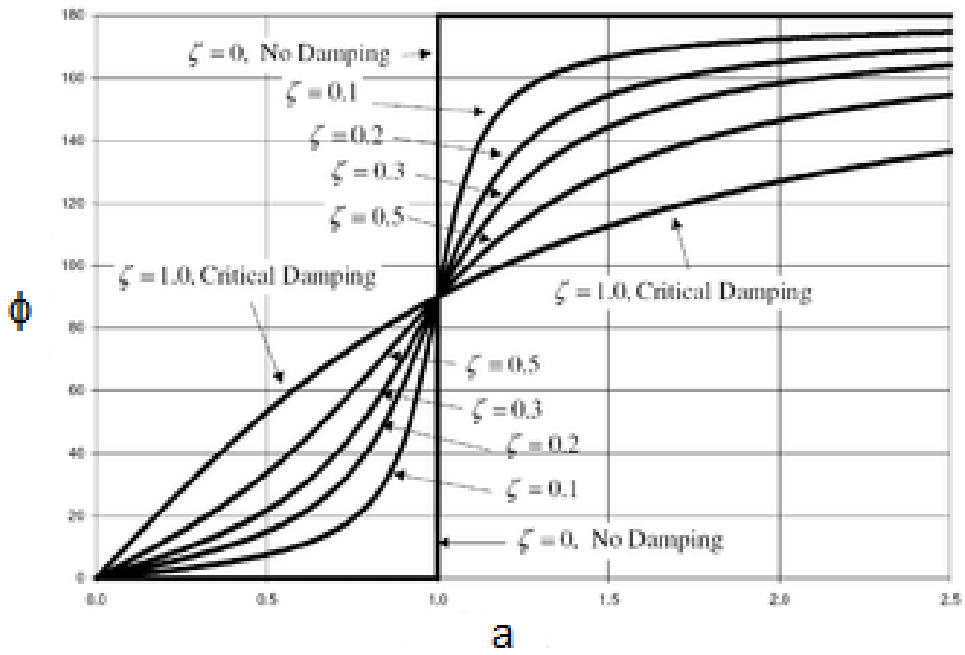

Figure 2.3: Damping ratio, ξ, as a function of phase: a frequency ratio and ϕ phase angle

$$\phi = \arctan \frac{c\Omega}{k - m\Omega^2}$$

where, appropriately replacing the expressions of a, ω_0 and ξ we obtain

$$\phi = \arctan(\frac{2a\xi}{1 - a^2})$$

If $\omega_0 << \Omega$ it follows that $a >> 1$ and the rate Z/Y tends to 1. This means that the relative displacement has amplitude Z equal to that Y of the body to which the transducer is connected but is in phase opposition, so the amplitude of the absolute displacement x of the seismic mass tends to zero. For $\omega_0 << \Omega$ the mass of the instrument must be considerable and the stiffness k must be small enough to be able to estimate the relative displacement without incurring measurement errors. A **seismograph** is a tool with a very small ω_0 that always operates at a frequency higher than its own resonance.

Given that the harmonic type solution (2.5) has an acceleration amplitude

$$\frac{Z}{\Omega^2 Y} = \frac{1}{\omega^2 \sqrt{(1 - a^2)^2 + (2a\xi)^2}}$$

where $\Omega^2 Y$ is the acceleration. If $\omega_0 >> \Omega$ it follows that $a << 1$ and

$$Z = \frac{\Omega^2 Y}{\omega_0^2}$$

where the amplitude of relative displacement Z is directly proportional to the acceleration of the body $\Omega^2 Y$. An instrument made in this way is the **accelerometer**. In particular, $a >> 1$ is called the seismographic zone and $a << 1$ is called the quasi-static zone.

Instead of measuring the displacement the force transmitted by the damping elastic element is measured, the equation of motion (2.3) can be rewritten:

$$m\,\ddot{z} + m\,\ddot{y} = -c\,\dot{z} - kz \tag{2.6}$$

That is, the force transmitted by the damping spring element is given by the sum of the two inertial terms due to the relative acceleration of the mass and the absolute acceleration of the constraint.

$$m\,\ddot{z} + m\,\ddot{y} = -c\,\dot{z} - kz = F \tag{2.7}$$

So, the $\ddot{y}$, absolute acceleration of the body, is obtained by

$$\ddot{y} = \frac{-c\,\dot{z} - kz}{m} - \ddot{z} \tag{2.8}$$

If $\omega_0 >> \Omega$ it follows that $a << 1$ and the term $\ddot{z}$, relative acceleration of the mass, is negligible. So, the (2.8) can be simplified as follows:

$$\ddot{y} \approx \frac{-c\,\dot{z} - kz}{m} = \frac{F}{m} \tag{2.9}$$

2.6.1 Speed transducers

The speed transducers can be: the seismometer or the interferometer.

The **seismometer** consists of a magnet connected by means of a base to the monitored structure. Inside the magnet we have two solenoids that move causing an electric current. From the current value it is possible to go back to the speed. For environmental vibrations they are the most suitable because they possess high sensitivity. They are characterized by a proper T period of vibration around 0.5 Hz, so they are not suitable in the case of very low frequencies. In fact they are used above 1 Hz.

The **interferometer** works with a laser beam that is pointed towards the structure and the phase variation between the electromagnetic waves sent and the retro-reflective waves is observed. This phase variation, due to the vibration of the object under study, is converted into a voltage signal proportional to the speed. This technique allows to detect vibration amplitudes smaller than 200 micron in the frequency range from 0.1 Hz to 150 Hz and allows to measure displacements, rotations and speeds with very high precision. It does not need to physically access the structure. The only disadvantage is that it is affected by vibrations that act directly on the transducer, which add up to the noise of the response.

2.6.2 Accelerometer

Depending on the frequency band to be measured, it consists of a more or less heavy mass whose movement generates an analog signal that can be: *piezoelectric* for high frequencies, *capacitative* for medium frequencies, *strain gage* for low frequencies.

2.6.3 Servo-accelerometer

It consists of an acceleration transducer and works like an accelerometer but benefits from a pre-amplification of the signal. It also detects small movements and the electrical signal is clearly visible.

2.7 Location of the instrumentation

From a theoretical point of view, a structure can be instrumented in all those points where it is considered interesting to evaluate its behavior. In practice, however, the number of sensors is closely linked to the available financial resources, both in terms of measuring devices and data acquisition. It is therefore very important to place a minimum number of devices on the structure in order to obtain all the necessary information. To achieve this, it is necessary to have, already, a rough idea of the proper ways that will be identified. In fact, it is necessary to pay great attention not to position the accelerometers in the modal nodes or in their proximity, because in these points the observability of the modes is null. For example, if you place a sensor in the middle of a supported-supported beam, you can see very well the acceleration given by the first mode, but on the other hand the sensor is indifferent to the second mode, fig. 2.4. In general, avoid placing the sensors on the symmetry axes to prevent the asymmetric modes from being hidden. In the illustrated case a good point to observe both the first and the second way, having only one sensor available, could be at a distance of 0.3 from one extreme or the other.

2.8 Implementation of a kit for structural monitoring and dynamic identification of case study ITI Monaco

As part of this research and in conjunction with the participation in some research projects[2], a kit was implemented for the structural monitoring of civil buildings and not only of road infrastructure as required by Italian law. The implemented

[2]STRIT (Strumenti e Tecnologie per la gestione del Rischio delle Infrastrutture di Trasporto), DOMUS (Distretto delle tecnologie infOrmatiche e di coMunicazione per lo svilUppo di ambienti intelligenti e Sostenibili), ALFORLAB (Ambi.Tec.Fil.Legno)

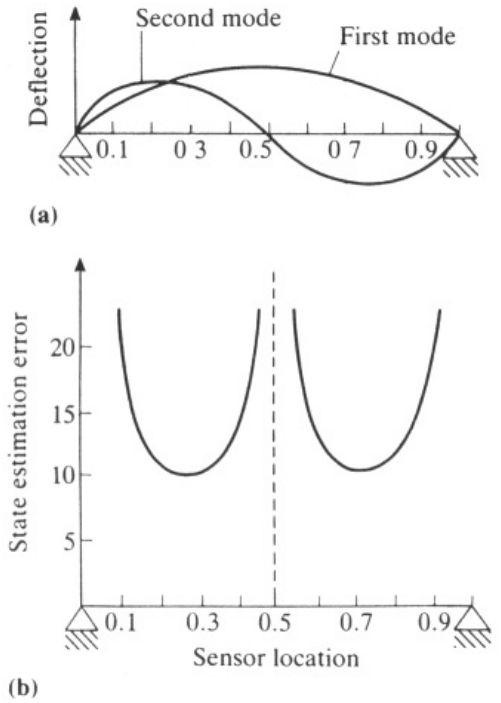

Figure 2.4: Sensor location: a) modal shapes; b) signal error

kit consists of an accelerometric network combined with a portable vibrodina. In particular, the vibrodina has been designed, built and tested in collaboration with the DRC Srl and thanks to the company EngineLAB Srl.

2.8.1 Accelerometric network

The accelerometric network consists of eight single-axial piezoelectric accelerometers with a shear-system, figg. 2.5, 2.6, 2.7.

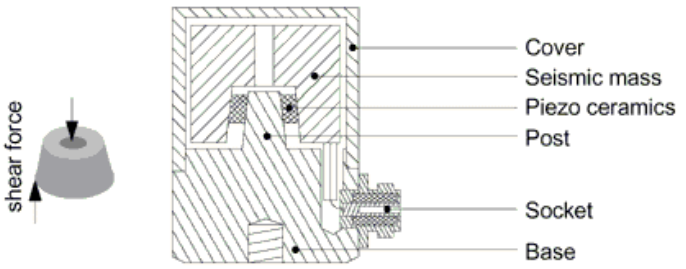

Figure 2.5: Accelerometer KS48C-model: shear design

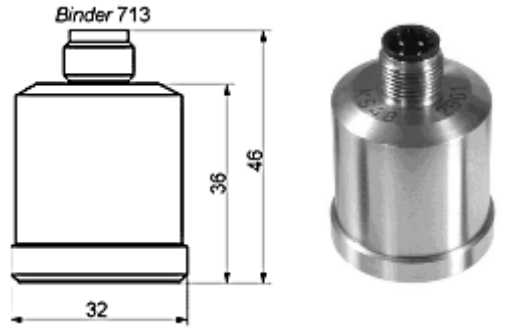

Figure 2.6: Accelerometer KS48C: measures

Figure 2.7: KS48C-model: magnetic attack, accelerometer, nut

A typical trend of the frequency response of this piezoelectric accelerometer is shown in fig. 2.8 in function of the type of assembly. As far as the electrical aspect is concerned, when an accelerometer is mounted on a conducting surface there is the possibility that the sensor will be disturbed by signals coming from other electrical devices or even from the power supply devices of the system itself, forming a *ground loop* (already seen previously), they concatenate with the acquired signals. It is therefore convenient to isolate the accelerometers from the structure on which they are mounted. Accelerometers must be connected to the acquisition system through strong connections to ensure continuous transmission without intermittences that would cause data loss. The output signal from a piezoelectric sensor is low, which means that a very sensitive signal conditioning circuit is required. ICP (Integrated Circuit Piezoelectric) type accelerometers, which incorporate a micro-amplifier which converts the signal from high to low impedance, were used for this application. The transducer needs a constant current supply which is supplied by specific acquisition systems and, in this case, it has been possible to use standard cables, even of considerable length, without the signal degrading significantly. Experimentation in the Auditorium of ITI Monaco buildings was carried out by creating an accelerometric network whose nodes were formed by high-quality piezoelectric accelerometers and the output of the ICP transducer permitted the use of a RG59 coaxial cable, fig. 2.9. The accelerometer used is the

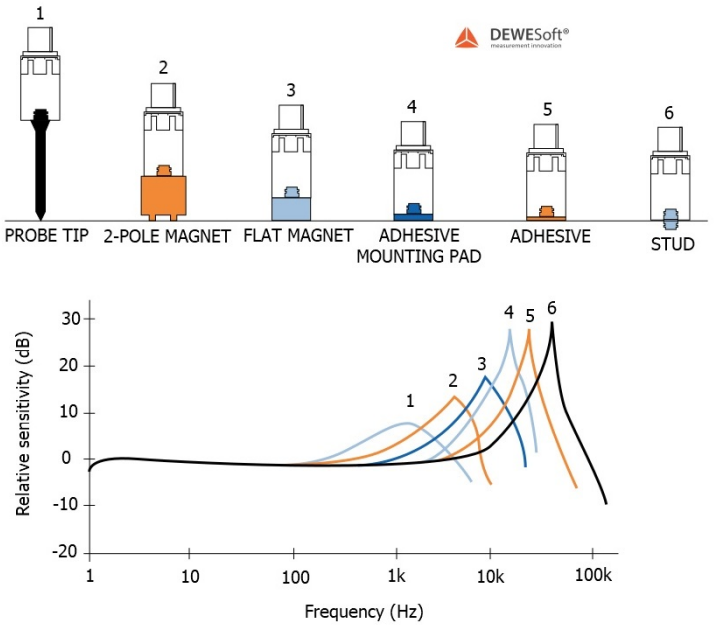

Figure 2.8: Frequency response of a KS48C-model and related to the type of assembly

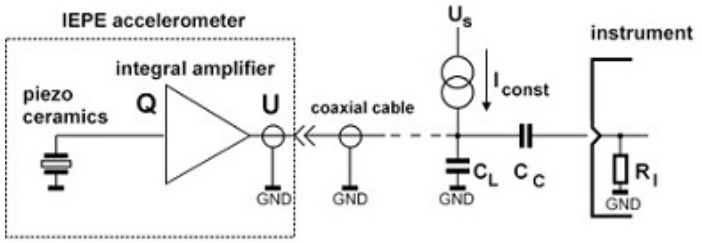

Figure 2.9: Equivalent circuit of the ICP-system: transducer and acquisition

KS48C model, tab. 2.1, with polarity positive on the output pin of the connector for an acceleration directed from the mounting surface into the body of the accelerometer and the current for the internal charge converter amount 2-20 mA at a supply voltage of 24-30 Volt. To avoid aliasing problems, it is important that the sampling rate is greater than or equal to twice the highest frequency contained in the signal. Considering that the range of frequencies to be explored is between $3Hz$ and $30Hz$, a *band-pass filter* has been applied, that is a device that allows the passage of the frequencies present within the range of interest and attenuates the frequencies outside its. The active element of accelerometer KS48C is a piezoelectric material. Piezoelectricity is the property of some crystals to generate a potential difference when they are subject to mechanical deformation. This effect

Piezo design	Shear-system
Voltage sensitivity	1000±20% [mV/g^3]
Weight	165 [g]
Residual noise (20-50000 Hz)	<13 [μg]
Material	stainless steel
Output bias voltage	8-12 [V]
Resonant frequency	>6.5 [kHz]
Transverse sensitivity	<5 [%]
Operating temperature range	-20/120 [°C]
Temp. coefficient of sensitivity	-0.16 [%/K]

Table 2.1: Main features of accelerometer KS48C-model

is reversible and occurs on scales of the order of nanometers. The operation of a piezoelectric crystal is quite simple: when an external pressure (or decompression) is applied, opposite charges are positioned on opposite faces. Crystallosis involves a capacitor to which a potential difference has been applied. If the two faces are connected to an external electric circuit, then an electric current called piezoelectric current is generated. On the contrary, when applying a potential difference to the crystal, it expands or contracts. Soliciting the crystal with two compressive forces F (or traction or cutting) are born on the faces greater electric charges proportional to the stress:

$$q = d_{ij} \cdot F \tag{2.10}$$

where d_{ij} is a piezo-constant, said sensitivity of the transducer, is linearly dependent on the proportionality constant of the piezoelectric material and on the entity of the seismic mass m. The crystal behaves like a condenser with the two charges $+q$ and $-q$ facing.

$$q = C \cdot u \tag{2.11}$$

$$C = \epsilon_0 \epsilon_r \frac{A}{d}$$

$$u = \frac{q}{C} = d_{ij} \frac{F}{C} = d_{ij} \frac{F \cdot d}{\epsilon_0 \epsilon_r \cdot A} = d_{ij} \frac{m \cdot a \cdot d}{\epsilon_0 \epsilon_r \cdot A}$$

By connecting the capacitor inside an electrical circuit, the potential difference between the two faces is proportional to the applied force and therefore to the acceleration of the body to be measured.

The sensing element of a piezoelectric accelerometer are piezoceramic material and seismic mass. One side of the piezoelectric material is connected to a rigid post at the sensor base. The so-called seismic mass is attached to the other side. When the accelerometer is subjected to vibration, a force is generated which acts on the piezoelectric element. According to Newton's law this force is equal to the product of the acceleration and the seismic mass. By the piezoelectric effect a

charge output proportional to the applied force is generated. Since the seismic mass is constant the charge output signal is proportional to the acceleration of the mass.

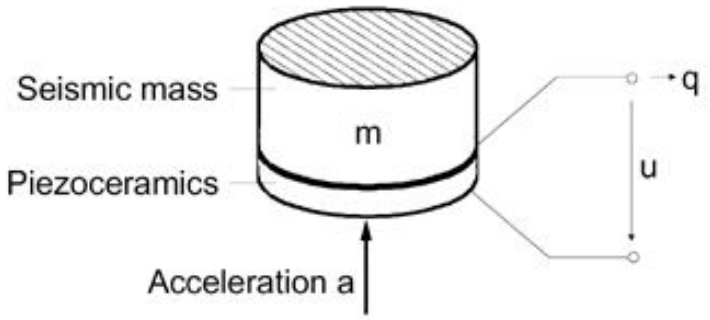

Figure 2.10: Seismic mass m

A compression disk looks like a capacitor with the piezoceramic material sandwiched between two electrodes. A force applied perpendicular to the disk causes a charge production and a voltage at the electrodes.

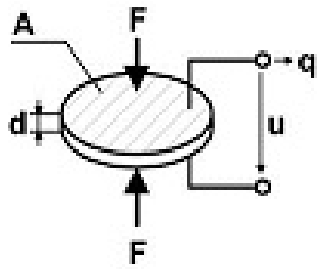

Figure 2.11: Piezoelectric effect for a compression disk: A electrode-area, d thickness, F force, q charge, u voltage, d_{33} and e_{33} piezo-constants

$$F = m \cdot a \tag{2.12}$$

$$q = d_{33} \cdot F$$

$$u = \frac{d_{33}}{e_{33}} \cdot \frac{d}{A} \cdot F$$

where

$$e_{33} = \epsilon_0 \epsilon_r$$

with ϵ_0 dielectric constant of the vacuum and ϵ_r dielectric constant relative to the ceramic material (i.e. quartz). Transfer factors for acceleration:

$$a = \frac{q_a}{B_{qa}}$$

$$a = \frac{u_a}{B_{ua}}$$

Charge sensitivity:

$$B_{qa} = \frac{q}{a}$$

Voltage sensitivity:

$$B_{ua} = \frac{u}{a}$$

2.8.2 Vibrodina: VIBRO 9001-E

For structural monitoring and dynamic identification of the ITI's Monaco Auditorium, a slider vibrodine (called VIBRO-9001) was built by the collaboration between the SMART Lab research team and the DRC factory, used to impress an external forcing structure in situ. Vibro 9001 is a mechanical system designed and manufactured entirely in Italy composed of Real Time Controller RTC 9001 Controller, RTC analysis and management software, electromechanical linear actuator. Vibro 9001 is the first and only vibrodine in the civil sector that allows you to solicit and guide the structures at their natural frequency. The Vibro 9001 system can be transportable on site manually by the operator thanks to its relative low weight for tests on existing structures. The system can be used on site for vibration analysis on scale models for research and teaching purposes. The Vibro 9001 system, complete with RTC 9001-S controller, is particularly suitable for sinusoidal low frequency stresses ranging from 0.5Hz to 30Hz. It is possible to generate sinusoidal waves, random, programmed paths, real simulations.

The uniqueness and uniqueness of the system consists in using a high performance linear motor in terms of position resolution and speed (frequency). Further uniqueness of the system linked to the use of the permanent magnet linear motor is the high efficiency guaranteeing a reduced energy consumption due to the higher overall efficiency: at full capacity it requires a maximum of 2 kW of power obtainable with any current generator. The system includes the following components:

- Vibra RTC software
- Real Time Controller - RTC VIBRA
- Drive
- Linear motor with moving coil
- Accelerometric sensors
- Position sensor - encoder
- Moving masses

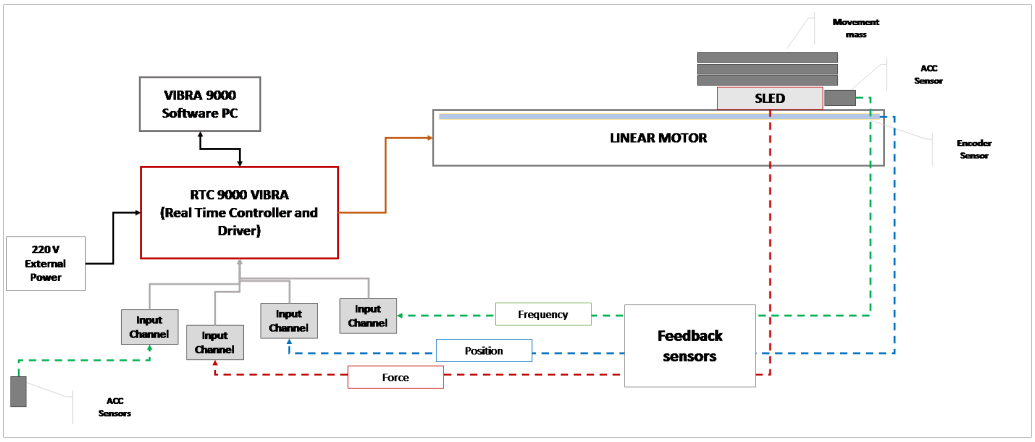

Figure 2.12: Vibrodina: operating scheme

The linear motor is composed of two guides on which two recirculating ball carriages move to which the slide is fixed. The slide is equipped with an accelerometric sensor and a position sensor (encoder) that detects the position of the slide same in every point of the linear motor. The sled has a top plate where you can apply masses. The linear motor is fixed to the ground by means of anchor plates that allow the oscillations to be transmitted to the structure to which it is anchored. The RTC software defines the frequency at which the slide must move and the forcing to be generated. The controller analyzes the data and generates the command on the drive that sends the electrical impulse to the motor (coil) which generates a magnetic field of sign congruent with the movement it must perform. The slide starts to execute a sinusoidal movement along the guides: the accelerometric sensor acquires the frequency of movement of the slide which signal is acquired in real time by the controller which processes the value using it as input to generate the command signal to send to the drive.

This operation is defined as closed loop.

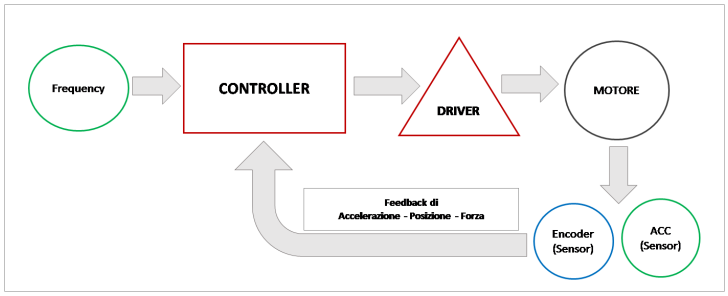

Figure 2.13: Operating diagram of the closed loop VIBRO 9001 instrumentation

The encoder position sensor is acquired simultaneously with the accelerometric

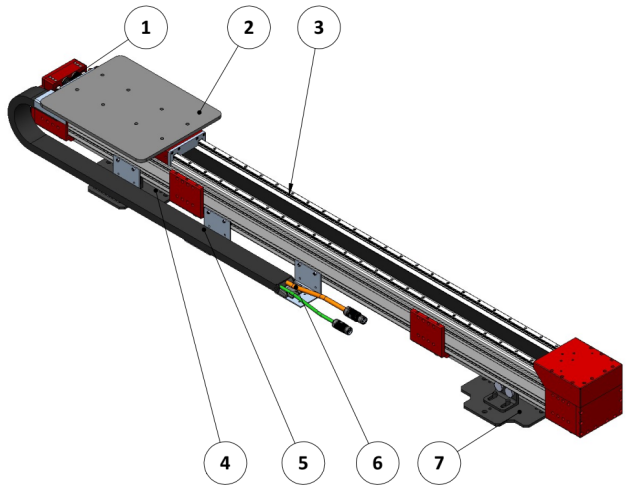

Figure 2.14: Graphic scheme: 1 slide protection limit switch, 2 driving masses and sled, 3 Linear motor-guides, 4-7 ground fixing plate, 5 cable chain, 6 motor drive connection cables

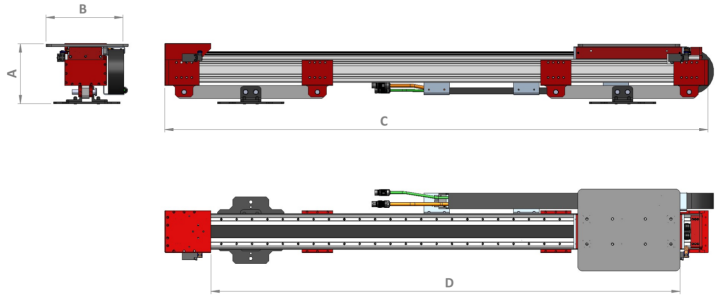

Figure 2.15: Graphic scheme: A 280mm, B 340mm, C 2200mm, D 1500mm (effective travel of the slide)

sensor in order to check the exact position of the slide and the travel that it actually travels. The position value is processed in real time to obtain the velocity values that are analyzed together with the acceleration values to obtain the value of the generated force. Also in this case the position value is a feedback to generate the command signal. A third channel acquires the accelerometric value of a sensor that is positioned on the structure or element to be measured.

2.8.3 Tromograph

Tromograph is an instrument specially designed for microtremor measurements in the frequency range of 0.1 to 500 Hz. This tool was developed at the SmartLab laboratory of the University of Calabria. The instrument is portable, light (2 kg)

Figure 2.16: VIBRO 9001 - E

and small (18 x 14 x 8 cm) with low energy consumption. It employs very small masses and a non-resonant rigid structure built with non-diffractive materials, fig. 2.17.

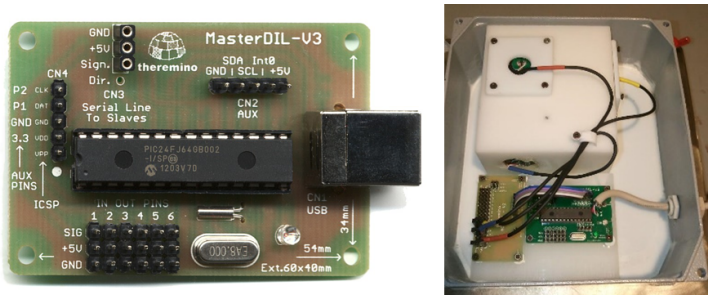

Figure 2.17: Tromograph

The sensors consist of a set of critically damped velocimeters that transmit the signal to a digital acquisition system, via the Theremino Datalogger card. The Theremino Data-logger (freeware hardware) is an economic an open source system, data acquisition system (ADConverter) but at the same time having great performance and being easy of use. Theremino is an open source system, completely free and open, designed to interface Windows, Linux, OSX and Android with the outside world. The modules of the system can communicate with each other, even via the Web. It is an Input/Output device, directly connectable via USB to various types of PC, without needing for special drivers, suitable for experimentation with sensors of various kinds and very simple in the mode of operation. The device is managed using the open source software HAL (Hard-

ware Abstraction Layer), which is easy to understand, easy to manage and well documented.

Chapter 3

Signal Analysis

3.1 Introduction

The transducers have the function of transforming a measured mechanical quantity, usually acceleration or speed, into an electrical signal. Instant by instant, therefore, the intensity of the electrical signal is proportional to the mechanical size of the structure to which it refers. The response signal recorded by the transducers can be analyzed both in the time domain and in the frequency domain. The frequency domain has been shown to be particularly suitable for gathering

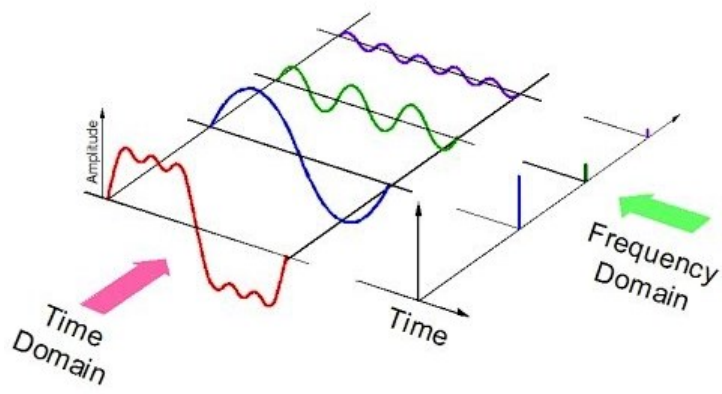

Figure 3.1: Response signal in the time domain and in the frequency domain

and studying the fundamental dynamic characteristics of a structure, such as its own frequencies and corresponding modal forms, and to solve the inverse problem of identifying the properties of the system starting from its response.

To calibrate a finite element model of an existing structure subject to a seismic event using direct recordings of the structure response, the time domain response (time-history) of the points at the base will be required in order to allow the

program to simulate the motion imposed on the ground and integrate with the step. If, on the other hand, it is intended to calibrate a linear finite element model through changes in stiffness and mass distribution, the representation in the frequency domain is the most suitable.

3.2 Vibration levels in the time domain

The analysis of a vibration signal expressed in terms of acceleration in the time domain is carried out by calculating different synthesis parameters that allow comparison with what we want to verify. These parameters are: Peak-to-Peak, peak, RMS and Average. The *Peak-to-Peak* indicates the maximum wave excursion

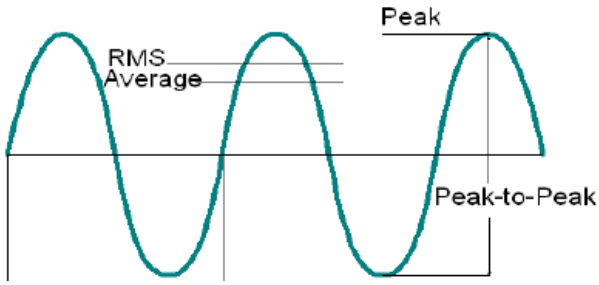

Figure 3.2: Parameters in the time domain

(maximum stress, mechanical play). The peak indicates the maximum positive or negative vibration excursion (short duration shocks). The *Root Mean Square*, *RMS*, is the most significant measure of amplitude in that it takes into account the history of the wave over time and gives an amplitude value directly related to the energy content of the vibration.

$$RMS = \sqrt{\frac{1}{T}\int_0^T x^2(t)dt} \tag{3.1}$$

where $x(t)$ is the trend of the signal as a function of time and T is the period, the duration of the signal itself. In the case of a sinusoidal magnitude of amplitude A, the (3.1) become

$$RMS = \frac{A}{\sqrt{2}} \tag{3.2}$$

In the case of digital signals consisting of N samples, the (3.1) become

$$RMS = \sqrt{\frac{1}{N}\sum_{i=1}^{N} x_i^2} \tag{3.3}$$

The duration T of the measurement is divided into T_i intervals and for each of them the corresponding RMS value is calculated. The measuring base of the T_i intervals, for the calculation of the RMS value in moving average, is usually $1second$ because in this way it is possible to plot the trend of the RMS value over time and verify its correlation with any local amplitude peaks.

The *equivalent acceleration to the energy of the vibration*, a_{eq}, is defined the linear mean of the effective value calculated over a time interval T

$$a_{eq} = \sqrt{\frac{1}{T}\int_0^T a_{RMS}^2(t)dt} \tag{3.4}$$

The *Crest Factor*, $C.F.$, is defined as the ratio between the peak value and the RMS value or the ratio between the peak value and the value of a_{eq}.

$$C.F. = \frac{Max.Peak}{a_{RMS}} \tag{3.5}$$

or

$$C.F. = \frac{Max.Peak}{a_{eq}} \tag{3.6}$$

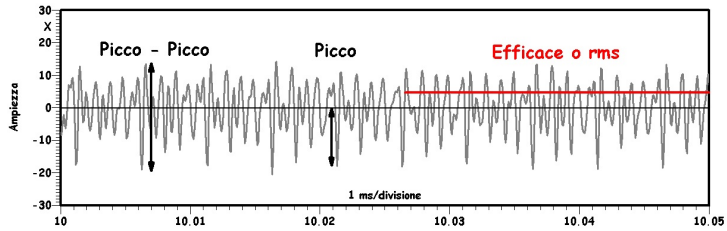

Figure 3.3: Equivalent acceleration to the energy of the vibration

The *Average* takes into account the history of the wave over time. For continuous signals is

$$Avg = \sqrt{\frac{1}{T}\int_0^T x(t)dt} \tag{3.7}$$

for discrete signals is

$$Avg = \frac{1}{N}\sum_{i=1}^{N} x_i \tag{3.8}$$

The vibration levels can be expressed, as well as in metric units, in logarithmic quantities: the scale used is that of the *decibel*, dB. It is given by

$$dB = 10\log(\frac{x^2}{x_{rif}^2}) \tag{3.9}$$

or

$$dB = 20\log(\frac{x}{x_{rif}}) \tag{3.10}$$

where, x is the measured effective level and x_{rif} is the standard reference level.

The use of logarithmic scales for the representation of vibrations is widespread in the practice of measurement if the signal is expressed in broadband[1], particularly if special filters should be applied frequency weighing as those imposed by $ISO2631$ and $ISO5349$ regulations. One of the advantages offered is that of compressing a very wide range of values within a reasonably reduced scale; in fact, there is the effect of dilating the lower amplitude frequencies or values on the graph and compressing the higher ones, thus giving the same percentage of resolution on the whole graph, while maintaining the dimensions within reasonable limits.

3.3 Measurement of signals

To pass from a signal in the time domain to a signal in the frequency domain, a very fast and effective numerical method is used: the *Fast Fourier Transform*, *FFT*. The hypotheses underlying the numerical method are:

1) the sampled signal in the time domain contains N values uniformly spaced with interval Δt expressed in seconds. The total sampling period begins at $t = 0$ and ends at $t = T_{TOT}$, then the sampled signal in the time domain is given by

$$T_{TOT} = N\Delta t \tag{3.11}$$

2) the sampling of the signal in the frequency domain assumes that the frequency spectrum contains $N/2$ uniformly spaced points with a frequency interval equal to Δf expressed in Hz. The frequency spectrum is therefore defined in the range between 0 and F_{max} with the maximum frequency obtained from the sampled signal given by

$$F_{max} = \frac{\Delta f N}{2} \tag{3.12}$$

3) the maximum frequency that can be identified with a given sampling frequency, when passing from the frequency domain to the time domain, is

$$F_{max} = \frac{1}{2\Delta t} \tag{3.13}$$

known as Nyquist's frequency.

By (3.13) we get that the maximum frequency of sampling $\Delta t = 1/2F_{max}$. This means that the maximum frequency F_{max} to be obtained from the sampling of a certain signal must have a frequency of sampling of the signal Δt equal to

$$\Delta t \leq \frac{1}{2F_{max}} \tag{3.14}$$

[1] octave band or 1/3 octave band

This means that the harmonics of higher frequency are to be discarded without affecting the resolution of the FFT. Replacing the (3.12) in the (3.13)

$$\frac{\Delta f N}{2} = \frac{1}{2\Delta t}$$

$$\Delta f N = \frac{1}{\Delta t}$$

$$\Delta f = \frac{1}{N\Delta t} \tag{3.15}$$

Replacing (3.11) in the (3.15) is obtained

$$\Delta f = \frac{1}{T_{TOT}} \tag{3.16}$$

In the practical process we start by choosing Δf and by the (3.16) we obtain the total sampling period T_{TOT}

$$T_{TOT} = \frac{1}{\Delta f} \tag{3.17}$$

and by the (3.12), once the maximum frequency F_{max} has been set it is possible to obtain N

$$N = \frac{2F_{max}}{\Delta f} \tag{3.18}$$

all in order to derive which sampling frequency to use.

3.4 Random functions

Given an aleatory variable $x(t)$ we define density of probability distribution the function $p(x)$ with the following physical meaning:

$$p(x)dx = Prob[x \leq x(t_0) \leq x + dx] \tag{3.19}$$

where, $p(x)dx$ represents the probability that at time t_0 the variable $x(t)$ has values between x and $x + dx$.

$$P(x) = \int_{-\infty}^{x} p(x)dx \tag{3.20}$$

where $P(x)$ is probability distribution function and represents the probability that $x(t_0)$ has values between $-\infty$ and x. The expected value of the aleatory variable $x(t)$ is given by

$$E(x) = \int_{-\infty}^{+\infty} xp(x)dx \tag{3.21}$$

Particular importance assumes

$$E(x^2) = \int_{-\infty}^{+\infty} x^2 p(x)dx \tag{3.22}$$

which expresses the average of the values of $x(t)$, elevated squared, and is also called the RMS Root Mean Square value. A time-dependent aleatory process is represented by the set of possible random functions $x_1(t), x_2(t), ..., x_n(t)$, called sample functions. To describe the signal $x(t)$, we can examine the distribution of the $x(t_1)$ values that the various sample functions have at the time $t = t_1$. The magnitude $x(t_1)$ is considered a random variable for which a first order probability distribution function can be defined. The same can be done for the set of values at the time $t = t_2$. Knowing the statistical distributions at times t_1 and t_2 can also be defined the probability distribution of the second order or joint distribution, which represents the statistical link between these two random variables. It can be a function of both t_1 and t_2 or the difference $\tau = t_1 - t_2$. With the stationary term it is indicated that the functions of probability distribution of order higher than the first do not depend on the absolute value of the time but only on the difference of the times τ. With the term ergodic[2], on the other hand, a stationary process is indicated in which the averages made on a single sample function when the time varies are independent of the sample function. That is, a sample function is completely representative of the set of sample functions.

3.5 Excitation signals

The excitation signals used in dynamic identification can be divided into two main categories: signals containing a single frequency and signals containing a frequency spectrum. The signals of the first category are instead of a sinusoidal type: swept sine and stepped sine. The signals of the second category can be divided into three subgroups: periodic signals (pseudo random, periodic random, periodic chirp), non-periodic (pure random) and transitory (burst random, burst chirp, impact).

3.5.1 Swept sine

It is an excitation consisting of a sinusoidal signal, with a slow and continuous frequency variation. It is one of the oldest methods of excitation and it was first applied to signal analysis techniques, such as band pass filters. In this type of excitation the structure is virtually excited at a single frequency, and given the slow increase in variation it can be assumed that the response is stationary. The peak/RMS ratio and signal/noise ratio are typical of this type of excitation. Moreover, the high control on frequency and amplitude makes it suitable for the

[2]In signal theory, a stochastic process is said to be ergodic when the statistical averages converge almost everywhere in temporal averages. A condition necessary for ergodicity is therefore the stationarity in a broad sense, up to the order for which the ergodicity property is to be verified. In particular, we talk about average ergodicity when the time average and the statistical mean coincide; we talk about ergodicity in correlation when statistical autocorrelation and temporal autocorrelation coincide.

characterization of structures with non linear behavior. The main limitation of this type of excitation is the slow frequency variation that results in a high test time.

3.5.2 Stepped sine

It is the modern version of the swept sine, obtained in fact, applying to this the modern techniques of digital signal analysis. Instead of a continuous frequency variation, the stepped sine provides a discrete frequency increase. We proceed by step:

step 1 definition of the frequency band of interest, through initial frequency, final frequency, and frequency increase.

step 2 conversion of the digital signal into analog and excitation of the signal amplifier and the shaker.

step 3 Acquisition of the analog signal from the accelerometer and the amplifier through an analog-digital conversion board, set at a scanning frequency equal to the product of the excitation frequency for the number of points desired in a wave.

step 4 Waiting to extinguish the transitory term of the structure response, then recording the acquired data and subsequent analysis. For each frequency increment the process is repeated.

3.5.3 Pseudo random

It is a stationary ergodic signal, with a spectrum containing only whole multiples of the frequency increment present in its Fourier transform. The amplitude spectrum is generally very flat while the phase spectrum is random. The generation of a signal of this type requires the use of an analog digital converter.

3.5.4 Periodic random

Similar to the pseudo random signal, the periodic random excitation has a spectrum that contains discrete frequencies consisting of the integer multiples of the frequency resolution used in its FFT. The signal is generated by joining a random number of generators in order to have an amplitude and random phase content. This generates a basic signal of a certain duration, whose repetition in sequence generates the excitation signal of the structure.

3.5.5 Periodic chirp

Periodic chirp[3] is a special case of the pseudo random. It consists of a sinusoidal signal whose frequency is varied during the excitation period. This variation is

[3]The term chirp derives from English and indicates a short, high-pitched sound, like that emitted by a bird; in fact, reproducing the chirp signal in acoustic waves produces a sort of whistle.

repeated in such a way as to obtain a periodic signal.

3.5.6 Pure random

It is a non-periodic random signal with a Gaussian probability distribution. Its spectrum presents all the frequencies contained in a specific band, and being defined in a random way it is essential to use a process of average measurements to estimate the FRF. Due to the low peak-RMS ratio, pure random excitation makes it possible to easily eliminate noise. It also provides a good linear approximation of a non-linear system in that, by making a sufficient number of averages, the non-linear effects of the system excitedly randomly tend to self-compensate. Another positive feature of this type of signal is the relative simplicity of the required equipment: an external noise generator. The main problem of this type of excitation is the leakage because, since the signal is not periodic in the observation time, this error can not be avoided.

3.5.7 Burst random

The signal starts as in the pure random but after a certain excitation time it is truncated to zero in such a way as to allow the structure to complete its oscillations within the acquisition period. The frequency spectrum has a random amplitude and phase and contains energy throughout the frequency band of interest. The excitation period, after which the signal is truncated to zero, depends substantially on the damping of the test structure.

3.5.8 Burst chirp

It is a sinusoidal signal, with variable frequency, which, like the random burst, is truncated to zero in the last part of the excitation period.

3.5.9 Impact

It is a transitory signal, consisting in a pulse of very limited duration with respect to the acquisition time. The shape, and the width of the pulse, mainly control the level of the spectrum, the duration, instead it influences the bandwidth. The maximum frequency in the spectrum is inversely proportional to the pulse duration. The most common impact test is the one defined with an errant hammer. In this test the accelerometer is fixed to a point in the structure and this is excited from time to time in different points in order to reproduce the frequency response matrix of the H_{ij} structure and thus obtain the modal shapes.

3.6 Data acquisition problems

The main problems deriving from the acquisition of data are: *ground loop*, *aliasing*, *windowing* and *leakage*.

3.6.1 Ground loop

When connecting two or more earthed equipment, for example a source and an amplifier, the ground voltage of one could be slightly different from that of the other; this creates a potential difference and therefore a current circulation through the cables that connect the two devices. Ground loops are particular situations that frequently occur when two or more devices share more than one ground connection or ground connection. This frequently happens in audio devices for cars because they have a common mass. Ground loops are one of the most frequent sources of buzzing in audio. Ground Loop is nothing but a buzz that occurs when connecting grounded audio devices. This problem is more frequent in the case of connections with unbalanced cables (the unbalanced cable has only one conductor plus the mass, the balanced cable has two conductors plus the mass), poor quality cables and is created especially when the mass voltage source unit (A) is different from the other final unit (B) creating a potential difference and therefore a current circulation. Furthermore, this problem is highlighted more when an amplifier unit is used. By connecting two devices (A - B) with a cable, these two points are joined together by mass, thus forming a loop. This ring behaves like an antenna that picks up the electromagnetic noises in the surrounding environment and adds them to the signal and then reproduces them together.

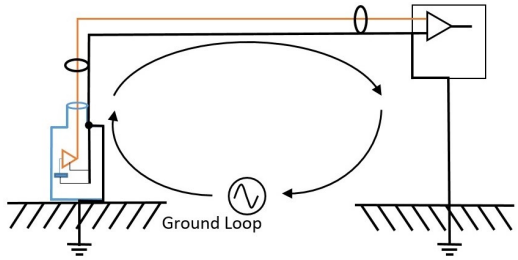

Figure 3.4: Ground loop

3.6.2 Aliasing

The sampling rate determines how often an analog-to-digital conversion (A/D) takes place. A high sampling rate acquires more points in a given time interval and can provide a better representation of the original signal than a low sampling rate. Sampling too slowly can cause an incomplete representation of the analog signal.

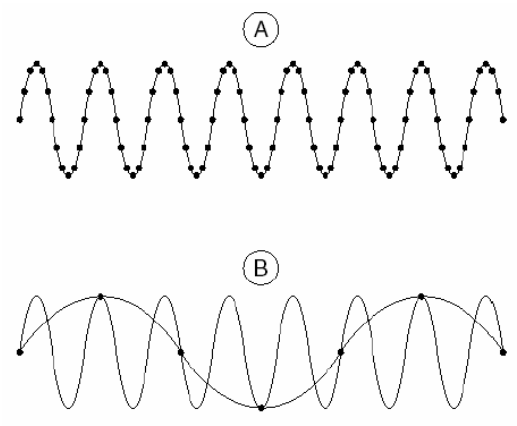

Figure 3.5: Signal sampling: A sampled appropriately, B sub-sampling aliasing

The effect of a subsampling is that the signal appears as if it had a different frequency from the actual one. This phenomenon occurs when the sampling frequency is lower than that of Nyquist, so we try to highlight a given signal using a too sparse sampling. And so it happens that high frequencies in the original signal seen at an insufficient sampling step appear as low frequencies in the reconstructed signal. According to Nyquist's theorem, it is necessary to sample at a frequency greater than twice the maximum component frequency of the signal you are acquiring to avoid aliasing. For a given sampling rate, the maximum frequency that can be accurately represented without aliasing is Nyquist frequency. The Nyquist frequency is half of the sampling rate. Signals with frequency components above the Nyquist frequency will appear replicated between the DC component and the Nyquist frequency. The frequency of the alias (phantom) is the absolute value of the difference between the frequency of the input signal and the integer multiple closest to the sampling frequency. For example, let's consider a sampling rate, f_s, equal to 100 Hz and suppose that the input signal contains the following frequencies: 25 Hz, 70 Hz, 160 Hz and 510 Hz. The frequency of Nyquist, $f_s/2$, is equal to 50 Hz. Then it happens that frequencies below the Nyquist frequency are sampled correctly, while frequencies above the Nyquist frequency are affected by aliasing. So, in this case, only the first frequency, 25 Hz, is returned to the correct frequency, while the other three frequencies, 70-160-510 Hz, will be reported incorrectly: they will have replicas (or alias) at frequencies lower than that of Nyquist. In particular, the alias frequencies will be equal to:

$$alias 70Hz = f_s - 70 = 30Hz$$

$$alias 160Hz = 2 \cdot f_s - 160 = 40Hz$$

$$alias 510Hz = 5 \cdot f_s - 510 = 10Hz$$

To avoid this problem we can resort to the introduction of anti-aliasing filters: which are low-pass filters, which cut the amplitude of the high frequencies so that they do not appear as low frequencies in the interval that interests us.

3.6.3 Windowing

The signal to be transformed with the FFT must complete an integer number of cycles within the window that is considered for analysis or must be completely included within it and therefore have a null value at the beginning and at the end. In practice, many signals do not respect these hypotheses of periodicity. In fact, a signal generated by a random excitation will very rarely present periodic character and the FFT will generate a frequency spectrum with "spots".

For this reason it is necessary to introduce sampling windows, that is, to multiply the signal in the time domain by suitable shape functions capable of overcoming these drawbacks. Sampling windows are chosen based on the type of results to be obtained:

- Rectangular or uniform window: allows to obtain a good frequency resolution;
- Hanning window: minimizes the effect of windowing when analyzing broadband signals, such as random signals;
- Flap-Top window: indicated for the determination of vibration amplitudes;
- Exponential window: it is used for structures with small damping in which the answer has not yet fallen to zero at the end of the acquisition window.

3.6.4 Leakage

Fourier analysis is formally applied to signals of infinitely extended duration and therefore also the sequence of the samples representing the signal in discrete form will have to be theoretically of infinite length. In practice, however, in a sampling process the sample sequence will necessarily have a beginning and an end, and therefore the number of samples available will be a finite number. Leakage is another type of signal distortion problem. To avoid the effect of leakage of the signal, a suitable time window must be chosen and therefore an adequate period of observation of the signal such as to make the duration seem infinitely extended.

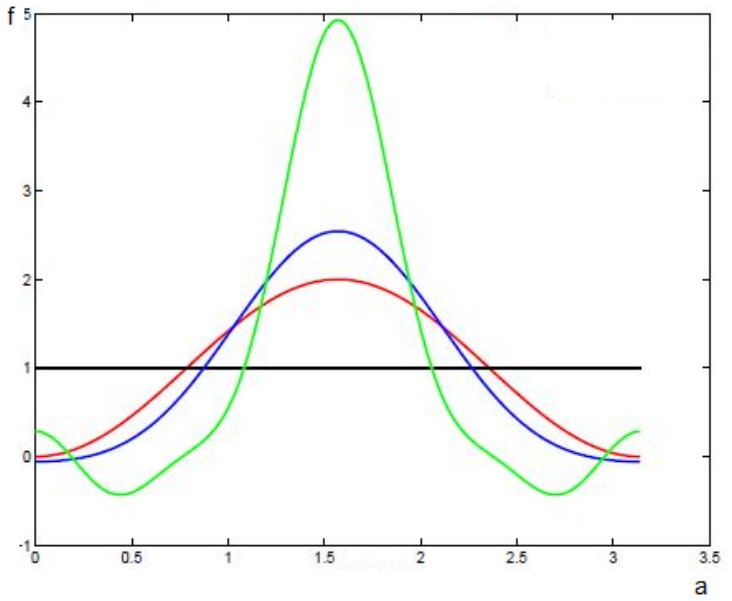

Figure 3.6: Temporal windows: Hanning, Rectangular, Kaiser-Bessel, Flat Top

Chapter 4

Case study: Bridges

4.1 Introduction

As part of this research activity and of the STRIT[1] project, together with the SmartLab team of the University of Calabria, we have carried out tests on some road infrastructures in the province of Cosenza.

The tests consisted in the survey of the structure with laser scanners for subsequent modeling of the same works to the finite elements [30, 31, 32, 33, 34] and installation of the accelerometric network to identify, in situ, the vibrating modes (which will subsequently be indicated with the experimental wording) of the road infrastructure. For the dynamic characterization of the bridges an accelerometric network of 8 wired elements was used and the good affinity of the results obtained in terms of both experimental and theoretical frequencies was ascertained.

For the dynamic characterization of Fiume di Mare Bridge and Caprovini Bridge, it is used, also an experimental tromograph [35].

4.2 Fiume Trionto Bridge

The object of study is represented by the bridge crossing over the long throat of Trionto river, which from the mountains of Sila, in province of Cosenza, flows toward the east until it flows into the Mar Ionian after a distance of about 40 km. It is located in the municipality of Longobucco, along the road that connects the Ortiano fraction of the same municipality to the SS 177, fig. 4.1. Its arched structure is completely made of reinforced concrete, covers a span of about 90 meters and reaches a maximum height, in the central part, about 20 m. The project, designed by the engineering firm of A. Martinelli, Rome, dates back to

[1]Strumenti e Tecnologie per la gestione del Rischio delle Infrastrutture di Trasporto, is a research project presented as part of the 2007-2013 National Operational Program for Research and Competitiveness Convergence Regions - Area: Environment and Ecology, Transport and Logistics.

1968, while the work was entrusted to Luigi Naccarato, and carrying out the work to the Company Ugo Coia, Trebisacce.

Figure 4.1: Fiume Trionto Bridge: view from downstream towards upstream.

From a geometric point of view the work can be divided into 4 parts, looking from upstream to downstream: a central part, at the arch, of 55.80 m, and three side parts, one of which is 10 m in the part of right and two 12 m each on the left side, fig. 4.2.

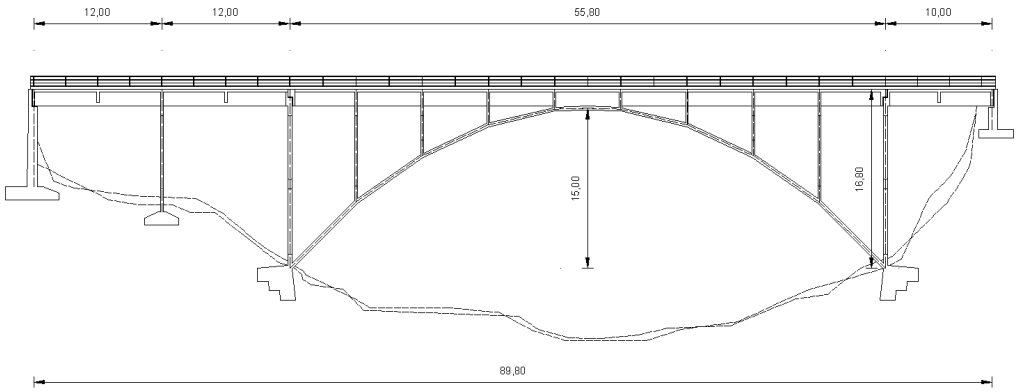

Figure 4.2: Fiume Trionto Bridge: longitudinal section

The supporting structure is therefore made up of two shoulders and 14 partitions on which the four main girders placed at a distance of 1.90 m are set, fig. 4.3.

The slab that carries the roadway is built on these trusses; the latter is also composed of lateral overhangs of 0.80 m at which a pavement of 0.20 m height was created, figg. 4.4, 4.5.

There are only two discontinuity joints in the road pavement located at the partitions located at the ends of the central arch. The main beams are also connected by crossbars, placed with a typical pitch of about 6 m, in order to increase the torsional stiffness of the deck.

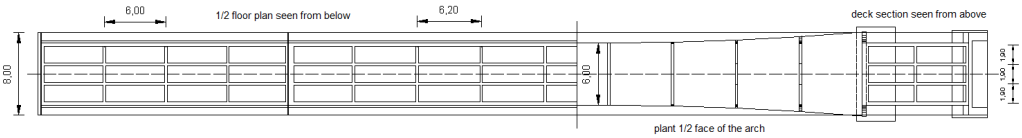

Figure 4.3: Fiume Trionto Bridge: plant

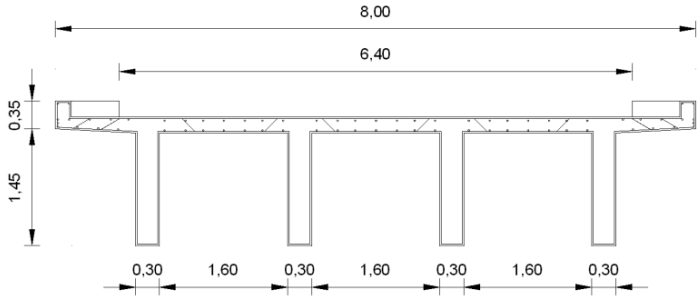

Figure 4.4: Fiume Trionto Bridge: cross section

Figure 4.5: Fiume Trionto Bridge: bottom view

The study of dynamic behavior was carried out by using finite element modeling, fig. 4.6. The FEM modeling was carried out with the aim of establishing a mechanical model capable of describing with a sufficient degree of accuracy the dynamic behavior of the bridge, or to determine the natural frequencies and the corresponding vibration modes. They have been used finite type of shell elements that require the definition of the thickness and the material. In particular, the

Mode	f_{Theo} [Hz]
1	2.67
2	3.48
3	5.04
4	6.15
5	7.99
6	9.18
7	9.66
8	10.07

Table 4.1: Theoretical frequencies by modal analysis

modeling was performed with the calculation code developed within the project and validated by comparison with two other commercial solvers available during the research project at the Unical-SMARTLab: MIDAS GEN and ABAQUS, FEM codes oriented structural analysis. For the geometric characterization we have been used to project carpentries available in CAD format digitized and converted into suitable mesh size to be submitted to the solver.

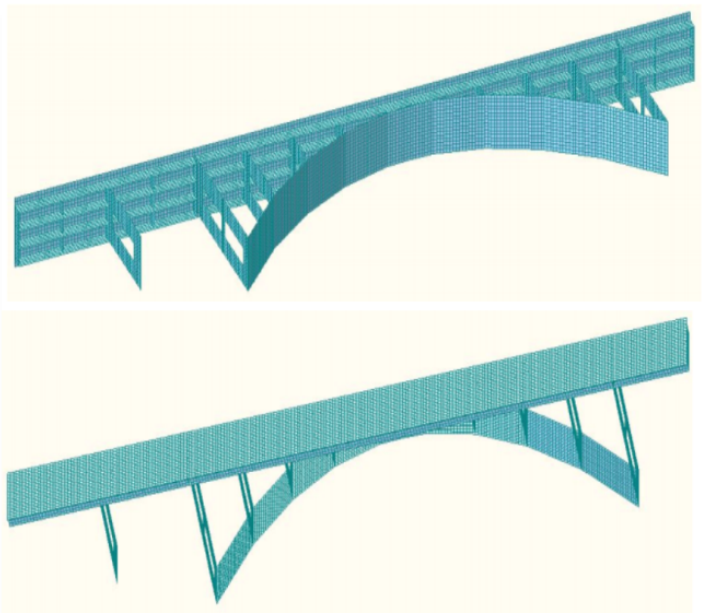

Figure 4.6: Fiume Trionto Bridge: finite element modeling

The first 8 modal forms are shown below, figg. 4.7, 4.8.

The evaluation of the resistance and structural performance in case of exceptional actions to strategic structures should be carried out using advanced

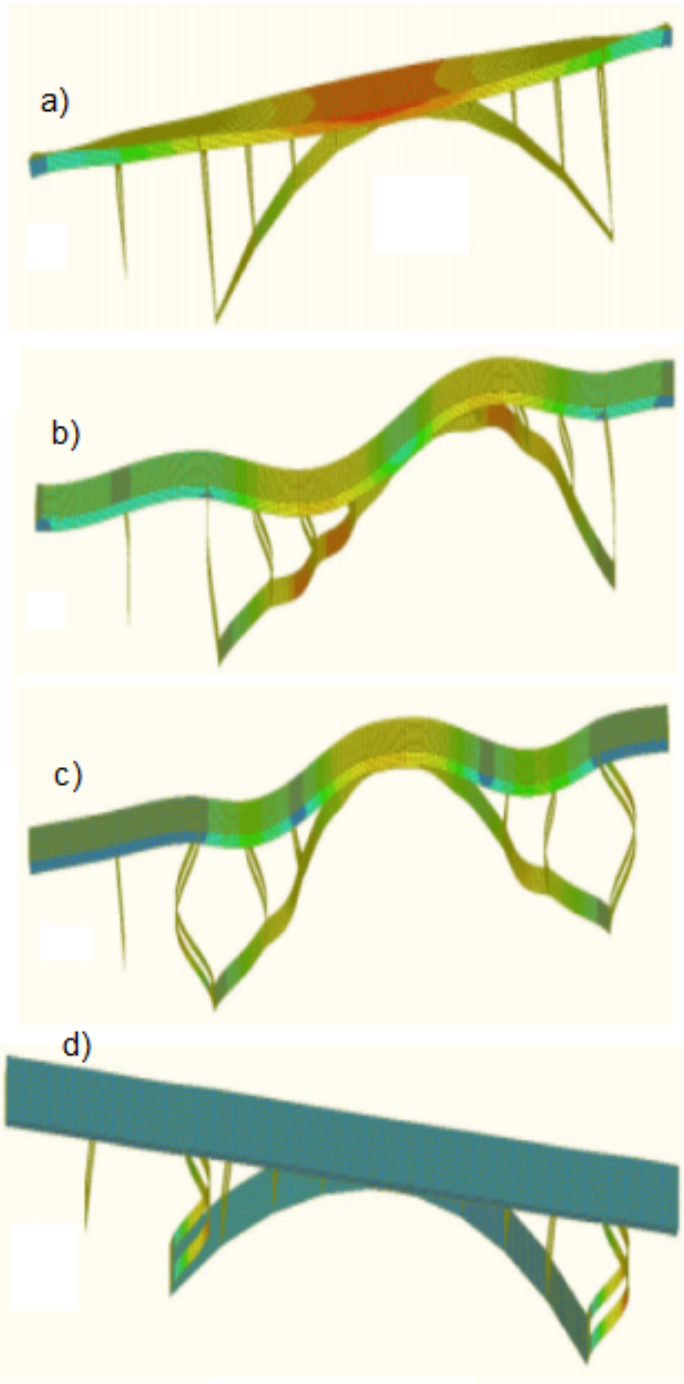

Figure 4.7: Fiume Trionto Bridge modal shapes: a) 1st mode, b) 2nd mode, c) 3rd mode, d) 4th mode

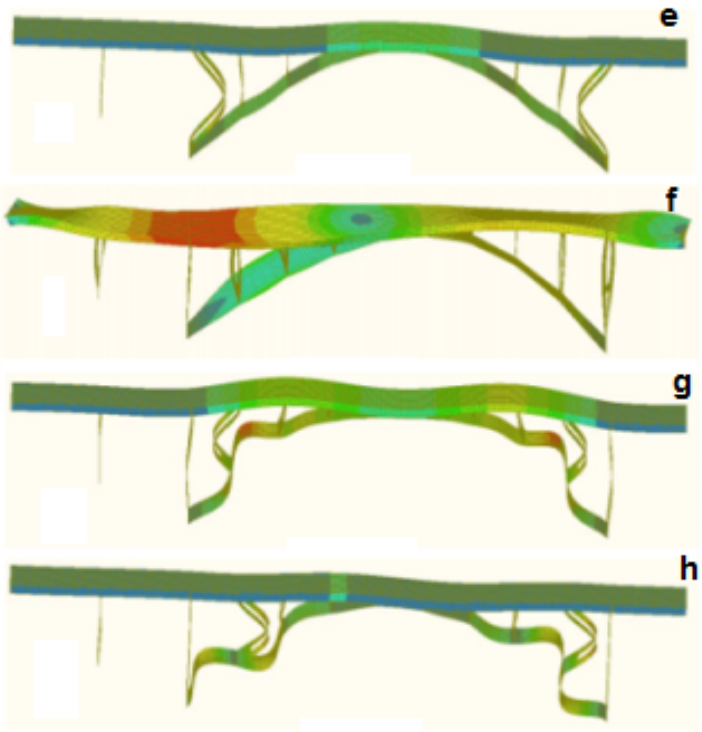

Figure 4.8: Fiume Trionto Bridge modal shapes: e) 5th mode, f) 6th mode, g) 7th mode, h) 8th mode

forecasting and modeling techniques; in this case it would require an accurate description of both the FEM model of the seismic who submit. For this reason, the characteristics of the material, of the constraint conditions and other aspects of modeling have been optimized by means of a fitting procedure of the parameters (Model Updating) which has allowed us to obtain an accurate linear model. The test apparatus consists of acceleration transducers, from the signal conditioners, from the data acquisition system and the power system. The eight acceleration transducers used, fig. 4.9, are of the piezoelectric type in stainless steel with sensitivity equal to 10 V/g.

Before proceeding, were prepared the tools, namely, it is checked for proper operation of all the accelerometers with relative calibration coefficient for the transformation of the electrical signal into acceleration. We have numbered in consecutive order all the cables and amplifiers in order to minimize the possibility of error in the connections.

The transducers were fixed on the structure, after application of steel cubes simply resting on the road surface of the bridge, and they were then connected to the signal conditioner, constituted by a unit which supplies the power and the amplification for the transducers and to the acquisition system by means of

Figure 4.9: Acceleration transducers: KS48C model

shielded coaxial cables of the required length to cover the stretch of monitored bridge, figg. 4.10, 4.11, 4.12. The cables were positioned in such a way as to keep them tense along the established route.

Figure 4.10: No.2 monoaxial accelerometers combined on the basis for biaxial readings

In particular, tests were carried out in ambient vibration under the action of the wind, in a forced vibration tests with traveling load, impulsive crash tests of train load and impulsive load tests of the vehicle caused by the impact of bumps made with wooden planks. In order to record the answer in as many points as possible to achieve a better identification of the dynamic response, given the size of the article, were necessary two distinct configurations for the placement of the instruments, hereinafter referred to as A and B, figg. 4.13, 4.14.

In the test setup A were placed no.6 measuring stations with no.8 trasducers: 4 accelerometers in the vertical direction in the 2-4-5-6 points, and 2 accelerome-

Figure 4.11: Acceleration trasducer uniaxial with base

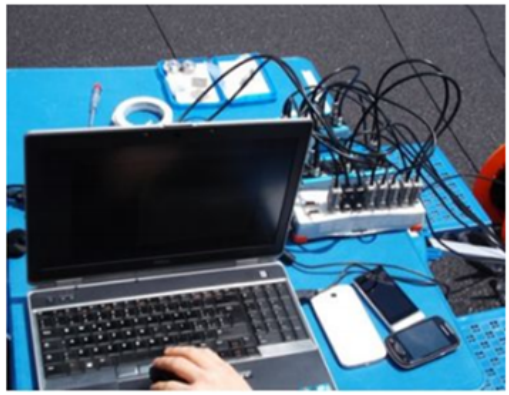

Figure 4.12: Data acquisition kit

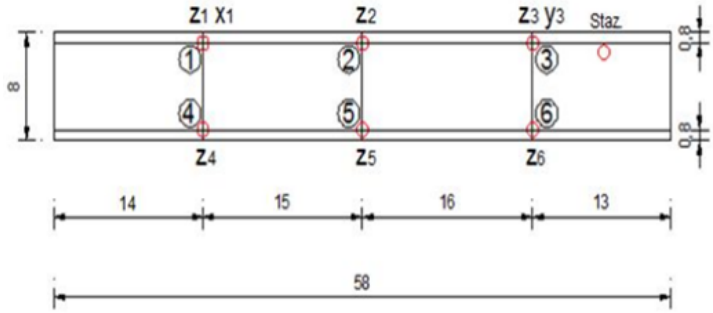

Figure 4.13: A configuration of accelerometer network

ters in the vertical directions and 2 accelerometers in the longitudinal directions (for biaxial readings) in the points 1-3, for a total of no.8 accelerometers. This configuration has allowed the measurement of the horizontal and vertical degrees

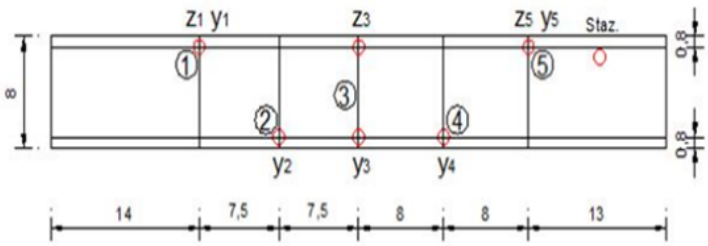

Figure 4.14: B configuration of accelerometer network

of freedom as well as the determination of any movements in the transverse direction.

In test B configuration were placed no.6 measuring stations with no.8 trasducers: 2 bi-axial in the points 1-5 (4 accelerometers), 2 accelerometers mono-axial in points 2-4 (opposite one another) and 2 accelerometers in point 3 (y-axis and z-axis), for a total of no.8 accelerometers. This configuration has allowed the measurement of degrees of freedom but predominantly vertical longitudinal horizontal ones.

The tests performed in both configurations thus include, white noise (wind) and vibration induced by traffic, performed along the bridge from both the right and left with the following modes:

1. Slow transit;
2. Fast transit;
3. Slow transit & slow transit with braking (impulsive stop);
4. Fast transit & fast transit with braking (impulsive stop);
5. Slow transit & zig-zag transit;
6. Fast transit & zig-zag transit;
7. Slow transit & slow transit on bumps;
8. Fast transit & slow transit on bumps.

The collected accelerometric recordings were processed using the Fourier transform thus obtaining the cross-spectra related to tests carried out, after having filtered the data with a low pass filter with 10 Hz cut-off frequency, which is nothing more than an electronic circuit which allows only the passage of frequencies below a given threshold (in this case 10Hz) said cut-off frequency.

In particular, each cross-spectrum has been calculated by considering all possible pairs of accelerometers, for both configurations, and for each test. They were

Test	Mode 1	Mode 2	Mode 3	Mode 4	Mode 5	Mode 6	Mode 7
1	2,8915	3,7346	5,0201	6,2447	7,8545	-	9,6474
2	2,8229	3,6926	4,9591	-	7,8278	8,4686	9,5215
3	2,8381	3,6926	4,9438	-	7,8735	8,4839	9,5215
4	2,8534	3,6469	5,0507	-	7,843	8,3771	9,5825
5	2,8687	3,7231	5,0964	-	7,8735	-	9,613
6	2,8381	3,7079	5,1422	-	7,843	-	9,2926
7	2,8381	3,5858	5,0354	-	7,843	-	9,3384
8	2,8076	3,6926	5,0201	-	7,8278	-	9,5978
9	2,8381	3,5248	5,0201	-	7,8278	-	9,3994
mean	2,844055556	3,666766667	5,031988889	6,2447	7,845988889	8,4432	9,501566667
variance	0,000540454	0,004285962	0,003352348	-	0,000289497	0,00222362	0,01455766

Table 4.2: Accelerometers in A-configuration: experimental frequencies by tests

Test	Mode 8	Mode 9	Mode 10	Mode 11	Mode 12	Mode 13	Mode 14
1	-	-	-	15,5487	16,4413	17,5018	19,8898
2	10,2692	-	13,6566	-	16,51	-	20,6146
3	-	-	13,6108	15,625	16,571	-	20,6604
4	-	-	13,6719	15,4724	16,46	-	20,7367
5	10,2844	-	-	15,5945	16,6626	-	20,5994
6	-	-	13,6108	-	16,6321	-	19,8364
7	10,2844	-	13,5345	-	16,5405	-	20,6909
8	10,8337	11,6119	13,5193	15,2893	-	-	20,6909
9	10,1929	12,207	13,5651	-	16,4948	-	19,2871
mean	10,37292	11,90945	13,59557143	15,50598	16,5390375	17,5018	20,33402222
variance	0,054230966	0,088536003	0,002927131	0,014380878	0,005443967	-	0,245950222

Table 4.3: Accelerometers in A-configuration: experimental frequencies by tests

Test	Mode 1	Mode 2	Mode 3	Mode 4	Mode 5
1	2,8381	3,6392	5,127	7,8888	-
2	2,7771	3,6316	5,0659	7,843	-
3	2,8229	3,7384	-	7,8278	-
4	2,8076	3,5706	5,0354	7,9041	8,4534
5	2,8076	3,54	5,188	7,843	8,4534
6	2,8381	3,7231	5,0354	7,782	-
7	2,7618	3,5858	5,0507	7,8888	8,4991
8	-	-	-	-	-
9	-	-	-	-	-
mean	2,8076	3,632671429	5,083733333	7,853928571	8,468633333
variance	0,000731783	0,004862488	0,003137499	0,001577785	0,000464109

Table 4.4: Accelerometers in B-configuration: experimental frequencies by tests

Test	Mode 6	Mode 7	Mode 8	Mode 9	Mode 10	Mode 11
1	-	-	12,5122	15,5792	16,6092	-
2	9,491	10,1624	13,4583	-	16,449	20,6604
3	9,2316	10,1471	13,504	-	16,3269	20,7062
4	9,3384	9,6436	-	-	16,51	20,8435
5	-	9,552	13,6108	-	16,4185	20,7214
6	-	-	13,6719	-	16,6016	20,8435
7	9,2468	9,5978	-	-	16,53	20,78
8	-	-	-	-	-	-
9	-	-	-	-	-	-
mean	9,32695	9,82058	13,35144	15,5792	16,49217143	20,75916667
variance	0,010639787	0,075308858	0,181795922	-	0,008860722	0,004774149

Table 4.5: Accelerometers in B-configuration: experimental frequencies by tests

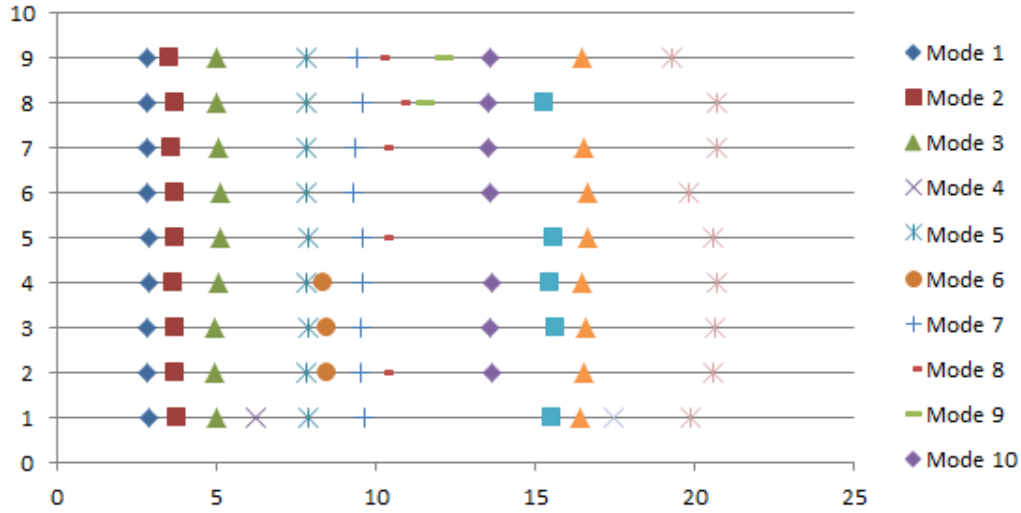

Figure 4.15: A configuration: experimental frequencies by tests [frequency - no. test]

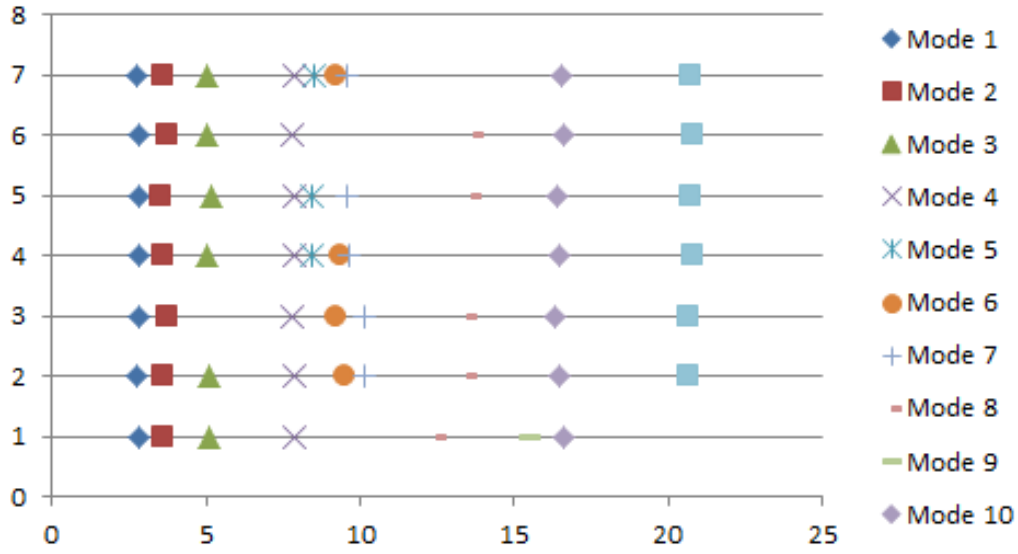

Figure 4.16: B configuration: experimental frequencies by tests [frequency - no. test]

thus obtained 128 vertical cross-spectra for the configuration A and 18 vertical cross-spectra and 60 for the horizontal configuration B. The calculations were carried out with a code written in Matlab that, on the basis of dynamic identification FDD technique, provides an estimate of the frequencies and mode shapes. For all

cross-spectra they were identified visually by the peaks in a progressive manner in a 1 to 10 Hz frequency range. The peaks sequences thus obtained were compared with each other and, for each level of frequency, the value has been selected that was repeated several times.

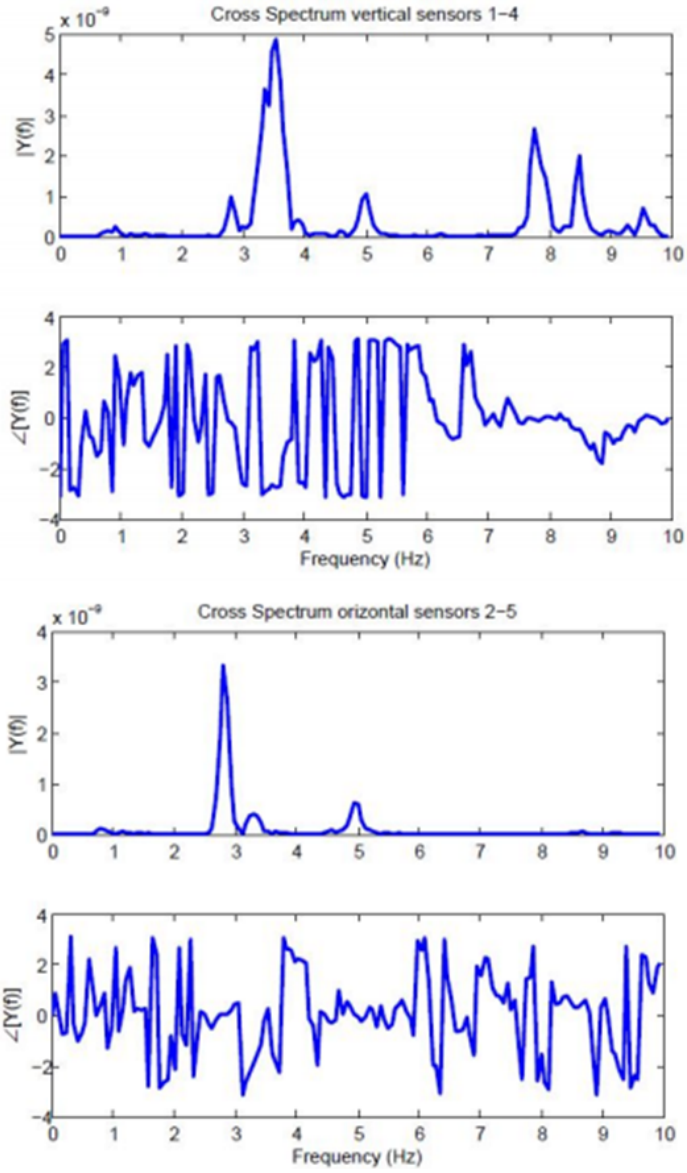

Figure 4.17: Cross-Spectra: vertical sensors and horizontal sensors

The frequencies and the experimental modal shapes were compared with those provided by the analytical model (FEM).

Mode	f_{Theo} [Hz]	$f_{Exp,A}$ [Hz]	$f_{Exp,B}$ [Hz]	Δf_A	Δf_B
1	2.67	2,844055556	2,8076	0.174	0.1376
2	3.48	3,666766667	3,632671429	0.186	0.153
3	5.04	5,031988889	5,083733333	0.008	0.044
4	6.15	6,2447	7,853928571	0.0947	0.136
5	7.99	7,845988889	8,468633333	0.144	0.478
6	9.18	8,4432	9,32695	0.074	0.14
7	9.66	9,501566667	9,82058	0.159	0.16

Table 4.6: Deviation between theoretical and experimental frequencies.

Preliminarily was made a verification considering only the frequency values and, once checked the correlation between these, the modal shapes were compared.

Already visually, by the modal shapes it is immediate univocally associating to each mode of vibration experimental a corresponding analytical mode.

The limited number of available accelerometers, made it possible to compare only few modes of vibration as the measuring points were placed only on the central span of the bridge. The result shows that the experimental frequencies calculated with the Matlab code ("data-driven") are almost coincident with those calculated by the FEM solver.

In fact, tab. 4.6, there has been an deviation almost null for all modes and for both configurations. Thus showing a good correlation between the two models: theoretical and experimental.

4.3 Fiume di Mare Bridge

The Fiume di Mare bridge, fig. 4.18, is located at Km 5 + 900 of the Provincial Road No.39 in the municipality of Fiumefreddo Brutio. It is a new construction of a single span consisting of beams in prestressed concrete burdening on shoulders with poles in concrete. The bridge is inserted in an old road layout of which some parts of the work remain, such as some spurs and a retaining wall both in stone.

For the geometric characterization the CAD files, figg. 4.19 4.20, available were used, processed and converted into a format suitable for being submitted to the solver.

The initial model was then transformed into a finite element model (FEM), fig. 4.21, and analyzed using the Abaqus structural analysis software, which imports the vectorized graphic model into a finite element mesh through solid procedures: solid 4-node tetrahedral elements with only 3 degrees of freedom per node.

From the modal analysis we have deduced the first three modes of vibrating the theoretical of the road infrastructure, are reported in fig. 4.22: modal shape

Figure 4.18: Fiume di Mare Bridge: aerial photo

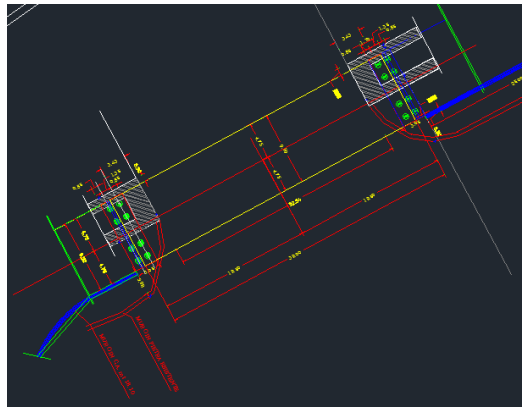

Figure 4.19: Fiume di Mare Bridge: plant scheme with supports on spurs and retaining walls

no.1 of the torsion-type with a frequency equal to 3.71 Hz and modal shapes no.2 and no.3 of the bending-type with frequencies equal to, respectively, 4.14 Hz and 11.17 Hz.

In order to record the answer in as many points as possible to achieve a better identification of the dynamic response, no 3 different configurations, fig. 4.23, for the placement of the instruments, hereafter referred to as A, B and C. On the bridge were carried out environmental vibration tests under the action of wind, forced vibration tests with traveling load, impulsive crash tests of the traveling load and impulsive load tests caused by the impact of the vehicle on bumps made with wooden planks.

In the test configuration A no.5 measurement stations where all the no.5 accelerometers are in the horizontal direction (transverse to the bridge) in the 0-1-2-3-4 points all on the same side of the bridge. This configuration allowed the

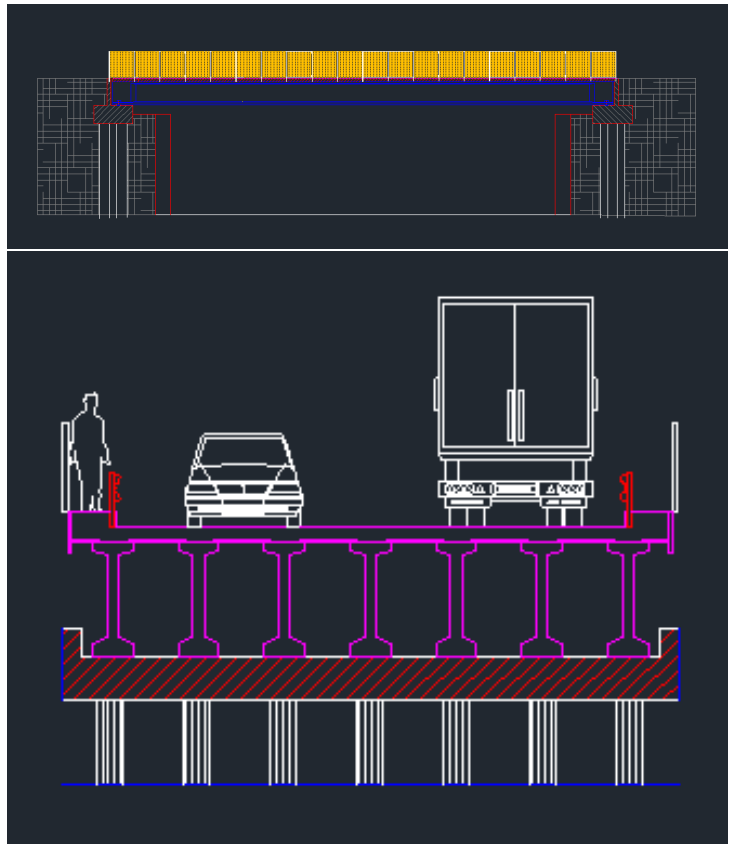

Figure 4.20: Fiume di Mare Bridge: longitudinal section and cross section

measurement mainly of the degree of horizontal (transversal) freedom.

The test configuration B is similar to A only that the accelerometers were all positioned in the vertical direction with the intent of measuring the degree of vertical freedom.

In the test configuration C, always has been placed no.5 measurement stations where all the no.5 accelerometers are in the vertical direction: no.3 in points 0-1-2 and no.2 in points 3-4 in a position opposite to the first ones. This configuration made it possible to mainly investigate the torsional vibrating mode.

The tests carried out in both configurations include the white noise, in particular the wind, and the traffic-induced vibrations, performed along the bridge both from the right and from the left in the following ways:

1. Slow transit;
2. Fast transit;
3. Slow transit & slow transit with braking (impulsive stop);

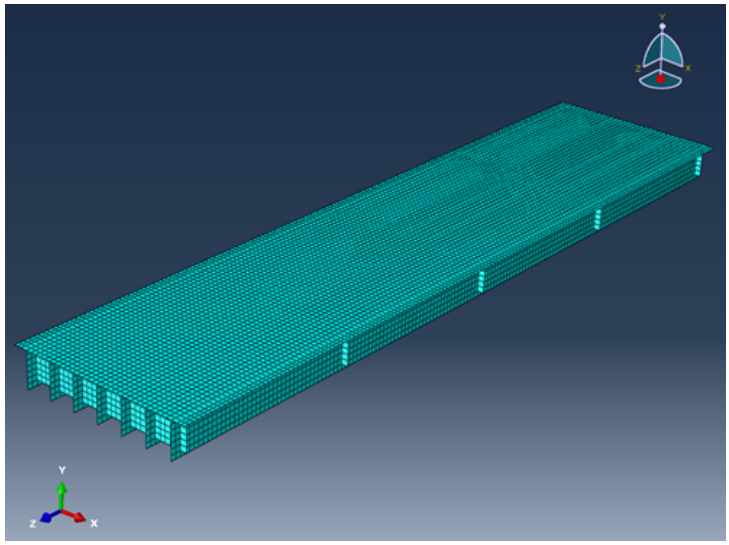

Figure 4.21: Fiume di Mare Bridge: finite element model

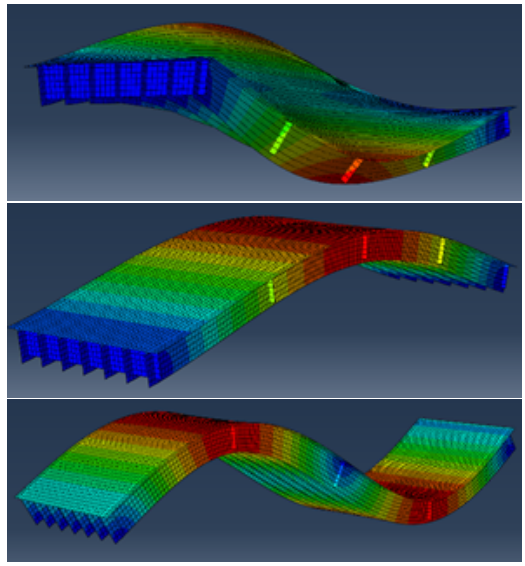

Figure 4.22: Fiume di Mare Bridge: the first three modes of vibrating

4. Fast transit & fast transit with braking (impulsive stop);
5. Slow transit & zig-zag transit;
6. Fast transit & zig-zag transit;
7. Slow transit & slow transit on bumps;

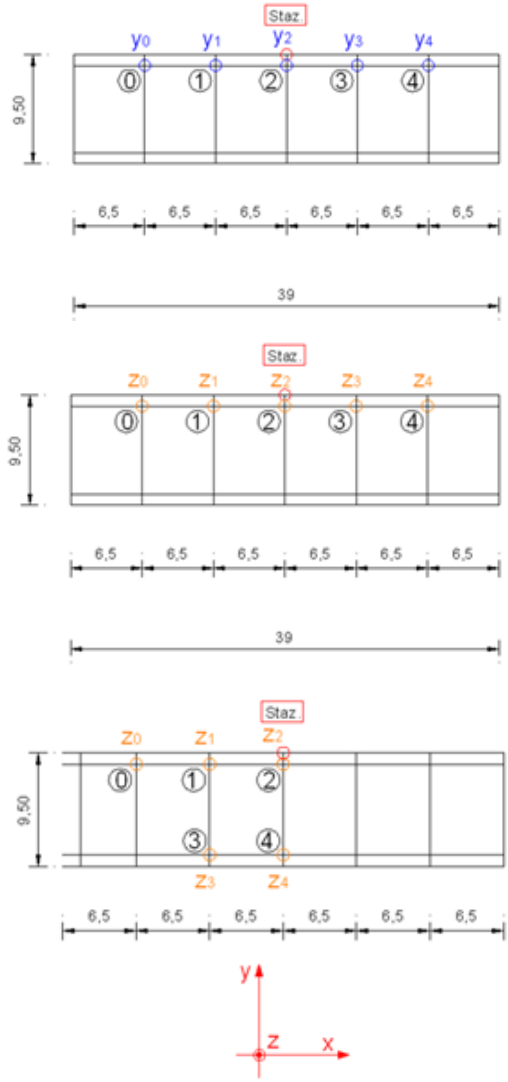

Figure 4.23: Fiume di Mare Bridge: A-configuration, B-configuration, C-configuration

8. Fast transit & slow transit on bumps.

The collected accelerometric records were processed using the Fourier transform (FFT) thus obtaining the cross-spectra relative to the tests carried out, after having filtered the data with a low pass filter with adequate cutting frequency, for this purpose the Matlab Data-driven code was used.

The tests that activated the first modes of vibration are shown below, tab. 4.7, with their respective frequencies, the mean, the standard deviation and the vari-

Test	Mode 1	Standard Deviation
1 white noise	3,5553	0,01252161
2 white noise	-	-
3 white noise	3,6621	$2{,}601 \cdot 10^{-05}$
4 slow transit	3,8147	0,02175625
5 zig-zag	3,6621	$2{,}601 \cdot 10^{-05}$
6 zig-zag	3,6469	0,00041209
7 zig-zag	3,6621	$2{,}601 \cdot 10^{-05}$
mean	3,6672	
variance		0,005794663

Table 4.7: A-configuration: experimental frequencies.

Test	Mode 1	Mode 2	Standard Deviation 1	Standard Deviation 2
1 three cars in a row	3,632	11,749	0,000227004	0,211753361
2 impulsive stop	3,723	11,322	0,005765871	0,001100028
3 slow transit	3,632	11,337	0,000227004	0,002320028
4 transit on bumps	3,601	-	0,002122138	-
5 transit on bumps	3,708	-	0,003712871	-
6 fast transit	3,632	11,047	0,000227004	
7 zig-zag	3,693	11,322		
8 white noise	3,5706	-		
9 white noise	3,632	10,956	0,000227004	0,110778028
mean	3,647066667	11,28883333		
variance			0,002046982	0,081487861

Table 4.8: B-configuration: experimental frequencies.

ance.

From the analysis of the experimental data we have been able to identify the first three modes of vibrating. In particular, the 1st mode with frequency equal to 3.66 Hz, the 2nd mode with frequency between 4.0 and 4.5 Hz, the 3rd with frequency 11.23 Hz. For the second modal shape it was not possible to find an exact frequency value, evidently the configurations and the modalities of the tests carried out did not univocally activate this way of vibrating.

From the graph showing, fig. 4.24, the experimental frequencies (FFT) that activated the second mode of vibrating of the infrastructure of the Fiumefreddo Brutio roadway, it is noted that the second frequency peak relative to the second modal shape is not well defined and oscillates between the values 4.0 and 4.5 Hz.

During the tests on this infrastructure environmental noise measurements were carried out by means of a further experimental instrumentation carried out within the Smartlab laboratory of Unical. The tromograph is a tri-directional acquisition

Test	Mode 1	Standard Deviation
1 impulsive stop	3,7842	0,01334355
2 transit on bumps	3,693	0,000591184
3 transit on bumps	3,601	0,004581356
4 fast transit	3,632	0,001345842
5 zig-zag	3,662	$4{,}46988 \cdot 10^{-05}$
6 zig-zag	3,6926	0,000591184
7 white noise	3,616	
mean	3,668685714	
variance		0,003981326

Table 4.9: C-configuration: experimental frequencies.

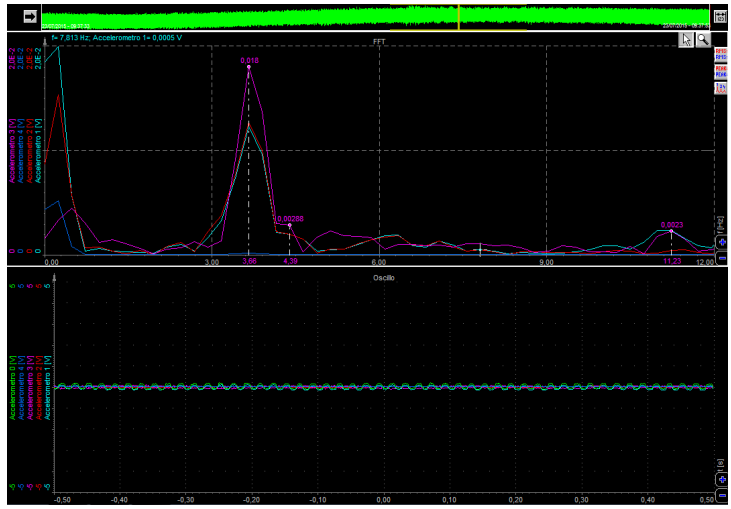

Figure 4.24: Fiume di Mare Bridge: experimental frequencies that activated the 2nd mode of vibrating

system characterized by a set of 3 geophones arranged along the X, Y and Z axes (with the Y-axis going north) of a horizontal plane in order to detect the tremor of the structure being investigated.

Only 3 measurements were made: at the two shoulders of the bridge and on the center line. The evaluation of the bridge vibration proper frequencies were carried out with the use of the following software: Dolfrang version 4.3 and Theremino HAL version 5.2; Geopsy processing software ver. 2.9.1 (geopsypack-2.7.0).

During the acquisitions with the tromograph, the external meteorological conditions showed light breeze coming from Est. Acquisitions took place via the USB port of the Theremino-SmartLab, with acquisition with a single gain. The frequencies of the 3 geophones are around 4.5 Hz with sampling frequency of 333

Modal shape	Theoretical frequency f_{Theo} [Hz]	Experimental frequency f_{Exp} [Hz]	Deviation Δf
1	3.71	3.66	0.05
2	4.14	4.0÷4.5	0.14÷0.36
3	11.17	11.28	0.06

Table 4.10: Deviation between theoretical and experimental frequencies

Hz. For the evaluation of the bridge vibration proper frequencies the duration of each single acquisition was 20 minutes and the total number of recorded data was 400.000 every 0.003 seconds. The processing was carried out with the lengths of the windows from 20 seconds to 50 seconds, 5% overlap, bad sample threshold 99%, anti-triggering signal on raw. During the test run, the wind was absent. The acquisition thus obtained, highlights, good signal spectra can be analyzed.

The oscillation frequency of the bridge, obtained from the H/V ratio, is around 10.5 Hz, fig. 4.25.

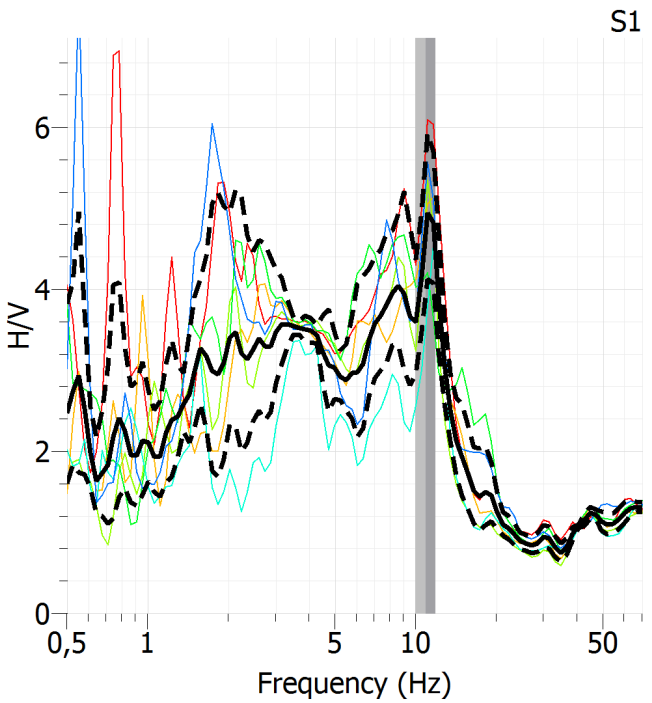

Figure 4.25: H/V ratio: peak frequency to 10.5 Hz

This means that, in case of earthquake, seismic components that will be am-

plified on the total of those generated by the earthquake will be those 9.5÷10.5 Hz which will be amplified by a factor of about 9 times.

The other frequencies are high compared to the terms of those generated by an earthquake and thus are irrelevant in case of earthquake. Pull the displacement spectra allows us to understand the spatial deformation that the structure undergoes at a particular frequency. It is important to emphasize that the overall deformation, ie the one that actually occurs, of the structure will be given by the sum of the various deformation modes, each to its own frequency, to which it is subjected.

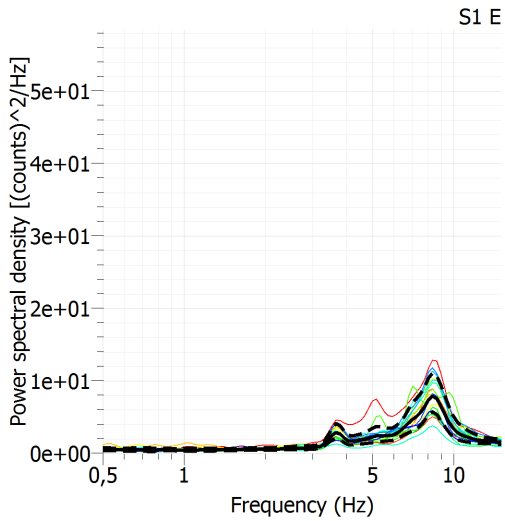

Figure 4.26: H/V ratio: spectrum of the X component, East direction, at the shoulders and along the central axis.

First mode of vibrating is transversal (y-axis) and the second mode of vibrating is vertical (z-axis), both at 4.4 Hz, figg. 4.27, 4.28. The deformed form obtained by the envelope of the spectral maximum shows that the amplitude of such motion increases progressively away from the center line up to a maximum located at about 2/3 of the deck and ends with values close to zero on the shoulder. The vertical components of motion, suffer an abrupt decrease, from external measures to the internal ones. This phenomenon can be justified by a torsional movement of the bridge. From this analysis it showed a clear acknowledgment of the data obtained with the experimental tromograph, with data obtained from the accelerometers.

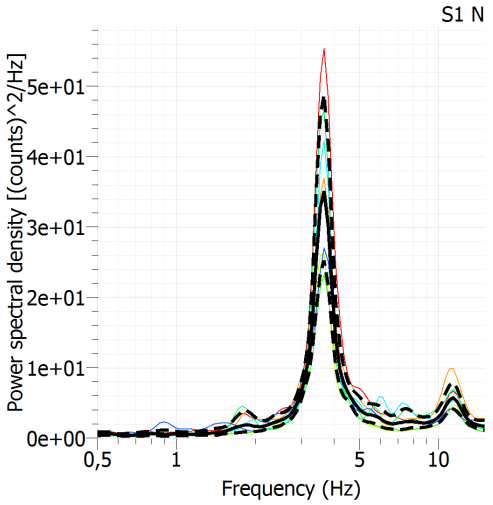

Figure 4.27: H/V ratio: spectrum of the Y component, North direction, at the shoulders and along the central axis.

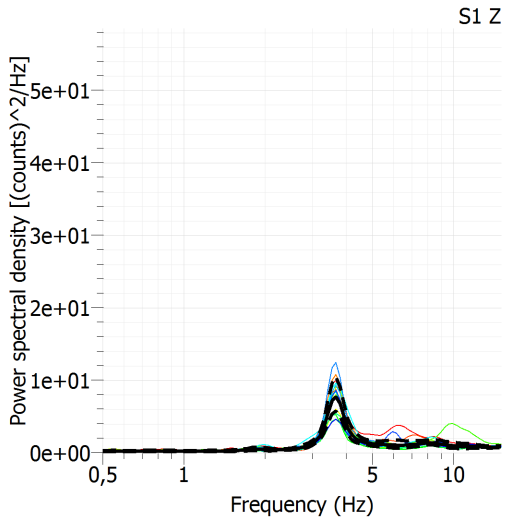

Figure 4.28: H/V ratio: spectrum of the Z component, vertical direction, at the shoulders and along the central axis.

4.4 Caprovini Bridge

The bridge crosses the river Aron in the locality of S. Angelo-Caprovini in the municipality of Cetraro. It is located along the Provincial Road 26, at km 1+900, about 2.5 km as the crow flies from the Tyrrhenian Sea and at an altitude of 130

m above sea level. The bridge, whose construction dates back to the 50s of the last century, has a three-span structure, built in reinforced concrete, symmetrical. The central span rests on a double parabolic structure with connecting beams. The side spans, in addition to being joined to the arched structure, rest on the shoulder in reinforced concrete and in the middle on a crutch in c.a. having a double column. From a geometric point of view the work has a length of 76 m approximately for a width of 7.40 m and a height from the ground of about 25 m. The supporting structure is therefore made up of two main beams placed at a center distance of 4.70 m. On these trusses the insole that houses the roadway is made; the latter also consists of lateral overhangs of 0.95 m at which a pavement of 0.10 m height has been created. The main beams are also connected by transoms, placed with a pitch of about 4 m, in order to increase the torsional stiffness of the deck, figg. 4.29 4.30 4.31.

Figure 4.29: Caprovini Bridge: view of the top road

Figure 4.30: Caprovini Bridge: view from the valley to the mountain

For the geometric characterization we used the laser scanner technology with integrated camera [36], so as to acquire large amounts of data, both geometric

Figure 4.31: Caprovini Bridge: view from below

and photographic, in limited time. A RIEGL VZ 1000 laser scanner with the acquisition characteristic of the return pulse waveform was used [37]. This characteristic allows to discriminate the ground or an artifact from the vegetation that covers it. Data processing was then performed with the RiscanPro and Geomagic softwares. Finally, the on-site surveys and the detailed measurements made it possible to integrate the survey results with a laser scanner and to fine-tune the geometric model in a more precise way, figg. 4.32 4.33 4.34.

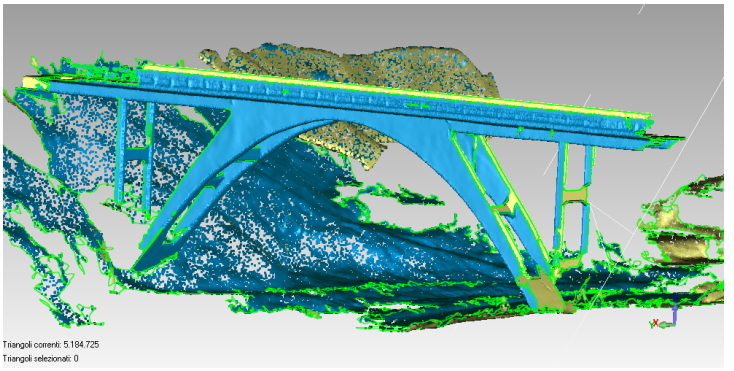

Figure 4.32: Caprovini Bridge: 3D mesh obtained from relief Laser Scanner

The initial model was then transformed into a finite element model, FEM, fig. 4.35, and analyzed using the Abaqus structural analysis software which, through automatic procedures, imports the vectorized graphic model and converts it into a finite element mesh: in this case, tetrahedral elements to 4 solid

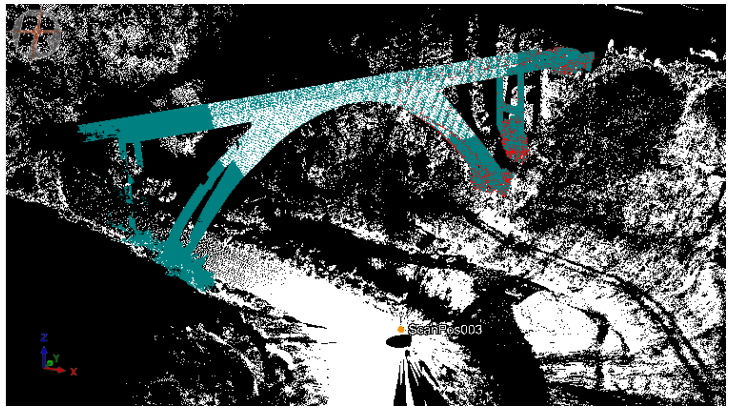

Figure 4.33: Ponte Caprovini: union of the various scans carried out with Laser Scanner

Figure 4.34: Caprovini Bridge: detail of scanning the support of the crutch parabolic reinforced concrete

nodes with only 3 degrees of freedom per node.

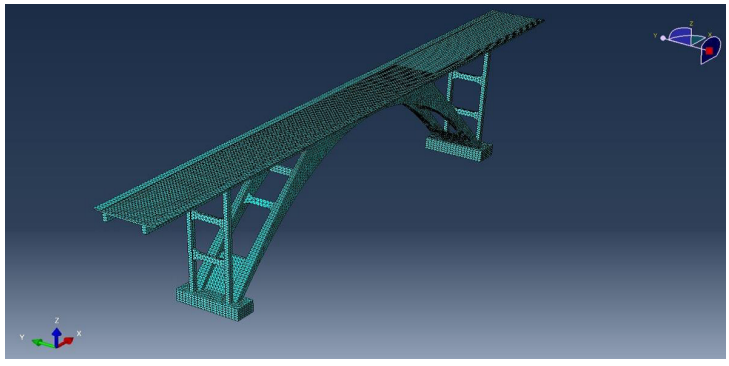

Figure 4.35: Caprovini Bridge: 3D model with finite elements

From the modal analysis of the Caprovini bridge, carried out on the finite element model, the first two ways of vibrating the infrastructure were taken into consideration, figg. 4.36, 4.37, which are characterized by the following so-called theoretical frequencies: mode 1 has frequency equal to 2.4286 Hz, mode 2 has frequency equal to 7.0818 Hz.

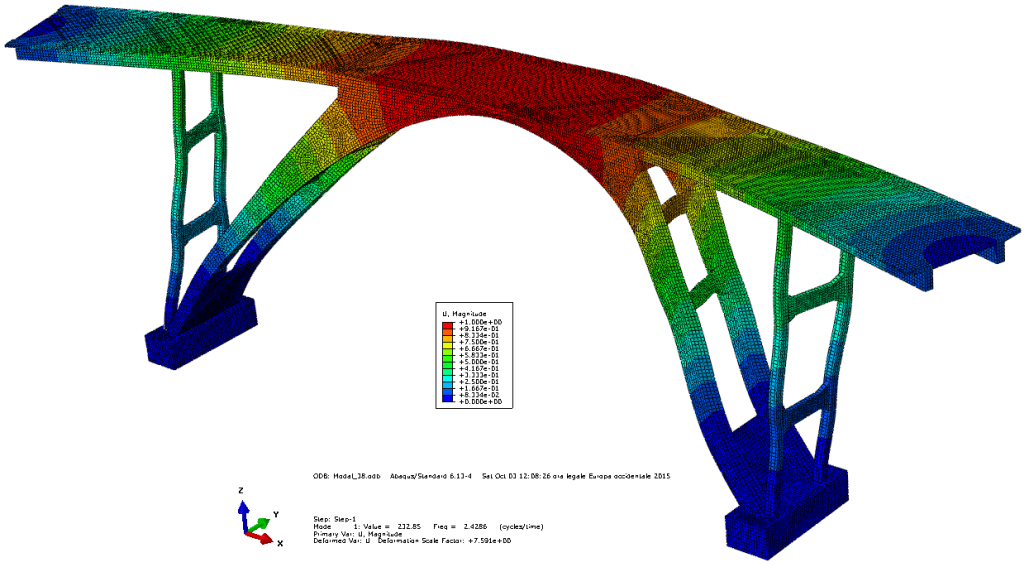

Figure 4.36: Caprovini Bridge: first modal shape of the FEM analysis

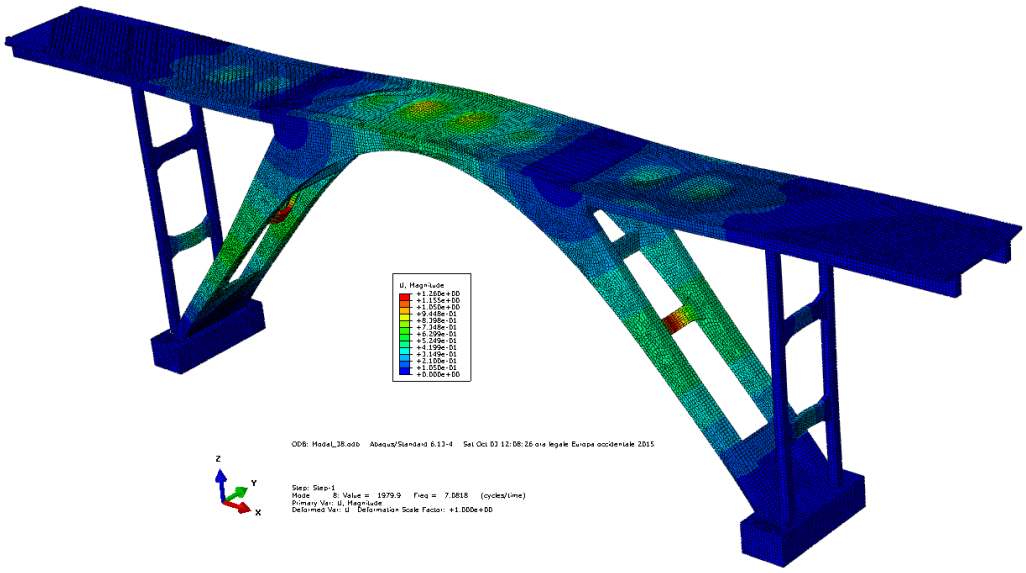

Figure 4.37: Caprovini Bridge: second modal shape of the FEM analysis

We proceeded by positioning on the work of the unidirectional acceleration transducers, suitably arranged, of piezo-electric type with sensitivity equal to 10 V/g. These sensors have made it possible to identify the real vibrations of the structure subjected to environmental noises and unsupervised stresses (FDD, Frequency Domain Decomposition). In particular, environmental vibration tests were carried out under the action of wind, forced vibration tests with traveling load, impulsive crash tests of the traveling load and impulsive load tests caused by the impact of the vehicle on bumps made of wooden planks. In order to record the answer in as many points as possible to achieve a better identification of the dynamic response, given the dimensions of the structure, two distinct configurations were needed for the placement of the instruments, hereafter referred to as A, fig. 4.38, and B, fig. 4.39.

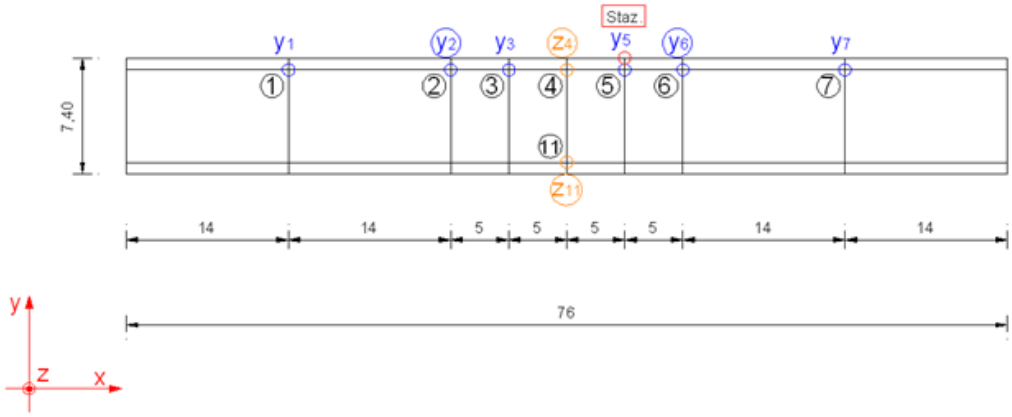

Figure 4.38: Test configuration A of the accelerometric network: so-called horizontal

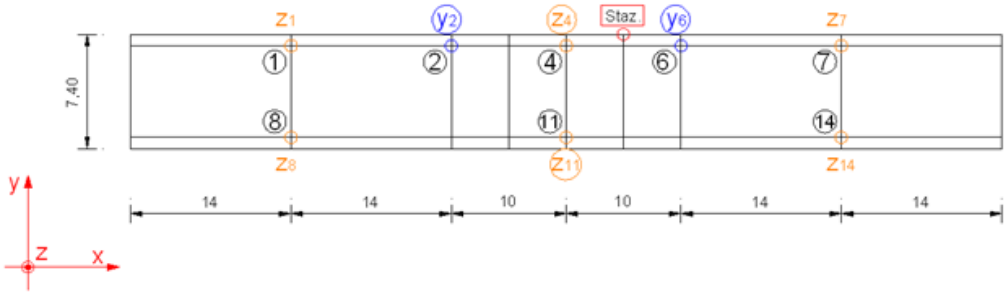

Figure 4.39: Test configuration B of the accelerometric network: so-called vertical

The preparation of the experimental apparatus (accelerometers, cables and control units) and the realization of the tests took place according to the following

steps:

- horizontal road marking;
- location of accelerometers in configuration A, connection of cables to the control unit and realization of the tests;
- location of accelerometers in the configuration B, connection of the cables to the control unit and realization of the tests;
- recovery of equipment.

In the test configuration A, no.8 measurement stations were placed, no.6 accelerometers in the horizontal direction (transverse to the bridge) in points 1-2-3-5-6-7, and no.2 accelerometers in the vertical directions in points 4-11, for a total of no.8 accelerometers. This configuration made it possible to measure the degree of horizontal (transversal) freedom as well as the determination of any movements in the vertical direction.

In the test configuration B, no.8 measurement stations were placed, no.6 accelerometers in the vertical direction at points 1-4-7-8-11-14, and no.2 in the horizontal directions (transverse to the bridge) at points 2-6, for a total of 8 accelerometers. This configuration allowed the measurement mainly of the degree of vertical freedom as well as the determination of any displacements in the horizontal (transversal) direction.

The tests carried out in both configurations include the white noise, in particular the wind, and the traffic-induced vibrations, performed along the bridge both from the right and from the left in the following ways:

1. Slow transit;
2. Fast transit;
3. Slow transit & slow transit with braking (impulsive stop);
4. Fast transit & fast transit with braking (impulsive stop);
5. Slow transit & zig-zag transit;
6. Fast transit & zig-zag transit;
7. Slow transit & slow transit on bumps;
8. Fast transit & slow transit on bumps.

On the basis of the results relative to the tests carried out according to the first configuration (configuration A with the sensors arranged mainly in horizontal direction transversely to the bridge carriage) presented in the following tables,

FREQUENCY [Hz]		
A-configuration	mode 1	mode 2
Test 1	2.41	5.74
Test 2	2.41	5.77
Test 3	2.42	6.22
Test 4	2.44	-
Test 5	2.41	6.16
Test 6	2.32	6.47
Test 7	2.38	6.29
Test 8	2.38	6.23
Test 9	2.32	6.23
Test 10	2.41	5.71
Test 11	2.40	-
MEAN	2.39	6.09
VARIANCE	0.001	0.06

Table 4.11: Experimental frequency in A-configuration

the mode at the frequency $f_{11} = 2.39Hz$ is considered with good reliability, with damping coefficient equal to 2%, while greater uncertainty is present on the second way, identified at the frequency $f_{21} = 6.09Hz$. The same way of vibrating was identified in the tests related to the second configuration (configuration B with the sensors placed predominantly in vertical direction perpendicular to the bridge driveability), at the frequency $f_{22} = 6.18Hz$ with a damping coefficient of just under 1%.

From the tests carried out on the road surface of the Caprovini bridge, it should be noted that with the B configuration the sensors do not lead to significant values of the frequencies and the dimensionless ratio of the damping. Even if it was right to test the positioning of the accelerometric sensors in this second so-called vertical mode.

The mean values of the frequencies determined experimentally on the Caprovini bridge, taken from the accelerometer readings of the sensors placed according to the configuration A, were compared with the so-called theoretical ones, taken from the modal analysis of the finite element model.

During the tests on this infrastructure environmental noise measurements were carried out by means of a further experimental instrumentation carried out within the Smartlab laboratory of Unical. The tromograph is a tri-directional acquisition system characterized by a set of 3 geophones arranged along the X, Y and Z axes (with the Y-axis going north) of a horizontal plane in order to detect the tremor of the structure being investigated.

DAMPING [%]		
A-configuration	mode 1	mode 2
Test 1	0.03	0.01
Test 2	0.02	0.009
Test 3	0.003	0.002
Test 4	0.05	-
Test 5	0.02	0.007
Test 6	0.04	0.02
Test 7	0.02	0.008
Test 8	0.04	0.02
Test 9	0.02	0.008
Test 10	0.01	0.006
Test 11	0.004	-
MEAN	0.02	0.01
VARIANCE	$2.08\text{x}10^{-4}$	$3\text{x}10^{-5}$

Table 4.12: Experimental damping in A-configuration

FREQUENCY [Hz]	
B-configuration	mode 2
Test 1	-
Test 2	-
Test 3	6.25
Test 4	6.23
Test 5	6.23
Test 6	6.03
Test 7	-
Test 8	-
Test 9	-
Test 10	-
Test 11	-
MEAN	6.185
VARIANCE	0.008

Table 4.13: Experimental frequency in B-configuration

DAMPING [%]	
B-configuration	mode 2
Test 1	0.01
Test 2	0.009
Test 3	0.002
Test 4	-
Test 5	0.007
Test 6	0.02
Test 7	0.008
Test 8	0.02
Test 9	0.008
Test 10	0.006
Test 11	-
MEAN	0.01
VARIANCE	$3x10^{-5}$

Table 4.14: Experimental damping in B-configuration

Modal shape	Theoretical frequency f_{Theo} [Hz]	Experimental frequency f_{Exp} [Hz]	Deviation Δf
1	2.4286	2.39	0.04
2	7.0818	6.09	0.99

Table 4.15: Deviation between theoretical (FEM) and experimental (FDD) frequencies

Only 3 measurements were made: at the two shoulders of the bridge and on the center line. The evaluation of the bridge vibration proper frequencies were carried out with the use of the following software: Dolfrang version 4.3 and Theremino HAL version 5.2; Geopsy processing software ver. 2.9.1 (geopsypack-2.7.0).

During the acquisitions with the tromograph, the external meteorological conditions showed wind coming from the North-West. Acquisitions took place via the USB port of the Theremino-SmartLab, with acquisition with a single gain. The frequencies of the 3 geophones are around 4.5 Hz with sampling frequency of 500 Hz. For the evaluation of the bridge vibration proper frequencies the duration of each single acquisition was 20 minutes and the total number of recorded data was 600.000 every 0.002 seconds. The processing was carried out with the lengths of the windows from 20 seconds to 50 seconds, 5% overlap, bad sample threshold 99%, anti-triggering signal on raw. During the execution of the test, the constant presence of wind sent into saturation the signal acquired with evidence of typical frequencies for wind noise. However, without the various filtering, in particular low-pass filter, it was possible to isolate the noise produced by the wind and the acquisition, thus obtained, highlights good signal spectra to be able to analyze. The spectral amplitude of the transverse component at 2.4 Hz is maximum at the center of the bridge and decreases moving towards the shoulders. The first way to cross the bridge to vibrate coincides in frequency with the first vertical mode: both at 2.4 Hz, fig. 4.40.

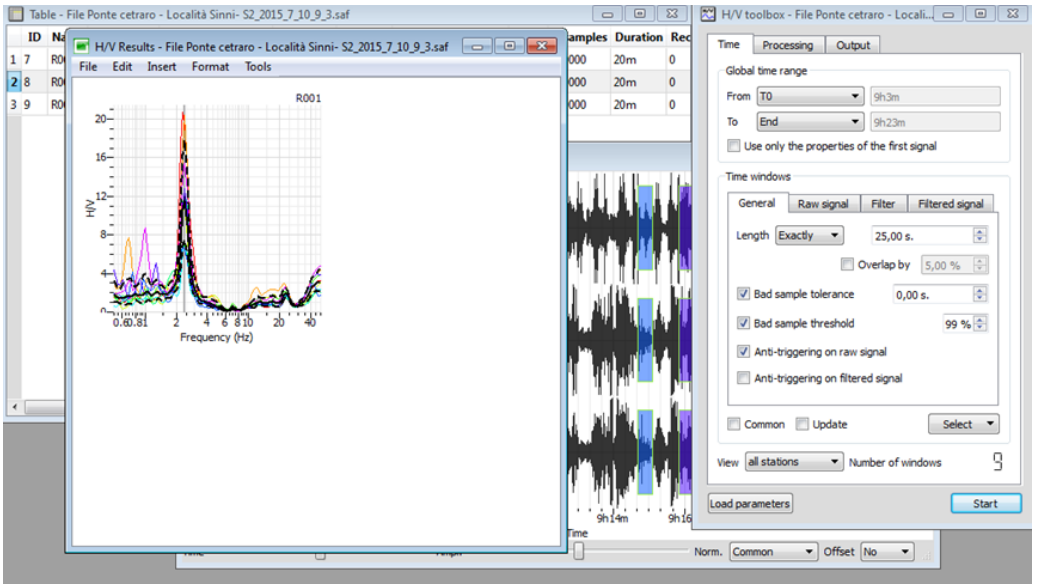

Figure 4.40: H/V ratio: resonance peak frequency to about 2.5 Hz.

The oscillation frequency of the bridge, obtained from the H/V ratios, comparing the data of the 3 measurements, figg. 4.41, 4.42, 4.43, is around 2.4 Hz. This

means that, in case of earthquake, the seismic components that will be amplified the total of those generated by the earthquake will be those 2.5÷3 Hz which will be amplified by a factor of approximately 3.5 times.

The other frequencies were elevated compared to the terms of those generated by an earthquake and therefore irrelevant in case of earthquake. By analyzing the spectra of the components X, Y and Z, ie the axis North, East and vertical, there is a peak at about 7.1 Hz, whereas the other two components have a frequency of about 2.5 Hz.

The results obtained with the H/V ratios are in clear correlation with the data results from the analysis FEM and FFD. This suggests that the experimental instrument has responded well to the acquisition data and confirms experiments with accelerometers.

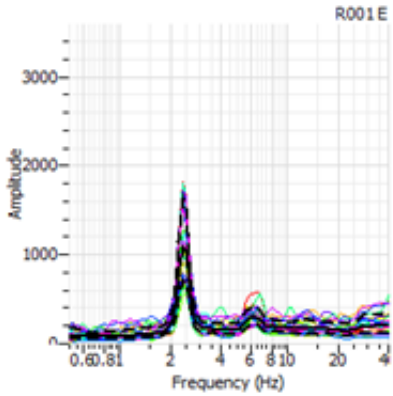

Figure 4.41: H/V ratio: spectrum of the X component, East direction, at the shoulders and along the central axis.

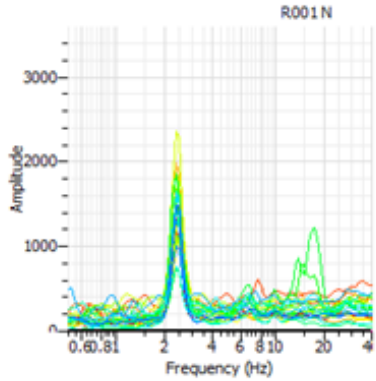

Figure 4.42: H/V ratio: spectrum of the Y component, North direction, at the shoulders and along the central axis.

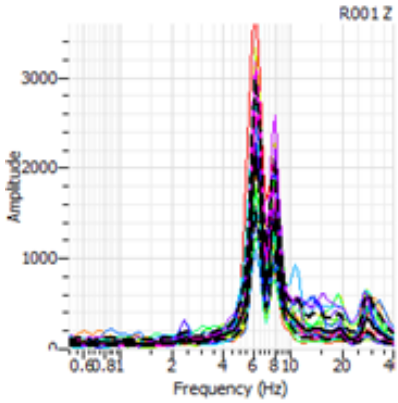

Figure 4.43: H/V ratio: spectrum of the Z component, vertical direction, at the shoulders and along the central axis.

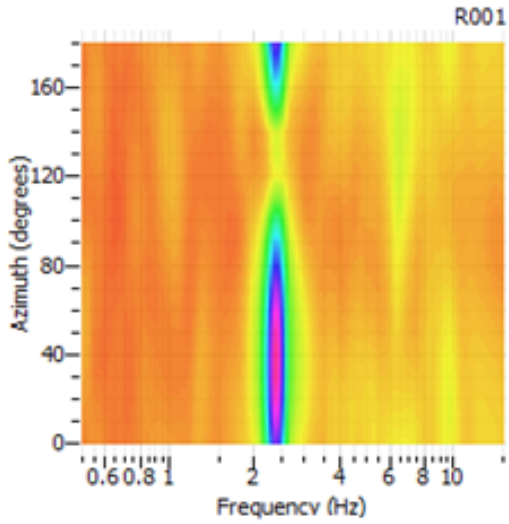

Figure 4.44: Frequency as a function of amplitude: 2.4 Hz resonance peak.

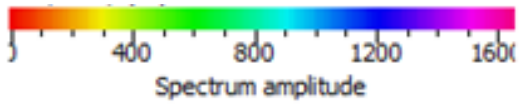

Figure 4.45: Spectrum amplitude.

Chapter 5

Case study: Auditorium of ITI A. Monaco

5.1 Introduction

The building's users not have cognition about its structural health, both for not having technical competences, so disregarding warning signals, and for hidden or slowly damaging processes, with fast and unexpected failure, sometimes effects of external causes. The high seismicity of most Italian territory requires the adoption of appropriate and effective measures to limit the effects of earthquakes on structures. The preservation of national building heritage against seismic risk can benefit by the indepth knowledge of the dynamic behavior of buildings. In this context, Structural Health Monitoring (SHM) has been growing in the last few years as a set of time-scale measures at significant points in the structure, for diagnosis and control of constructions. It is, therefore, a non-destructive *in situ* technique of analysis and structural features that underlines the real-time control and monitoring of a phenomenon by measuring physical-mechanical parameters describing the interaction between the environment and the state variables of the structure under consideration.

A monitoring system usually consists of sensors of various nature to detect environmental magnitudes and the structural response to stresses. The purpose of such a system is not only the assessment of the resistance to a building's earthquake but also the performance control of the structure under operating conditions is of great importance for both the protection against vibration risks and the reinforcement of critical structures or of strategic interest [38, 39, 40]. The typical architecture of the monitoring systems involves the use of peripheral sensors directly connected by cables to a central data acquisition system. However, a large number of sensors involves a large number of measurements and the acquisition system may be overloaded, especially if it has to process the data for damage identification: its algorithms would be particularly burdensome from a computational

point of view.

The research work described in this chapter is intended to make the building not only able to communicate its structural health, activating automatic procedures or, if necessary, asking human intervention, but also capable of preparing for probable future events. The changes of the principal vibration frequencies and vibration modes over time, obtained from the sensors by using seismic noise, when the variations between one and the other overpass the alert threshold, make possible alerts to be used for maintenance or to manage emergency situations.

A prototype was realized on a school building, *Industrial Technical Institute A. Monaco* in Cosenza, demonstrating the validity of the proposal [41].

Figure 5.1: Top view of the school complexes: I.T.I. A. Monaco

5.2 Dynamic identification

In this paragraph are resumed the main aspect of the dynamic identification already described in detail in the previous chapters to facilitate the comprehension of the particular experimental work carried out at the ITI Monaco Auditorium.

Identifying the dynamic response of a structure in terms of its own frequencies, vibrating modes and damping coefficients means carrying out the dynamic identification of the structure in question and it is possible to proceed according to two possible and distinct approaches: *analytical* and *experimental*.

The analytical approach, starting from the knowledge of the geometry of the structure, the boundary conditions and the characteristics of the materials and expressing the distribution of masses, stiffness and damping by matrix representation, from the resolution of a problem to eigenvalues, provides the modal

parameters of the system, i.e. natural frequencies, damping factors and modal shapes.

The experimental approach, starting from the measurement of the dynamic input on the structure and from the acquisition of the structural response in terms of displacement, allows to evaluate the frequency response functions and to estimate, starting from them, the dynamic parameters of the structure.

In the case study of ITI Monaco both approaches were followed: the analytical one in the case of white noise and the experimental one in the case of forced induced artificially by means of vibrodin.

A dynamic system with more degrees of freedom can be considered as a system subject to a series of forces $f(t)$ that produce a motion of the structure, which depends on the characteristics of the forcing and the characteristics of the system. It is, therefore, a system that, prompted by a certain input, forcing $f(t)$, produces an output represented by the motion $x(t)$ of the system itself. The equation for a system with several degrees of freedom assumes the form already seen in the previous chapters (1.1):

$$M\ \ddot{x}\ (t) + C\ \dot{x}\ (t) + Kx(t) = f(t) \tag{5.1}$$

where $\ddot{x}$, $\dot{x}$ and x are the vectors of size n respectively of acceleration, speed and displacement corresponding to the various degrees of freedom; M, C and K are the matrices with dimensions n x n respectively of mass, damping and stiffness and $f(t)$ is the vector of dimension n of the external forces applied. n is the number of degrees of freedom of the system.

In the hypothesis of axially indeformable uprights and without mass and infinitely rigid cross beams at the level of which the mass of the deck is concentrated, the system's response is determined considering the two degrees of freedom coinciding with the horizontal displacements $x_1(t)$ and $x_2(t)$ of the cross baricentres. The equation of motion (1.1) takes the form:

$$M\ \ddot{x}\ a(t) + C\ \dot{x}\ (t) + Kx(t) = 0 \tag{5.2}$$

where $\ddot{x}\ a(t)$ is the vector of absolute accelerations in the presence of seismic motion $u_g(t)$

$$\ddot{x}\ a(t) = \ddot{x}\ (t) + \tau\ \ddot{u}_g\ (t) \tag{5.3}$$

where $\ddot{u}_g\ (t)$ represents the assigned accelerogram, τ is said dragging vector and provides the displacements in the direction of the degrees of freedom of the system for a unit displacement of the ground. Therefore, τ is made up of unit in correspondence with the parameters subjected to seismic acceleration and null values in the other cases. So, the equation of motion (5.2) for the system subject to seismic motion takes the form:

$$M\ \ddot{x}\ (t) + C\ \dot{x}\ (t) + Kx(t) = -M\tau\ \ddot{u}_g\ (t) \tag{5.4}$$

This vector equation represents a system of differential equations with constant coefficients, with as many unknowns as the degrees of freedom of the system. To solve this system, *modal analysis* is used, a process through which one passes from a system consisting of n differential equations coupled to n decoupled differential equations, which can be resolved separately. The modal analysis allows to obtain useful information on the dynamic behavior of the structure. In particular, the modal analysis solver is used to calculate own frequencies, vibration modes and damping coefficients.

5.2.1 Experimental Modal Analysis

Often, however, one realizes that the dynamic properties calculated with the finite elements differ from the real properties of the structure. The causes to which this difference can be attributed are the following: 1. it is very difficult to evaluate the damping, as it is extremely variable in the structure and hardly reproducible virtually in the model; 2. the discretization of the reality underlying the finite element theory involves an approximation of the displacement fields through predefined form functions within each element; 3. there can be approximations related to interactions with non-structural elements; 4. the actual geometry could be different from the one considered in the model.

The experimental techniques allow, therefore, to bridge the difference between the model and the real structure, comparing the results obtained from the virtual model with the data acquired experimentally by means of dynamic monitoring techniques. *Experimental Modal Analysis* (EMA) is also known as *inverse problem* (in analogy to the so-called direct problem in which, known input and structure, one wants to know the answer) being a problem in which the answer is known and what the cause (input) and you want to know the structure.

The main reason for interest in the experimental dynamic identification is due to the fact that the dynamic behavior of a structure is considered a sort of *digital fingerprint*, in the sense that it depends only on its intrinsic characteristics (mass, stiffness, damping, degrees of constraint, etc.) and not from the entity and/or type of load applied. Therefore, if there are no internal changes to the product, for example structural damage, the behavior of the structure remains unaltered. Otherwise, you will notice a variation of the frequencies and the proper ways of vibrating.

Furthermore, structural identification is a technique in itself non-destructive and, as such, can be applied to both new structures, for example in the testing phase, or to existing or historical structures. It is precisely in the context of the dynamic identification of the structures that the Experimental Modal Analysis is located. It is a procedure that allows to identify the dynamic behavior of civil structures through experimental tests conducted using known inputs. The fundamental hypotheses on which the experimental modal analysis theory is based are: linearity, stationarity and observability.

The dynamic behavior of the structure is linear, so the response to a certain combination of input to the system is equal to the same combination of the respective responses. This means that the overlapping effect principle can be applied. The dynamic characteristics of the structure do not change over time. Therefore, the coefficients of the differential equations that support the problem are constant with respect to time. The data necessary to determine the dynamic characteristics of interest must be able to be measured. Thus, we enter a very wide field concerning the theory of the choice of measurement points for positioning the sensors of the monitoring system. In fact, it is necessary to choose carefully the measurement points, avoiding to place the measuring instruments in those points, called modal nodes, in which the observability of the modes is null. Therefore, the EMA allows the identification of the dynamic characteristics of the structure by applying input-output identification procedures. The limitations of the EMA are that *artificial excitation* is needed to measure the usually expensive frequency response functions and in some cases, such as large civilian structures, adequate excitement carries the risk of damaging them. The case study of this chapter was also an opportunity to design, implement and test a so-called *portable vibrodina*.

The success of the modal analysis of a structure depends on the use of an adequate instrumentation. This instrumentation is basically constituted by an excitation system, sensors for the acquisition of accelerations and displacements and a system for analyzing and measuring signals, as already seen in the previous chapters.

Basically, the task of an excitation system is to transmit a force to the structure; the transducers measure the amount of force applied, the displacement and the accelerations that the structure undergoes, converting them into electrical signals; these signals are then recorded by the analysis system, which generally analyzes the frequency content.

The most used fixed excitation systems are the shakers. Their main characteristics are the amount of force and displacement they can generate and the frequency range they can cover. They are mainly used in tests conducted at low frequency $(0 - 20Hz)$ where high levels of force and displacement are required. They consist of an electronic control system that allows you to easily generate and adjust the vibration signal. Among the main types of shakers are the electrodynamic and the mechanical.

The electrodynamic shakers are characterized by greater versatility; they are essentially made up of a mobile coil, connected to the connection support, positioned inside a magnetic field. An electronic system generates a signal that, appropriately amplified, feeds the moving coil. In this way, a force and a motion are generated which are transmitted, through the connecting support, to the structure.

5.2.2 Operational Modal Analysis

Modal analysis can also be performed in the case of *environmental excitations*, considered as a *white noise*. In this case, the input of the structure is not known (in general, it can not be measured), but it is nevertheless possible to evaluate the dynamic parameters of a structure. The different methods developed work, therefore, using only the output data. So, with the expression *Operational Modal Analysis* (OMA) we indicate a series of dynamic identification procedures based only on outgoing information, so much so that we speak of output-only techniques. In this case, it is assumed that the unknown input is characterized by a white noise with a Gaussian distribution at a mean value of zero. The OMA theory is based on the fundamental hypotheses of linearity, stationarity and observability, as in the case of experimental modal analysis, EMA. Environmental excitement includes vibrations induced by vehicular traffic, both on the road and rail, both on the surface and underground, from industrial activities, from wind and, finally, from earthquakes. These vibrations propagate first through the ground; as a consequence they undergo filtering, reflection and refraction phenomena; subsequently they propagate through the foundations reaching the superstructure. The hypothesis according to which the unknown input is well represented by a white noise with Gaussian distribution at mean value nil implies that the input is characterized by a flat spectrum in the range of frequencies of interest. As a result, all modes are excited and the outgoing spectrum contains all the information related to the structure. From a mathematical point of view, the signals are completely described by their correlation functions. The white noise, usually used to represent environmental excitement, is a particular type of noise characterized by the absence of periodicity and a constant amplitude over the whole frequency spectrum.

5.3 Application of geomatics techniques

The case study is the *Auditorium* of the Industrial Technical Institute A. Monaco in Cosenza which is one of the independent building blocks that make up the whole Institute. The building, with reinforced concrete bearing structure, occupies an area of about $400m^2$ and consists of two distinct areas: zone A and zone B, both with rectangular shape and height of $10.20m$. Zone A has dimensions of $13.65m$ by $9,85m$ and has 3 levels. Zone B, with dimensions of $24.00m$ by $11.15m$, has 2 levels. The second level of zone B coincides with the third level of zone A and can only be reached through the stairs present in this area. At the second level of zone B, there is a footbridge of about $7.50m$ in length, which is the covered passage, on pilotis, between the auditorium and the school complex.

The first operations carried out were the acquisition of the 1976 working project, figg. 5.3 and 5.4, and the visual analysis of the structure, in order to identify *in situ* a cracking map and the possible degradation phenomena. Con-

Figure 5.2: Auditorium of the Industrial Technical Institute A. Monaco

cerning the survey of the plants, the Leica $DISTO^{TM}$ D8 was used. It is an EDM with a $100m$ range and $2mm$ accuracy. The comparison between the dimensions of the original project and those obtained from the survey showed a substantial correspondence, taking into account the tolerances of reinforced concrete works (a few centimeter) and the thickness of the coating. For this reason, for the area not accessible of the attic, the foundations and the roof, the project drawings were considered valid. The Leica 1201+ robotic total station and the Nikon D3200 Digital Camera were used for the elevations survey. The total station has a range of 1 km, without a prism, with a precision of 1mm+1ppm; the angular precision is 1". The Nikon D3200 Digital Camera has a 24.2 megapixel APS-C (1.5x) sensor. The lens used, 55mm Nikkor, was calibrated using the Toolbox Camera Calibration for Matlab. The knowledge of the calibration parameters of the coupling lens-camera body allows resampling the images eliminating the distortions. The reconstruction of the elevations was carried out by photographic rectifying, with an analytical procedure. Using at least four coplanar points of known coordinates, measured by total station, orthogonalized images were obtained. Once obtained the rectified frames, for each zone of the facade, we started the mosaicking. This technique allowed us to generate a single image of the facade, mosaic of all photos reproducing the various zones. The rectified image of the facade was subsequently used as a texture of the auditorium 3D-model, in order to make it more realistic. The position of the openings was consistent with that obtained through the measurements inside the building. Once all the elevations have been reconstructed and, therefore, all the relevant orthogonalized images have been obtained, the degradation state has been analyzed. The analysis showed that: on the facades there are no cracks or traces of settlements; the painting run-off on the whole cornice and in correspondence of the drainpipes is visible; the marble slabs are missing at the corners of the building; there are some stains and there is vegetation. In order to be able to assess the presence of any instability due to movements of the foundation, the verticality of the edges of the building was verified. The measurements were performed with a Leica 1201+ total station. The instrument has been positioned, on different station points, in such a way as

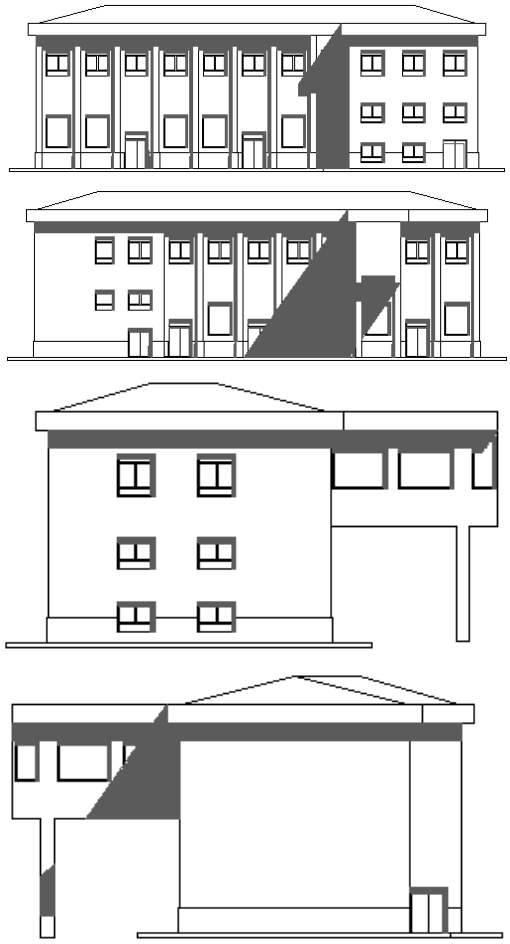

Figure 5.3: Auditorium ITI Monaco: north front, south front, west front, east front

to be able to collimate the various edges optimally. Points were scanned on each corner, lying on a vertical plane passing through the station axis (z axis). For each scan, the x and y average were obtained. It is observed that the edges are all vertical. The deviations are contained within the limits of manufacture tolerances and reach maximum values of about one centimeter.

In conclusion, a 3D-model of the building has been realized, with particular attention to the reinforced concrete bearing structure, to be used for the finite element modelling, in order to evaluate its structural vulnerability.

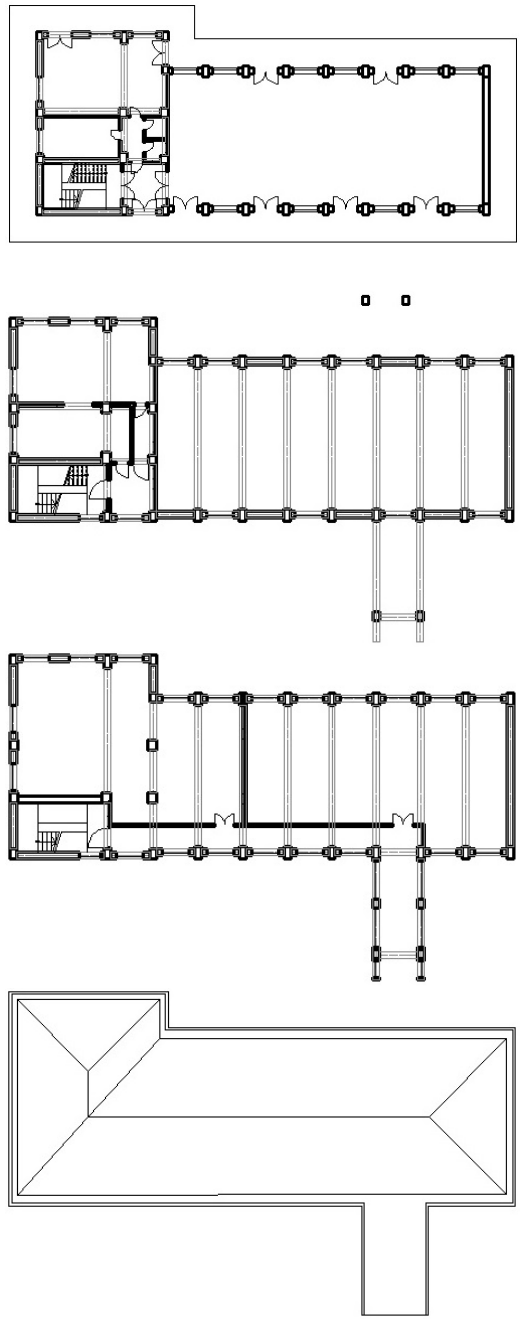

Figure 5.4: Auditorium ITI Monaco: ground floor, 1th floor, 2nd floor, roof floor

5.4 Test application on mechanical properties

The methods used on the Auditorium for the characterization of structural concrete are those based on: sclerometer test results (NDT); pull-out test results

Figure 5.5: Reconstruction of an elevation from orthogonalized images

(SDT); extraction of core samples (DT). All tests were preceded by:

1. Carbonation tests in order to evaluate the degradation process in concrete, fig. 5.6: the concrete surface is humidified with a 1% phenolphthalein solution in ethyl alcohol, which turns red when in contact with material whose pH is greater than 9.2 and remains colorless for lower pH values (the non-carbonated surface is color of red);

2. Pacometric investigations for the verification/identification of the position of steel bars immersed in concrete, fig. 5.7.

Figure 5.6: Test of concrete's carbonation: Plaster removal; Surface sanding; Test for phenolphthalein

Sclerometric test consists in causing the impact of a conventional mass against the material surface and in measuring the rebound height of the mass; the measure is expressed in terms of percentage of the rebound height with respect to the distance made by the mass between the moment it is released and when it hits the concrete surface. This percentage is known as Rebound Index, IR. The use of the rebound index involves many uncertainties and the probable accuracy in estimating the *in situ* compressive strength of concrete, which is about 25%. For this reason, this kind of test is used to evaluate the uniformity of *in situ* concrete and to identify and delimit areas characterized by poor quality or deteriorated concrete. Sclerometric tests [42] performed on the structural elements of the

Figure 5.7: Pacometric investigations

Auditorium, fig. 5.8, showed a good degree of homogeneity of concrete, providing an average value of the rebound index $IR = 41$.

Figure 5.8: Sclerometric test

Pull-out test [43, 44] is based on the correspondence between the maximum compressive load of concrete and the force necessary to extract a metal bar anchored to the structural element through a metal expansion plug inserted in a special housing in the hardened concrete. A pull-out test, fig. 5.9, is performed by a manual pressurisation unit equipped with a pressure gauge (with a peak indicator) that activates a hydraulic jack connected to the plug inserted into the material to be tested. Because of its shape, the metal dowel is pulled out with a cone of concrete whose surface slope is approximately 45 degrees to the vertical, highlighting that the collapse condition of the material is due to the overcoming of the tensile strength on the lateral surface of the cone.

Figure 5.9: Pull-out test

The ultimate force obtained from the test is then used to define the strength parameters of concrete through calibration curves and/or by relating the test with other non-destructive testing methods. Therefore, this test consists of a direct measurement of the tensile strength from which, with essentially empirical correlations, the compressive strength of concrete is deduced. The compressive strength is therefore deduced with empirical correlations but it shows a smaller margin of error if compared to the sclerometric test. Test results were obtained considering as extraction force:

$$F[kN] = 0.3047P[bar] \tag{5.5}$$

where P is the pressure value read on the digital pressure gauge. The following relation between the pull-out force and the equivalent concrete cube strength:

$$1[kN] = 0.94[N/mm^2] \tag{5.6}$$

The pull-out tests carried out provided compressive strength values between $22MPa$ and $27MPa$. The Core test [45] consists in the extraction of cylindrical specimens from the structural element through perforation with a hollow steel tube called diamond core drill, fig. 5.10. A kind of sled is fixed on the structure, on which the core drilling machine is mounted; the adoption of a water cooling system makes the coring operation rather invasive if carried out on buildings in operating conditions.

A carbonation test is generally performed on each extracted cored specimen: the phenolphthalein indicator solution is applied on the carrot's surface causing a concrete color change from transparent white, in the carbonated part, to violet red, in the non-carbonated part. All holes resulting from the extraction of the carrots must be sealed adequately with thixotropic, premixed, expansive or non-shrink cementitious grout.

Figure 5.10: Core test:HILTI DD150-U diamond drilling systems, Measurement of hardened concrete carbonation depth, Hole sealing material

Identification of the areas of structure in which to perform drilling is a delicate operation. It is necessary to choose those parts of the structure where the concrete is less stressed (for example at half height in columns).

Laboratory direct compression tests were performed on each cored specimen to determine the compressive strength of concrete. Concrete core drilling is the

best method to determine the compressive strength of concrete because it consists in a direct measurement of the original material of the structure. The limit to the number of cores resides, as well as operational and economic issues, in the damage to the structure that must always be reduced.

Correlation between the sample resistance and the cylindrical or cubic strength of concrete is defined by well-known standardized procedures. Carbonation tests on the cylindrical concrete specimens provided values of carbonation depth ranging between $3cm$ and $5cm$, while an average compressive strength equal to $29MPa$ was found from compression tests. The cylindrical compressive strength deduced from the pull-out test is

$$F_{ck}(pull-out) = 22 \div 27[N/mm^2]$$

The cylindrical compressive strength deduced from the core test is

$$F_{ck}(core) = 29[N/mm^2]$$

For reinforced concrete, the compressive strength calculation of concrete is:

$$F_{cd} = 0.85\frac{F_{ck}}{1.50} \tag{5.7}$$

so, we get

$$F_{cd}(pull-out) = 0.85\frac{(22 \div 27)}{1.50} = 12.47 \div 15.30[N/mm^2]$$

$$F_{cd}(core) = 0.85\frac{29}{1.50} = 16.43[N/mm^2]$$

The two results fall into different resistance classes:

$$C25/30 \Rightarrow F_{ck} = 25[N/mm^2] \Rightarrow F_{cd} = 14.16[N/mm^2]$$

$$C28/35 \Rightarrow F_{ck} = 28[N/mm^2] \Rightarrow F_{cd} = 15.86[N/mm^2]$$

so

$$F_{cd}(pull-out) > 14.16[N/mm^2] \Rightarrow C25/30$$

$$F_{cd}(core) > 15.86[N/mm^2] \Rightarrow C28/35$$

Considering also that there are no signs of deterioration of the material from the visual surveys, it was considered, for FEM modeling, a concrete with the following characteristics: $\gamma_{cls} = 2500[kg/m^3]$, elastic module $E = 25000[N/mm^2]$ and Poisson coefficient $\nu = 0.27$.

The accurate knowledge of mechanical properties of structural materials, obtained from experimental tests, allows having some parameters that can optimize and make numerical analysis more reliable, such as finite element modeling. Estimation of the *in situ* concrete strength has a fundamental importance in seismic assessments of existing reinforced concrete buildings, according to the most recent regulations.

5.5 FEM modeling

The Auditorium of I.T.I. Monaco was modeled in the context of FEM (Finite Element Method), fig. 5.11, in order to know its mechanical behavior [46]. The spatial model of the experimentation structure was realized with the help of the finite element software SAP2000. Beams and columns have been schematized as

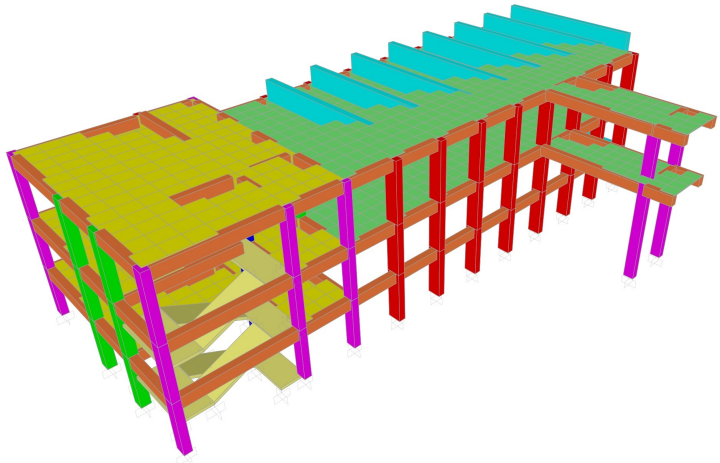

Figure 5.11: Spatial model of the Auditorium

beam elements, while for the floors and stairs has been made to the shell area elements. The results that can be obtained from a beam element are the torques, forces, displacements and rotations at the nodes. While the finished shell element is a three or four-node plane element (triangular or quadrangular), with both flexural and membral stiffness. The thick shells, used in the modeling of the halls of the Great Hall, represent a particular category of shell elements which, compared to the thin shell elements, also consider the shear deformability. Unlike the classical formulation (Kirchoff), in the thick shell formulation (Reissner-Mindlin) the flat surfaces initially perpendicular to the average surface remain flat but not perpendicular to the latter. The thick shell, used in the modeling of the floor of the Auditorium, represent a part of the casting shell elements category which, compared to the thin shell elements, also consider the deformability shear. It is, fig. 5.12, flats latero-cementitious, $25m$ thickness in the zone A (yellow) and $20cm$ thickness in the zone B (green).

Unlike the beam elements, for which the shape functions are well studied and it is possible to arrive at an exact solution also considering elements at two nodes, for shell elements it is necessary to proceed with the meshatura, which consists in subdividing them into sub-elements having a ratio next to one between the sides. The stairs were modeled as shell-thin elements of a thickness of $15cm$ bound to the beams and perimeter columns by interlocking. As regards non-load-bearing structural elements, infill panels and partitions, it was decided to represent them

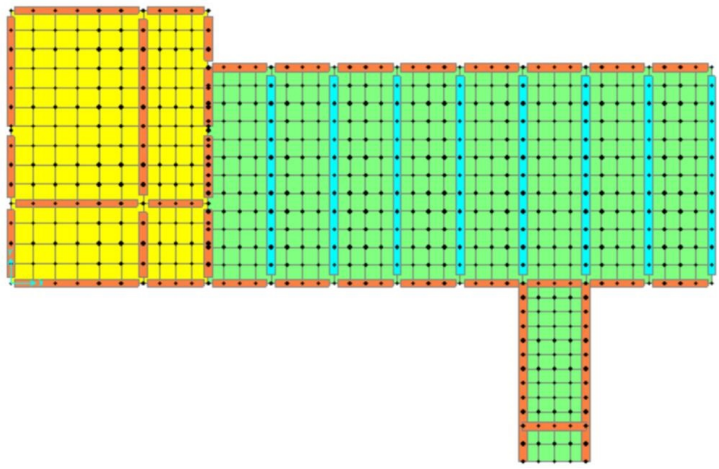

Figure 5.12: Shell area elements: in yellow the zone A, in green the zone B

as loads acting on the beams. The analysis of construction details showed that the roof is simply resting on brick walls along the perimeter and in the central part and does not have a rigid behavior on its floor. Therefore, since its contribution to the overall stiffness is small and difficult to assess, the roof has not been geometrically modeled. In any case, its own weight and the loads acting on it (snow load) were taken into consideration and applied directly to the relative members. Given the lack of documentation concerning the foundation structures and the type of soil, the soil-structure interaction has been imposed on the ground floor by binding the ends of the pillars with perfect interlocking constraints.

5.6 Modal analysis and theoretical frequency

Once the finite element model of the structure was completed, the modal analysis was performed [47], which provided results in terms of frequencies and periods of vibration [48]. The contribution of the generic mode of vibration to the structural response, considered as a translational or rotational contribution, is established on the basis of the percentage of participant mass [41, 49]. While, the number of modes to consider is fixed, according to the current legislation [50, 51], by the percentage of total participant mass that must be higher than 85%. One of the results provided by the modal analysis is the modal participation coefficients. Each way of vibrating will have its own coefficient of participation. These coefficients are a measure of the contribution of each mode of vibration to the seismic response of the structure.

These coefficients depend on the modal form of each mode of vibration and on the seismic mass of each deck. If you perform a seismic calculation with two different calculation software you could have different values of the participation

coefficients for the same structure. This happens because the participation coefficients depend on how the system's vibration modes are scaled. In fact, modes are nothing but forms, they are defined as less than a constant. This means that if I multiply the displacements of the decks of a single way of vibrating by a constant, the result will still be a modal form. That is, the displacements of each deck for each modal form have no meaning in their absolute value, but have meaning in relation to one another.

Therefore, by comparing the participation coefficients of the vibration modes with each other, we could get an idea about the extent of the contribution of each mode to the response of the system.

The participating mass instead tells us how much mass is excited for each mode of vibrating. That is the mass that for each mode of vibrating, multiplied by the spectral acceleration corresponding to the period of the mode, gives us the seismic cut at the base relative to that mode.

Consequently also the participating mass of each mode tells us the extent of the contribution of the individual mode to the response of the system. There is however a difference with respect to the modal participation coefficients. The participating mass does not depend on how modal forms are scaled. With any software we will perform the modal analysis, for the same identical structure the participating mass of each single mode will always be the same.

Usually the participating mass is expressed as a percentage of the total seismic mass with seismic mass calculated using the characteristic values of the permanent loads (structural and non-structural weight) and the characteristic value of the accidental loads reduced by the coefficient ψ_{2j} (see table 2.5.1 NTC2008). In essence, if you do not exceed 85% the calculation has no value.

Thus, the modes of vibration to be considered were chosen considering the participating mass of each mode of vibration and the total sum of the participating masses corresponding to the number of ways we are going to consider.

Each way of vibrating will contribute to the total seismic action with its own seismic cutter at the base. The seismic cutting of each mode will be given by the spectral acceleration corresponding to the vibration period of the mode for the participant mass of the vibrating mode. Therefore, if a sufficient percentage of the participating mass is not considered, a part of the agent seismic action is neglected.

The Italian Technical Regulations prescribe to consider a number of ways for which the participating mass is at least equal to 85% of the total seismic mass. Below is the extract of the Regulations, paragraph 7.3.3.1 NTC2008: *All modes with significant participant mass must be considered. In this regard, it is appropriate to consider all modes with a participating mass greater than 5% and in any case a number of modes whose total participating mass is greater than 85%.*

In the present case study the structural response is defined by the first eight vibration modes, tab. 5.1. By examining the deformations of the first three modes of vibrating of the structure, figg. 5.13, 5.14, 5.15, we have that: the first mode

		Translation x		Translation y		Rotation z	
Mode	f_{theo} [Hz]	Mass [%]	Sum [%]	Mass [%]	Sum [%]	Mass [%]	Sum [%]
1	4,9001	1,58	1,58	50,00	50,00	87,00	87,00
2	6,5951	59,00	60,58	3,20	53,20	0,53	87,53
3	9,1927	0,24	60,81	19,00	72,20	1,06	88,59
4	11,519	0,43	61,24	5,13	77,33	0,10	88,69
5	14,759	21,00	82,24	0,03	77,36	1,52	90,22
6	15,335	0,00	82,24	7,00	84,35	0,46	90,68
7	15,747	0,87	83,11	0,39	84,74	2,55	93,23
8	17,003	2,35	**85,45**	2,65	**87,39**	1,03	**94,26**

Table 5.1: Contributions of the vibration modes

vibrates at a frequency of $4.9Hz$ and is torsional with rotation around z-axis. In fact, in zone A, the presence of the stairs and the greater thickness of the floor greatly increase the rigidity with respect to zone B. The second mode, which corresponds to a frequency of about $6.6Hz$, is translational in the direction x. The third mode is translational in the y direction and vibrates with a frequency of $9.19Hz$.

Given that the Italian Technical Standards for Construction define torsional stiffness as the ratio $\frac{r^2}{l_s^2}$ in which:

r, torsional radius is, for each plane, the ratio between the torsional stiffness with respect to the center of lateral stiffness and the greater of the lateral stiffnesses, taking into account only the primary structural elements, for frame or wall structures (provided that they are slender and mainly deformation flexional), r can be evaluated, for each plane, referring to the flexural moments of inertia of the sections of the primary vertical elements.

l_s turning radius of the masses for each plane, is the ratio between the polar moment of inertia of the mass of the plane with respect to a vertical axis passing through the center of mass of the plane and the mass of the plane itself; in the case of a rectangular plan $l_s = \sqrt{\frac{L^2 + B^2}{12}}$ being L and B the plan dimensions of the plan.

The l_s parameter can also be calculated with a discretized distribution of the masses according to the indications reported in Eurocode 8[1] since for generic structural forms it is possible to define the mass concentrated in the nodes of the calculation model. $l_s = \sqrt{\frac{\sum m_i \cdot d_i^2}{M_{tot}}}$

Furthermore, in paragraph 7.4.3.1 of the NTC18, the structures, consisting of

[1] square root of the ratio (a) the moment of polar inertia of the mass of the plane in plan with respect to the center of mass of the plane and (b) the mass of the plane

Mode	Torsional stiffness	NTC18	NTC08
1	0.947	unchecked	checked
2	0.171	unchecked	unchecked
3	0.333	unchecked	unchecked
4	0.523	unchecked	unchecked
5	0.859	unchecked	checked
6	0.092	unchecked	unchecked
7	0.978	unchecked	checked
8	0.114	unchecked	unchecked

Table 5.2: Modal periods and torsional stiffness

frames and/or walls, are defined torsionally deformable if the torsional stiffness does not satisfy the condition of having a value greater than or at least equal to 1. While in the previous version, NTC08, this condition had a limit value of 0.8.

A more generic method to classify the structure is to use the vibration modes calculated by a dynamic modal analysis. This method compares the vibration frequency of the decoupled torsion mode, ω_{rot}, with the frequencies of the pure translational modes, ω. If the ratio Ω is greater than 1 the answer is mainly translational, if it is less than 1 the response is dominated by a torsional behavior.

From the modal shapes, we can identify the areas that undergo greater deformations for the planning of the positioning of the sensorial instrumentation. It is precisely at the structural parts affected by excessive displacements that the transducers are positioned.

In the case studied, there were eight accelerometers available. Following the analysis carried out with the SAP2000 software, which allowed us to get an idea of the structure's own modes, we chose to place them at the points indicated in the fig. 5.16, which also show the share of each accelerometer and the direction reading, chosen so as to obtain information also on the twisting component of the motion [22]. The acquisitions were all made within 6 hours. For the modal identification of the Auditorium, a wired network composed of eight high-sensitivity monoaxial piezoelectric accelerometers was created. In general, the choice of accelerometers to be used considered the acceleration levels to be measured so that they fall within the measurement range and the sensitivity of the sensor, that is, the potential difference produced on the element for a given level of acceleration. This last parameter is imposed when the accelerometer is manufactured and cannot be changed, it is measured in tension per unit of acceleration [mV/g]. The minimum and maximum measurable values are obtained experimentally during calibration.

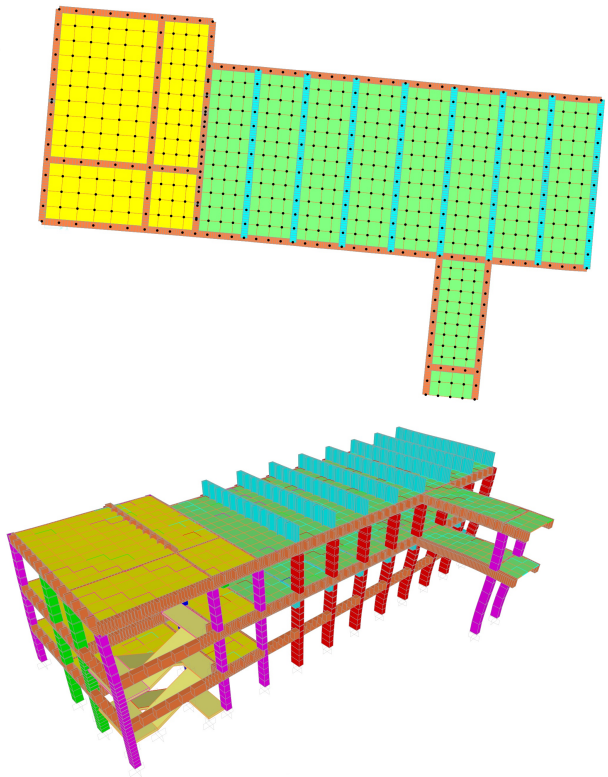

Figure 5.13: Deformed shapes of 1st vibration mode

5.7 Fourier algorithms

Structural vibrations are measured by electronic devices that convert vibrational motion into electrical signals. The analysis of these electrical signals can provide information regarding the nature of the vibrations, more particularly the signals are divided into the time and frequency domain, offering a different view according to the nature of the signal. The analysis in the time domain of a function (or signal) indicates its standard description with respect to the time variable, as opposed to the representation in the frequency domain, i.e. the graphic representation of the instantaneous values of signal in function of frequencies $s(f)$. In the Cartesian diagram the frequencies, f, are generally indicated on the abscissa axis, while the instantaneous values of the signal, $s(f)$, are indicated on the ordinate axis. The information provided by this double description is complementary to each other and helps to have a more complete view of the observed phenomenon. The advantage that derives from the introduction of the two domains is the possibility of changing the perspective with which we observe a given phenomenon. In this way, a problem that seems difficult to solve in one domain can be much simpler in the other.

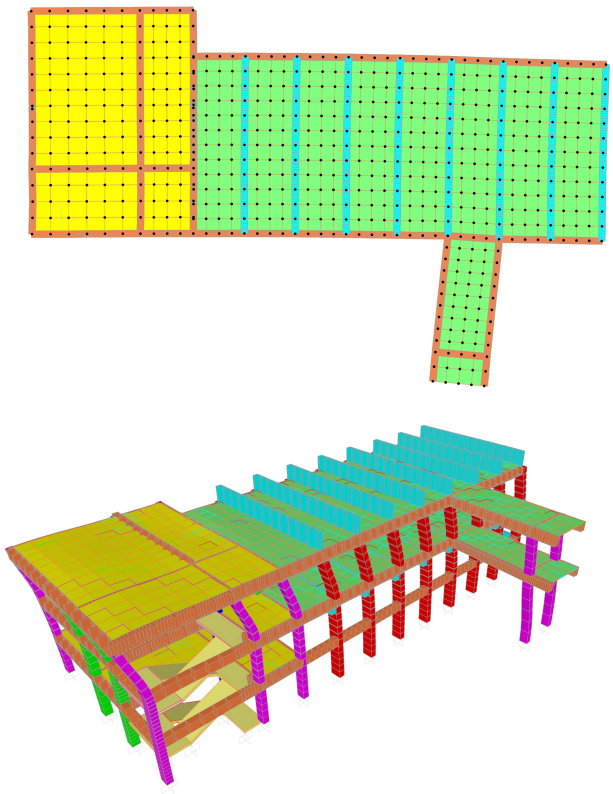

Figure 5.14: Deformed shapes of 2nd vibration mode

The mathematical tool used to transfer the study of signals and systems from the time domain to the frequency domain is the Fourier transform. Basically the Fourier transform indicates which weights (the intensities) of the different frequency components of a given signal. The Fourier transform can not be evaluated for all possible values of the continuous variable f, because this would mean an infinite number of times the calculations necessary for its implementation. On the other hand, from the point of view of the information on the spectrum of a sampled and truncated signal (therefore characterized by N numbers) it would be strictly sufficient to know the trend of the spectrum only in the frequency repetition interval. The discrete Fourier transform (Discrete Fourier Transform, DFT) allows to evaluate the harmonic content in this interval by means of an N number of discrete components. The repetition of the frequency spectrum depends on the sampling over time, as the frequency sampling is due to the periodicity of the signal over time. Periodic signals are of particular practical interest. In such cases, the harmonic analysis using DFT requires some caution, especially in relation to the selection of the truncation window and the fact that the sampling frequency is synchronized with the fundamental frequency of the signal to be an-

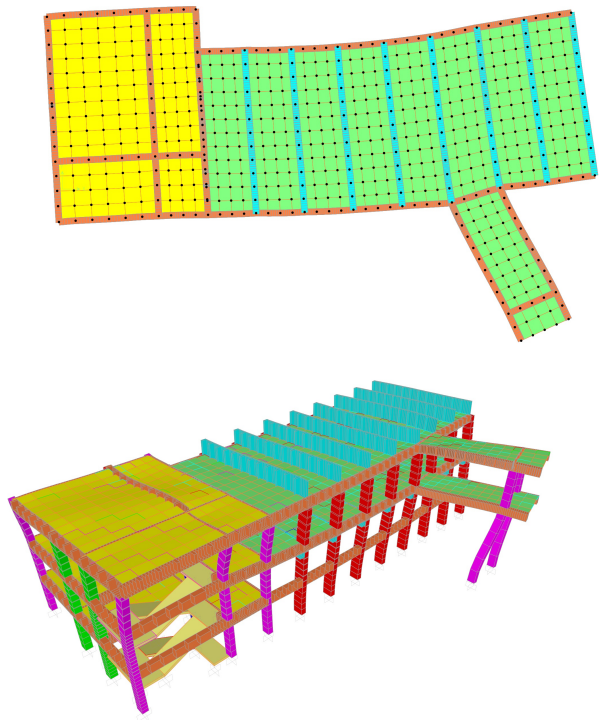

Figure 5.15: Deformed shapes of 3rd vibration mode

alyzed. DFT is a very useful tool for determining the frequency spectrum of a signal, but the computational burden required to implement this technique can be high. For example for $N = 1000$ 106 operations are necessary. For this reason several Fast Fourier Transform (FFT) transform algorithms have been developed that, by exploiting the symmetry properties of the DFT, allow a faster evaluation. Among these, the most common is the $radix - 2FFT$, which reduces operations to a number equal to $Nlog2N$. For example, to perform a 512-point DFT, this algorithm requires 4608 operations instead of 262144. The only constraint for its application is that the number of samples considered is equal to a whole power of 2.

5.8 Experimental data by OMA technique: activation of modes of vibration by white noise

These sensors measure the amount of force applied, the displacement and acceleration of the structure by converting them into electrical signals that are recorded by the analysis system and converted into frequency. The accelerations recorded by accelerometers 1, 3, 5 and 7 are shown below in fig. 5.20. The accelerations

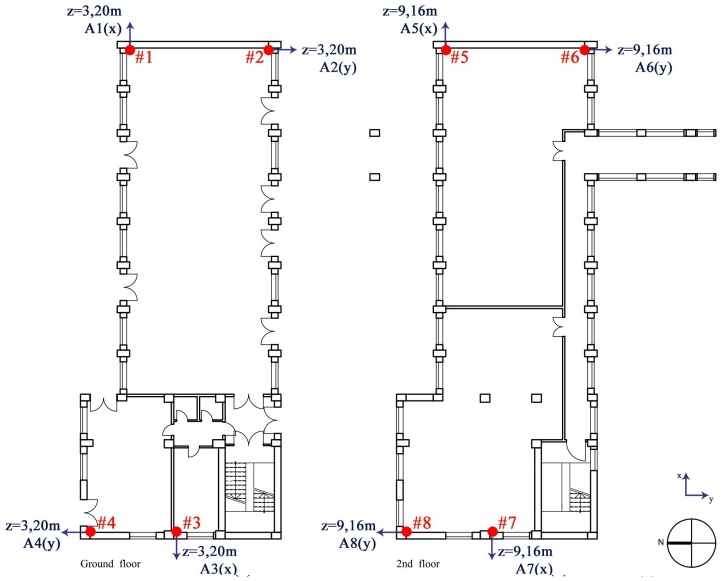

Figure 5.16: Position, elevation and reading direction of the accelerometers at the ground floor and 2nd floor

Figure 5.17: Position of accelerometers (no.1, no.2): ground floor

recorded by accelerometers 2, 4, 6 and 8 are shown below in fig. 5.21.

The final aspect is a graph with the superposition of power spectra relative to the various recorded signals, fig. 5.22.

Figure 5.18: Position of accelerometers (no.3, no.4): ground floor

From the graph, in correspondence with the values of the frequencies of the first three modes provided by the modal analysis (theoretical frequencies), there are increases, peaks, in terms of experimental frequency (frequency measured by the sensors). This identifies a sufficient precise correspondence between the theoretical and experimental frequencies. For the first mode, the FEM analysis had provided a frequency of 4.9Hz. As a way of translational vibration in the y direction, it is expected that the accelerometers capable of providing more information are 2, 4, 6 and 8. Although this, the PSD (Power Spectral Density) charts related to accelerometers 4 and 8 do not have evident peaks around 4.9Hz, since the structure, in the part that in the description phase of the work was referred to as zone A, is rather rigid compared to zone B.

For the same reason, from the results obtained from the FEM model it is possible to notice the non-symmetry of the deformed one justifies the fact that there are also high peaks in the PSD graphs related to accelerometers 1 and 5.

Finally, the data taken into account for the determination of the first frequency are those related to accelerometers 1, 3, 5 and 7, i.e. those placed at the corners at the end of the zone B, that is, at the part of the structure most affected by the

Figure 5.19: Position of accelerometers (no.5, no.6, no.7, no.8)

translational motion in the direction y.

By way of example, the graph of the PSD relative to the accelerometer number 6 is shown with the indication of the experimental frequency associated with the first mode of vibrating, fig. 5.23.

From the average of the frequencies provided by the graphs of the power spectral density relative to the accelerometers of interest, it was possible to determine an experimental frequency for the first mode equal to 4.852Hz.

For the second vibration mode, which corresponded to a theoretical frequency of 6.59Hz, the FEM analysis of the model showed how it was a translational mode in the x direction. Therefore, it is expected that the greatest information is provided by accelerometers 1, 3, 5 and 7.

Actually, the greatest peak is present in the PSD graph related to accelerometer 7. This is due to the fact that, in zone A, passing from the intermediate level to the last level, there is a considerable reduction in rigidity due to the absence of the stairs. This aspect is highlighted in fig. 5.24, which shows the position of accelerometer no. 7 on the deformed 3D structure according to mode 2.

Furthermore, by way of example fig. 5.25, the graph of the PSD relating to accelerometer number 7 is shown, with indication of the experimental frequency associated with the second vibrating mode equal to 6.067Hz.

Each accelerometer was connected via cable (RG59) with the acquisition system (DAQ, Data AcQuisition) consisting of an acquisition device with eight analog channels and eight amplifiers with IEPE (Integrated Electronics Piezo-Electric) interface.

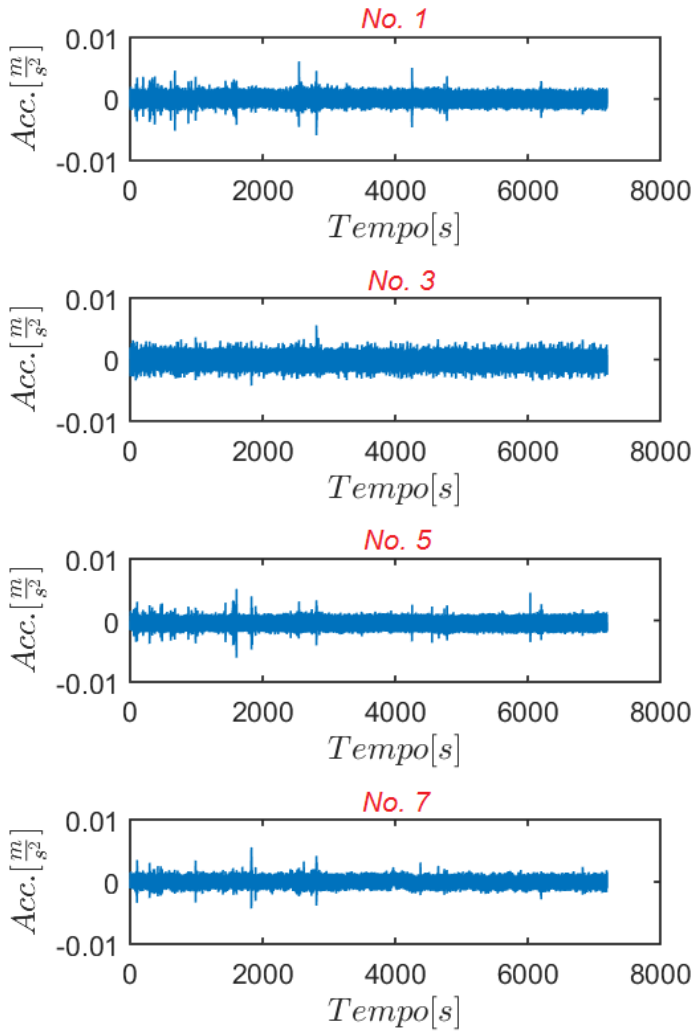

Figure 5.20: Acquisitions of accelerometers no. 1-3-5-7 with input environmental

The acquisition device has been connected to a PC equipped with DEWE-Soft software for the recording and analysis of the data coming from the various accelerometers. The various accelerometers have been installed in position and direction of reading such as to be able to provide, on the whole, information on the torsional mode, fig. 5.16.

Therefore, as far as the third way of vibrating is concerned, it is expected that, more or less, all accelerometers will be able to provide adequate information. Despite this, around the theoretical frequency of 9.19Hz, the PSD charts with the most noticeable peaks are those relative to accelerometers 5, 7 and 8. For the third mode of vibration, an experimental frequency of 8.869Hz was determined.

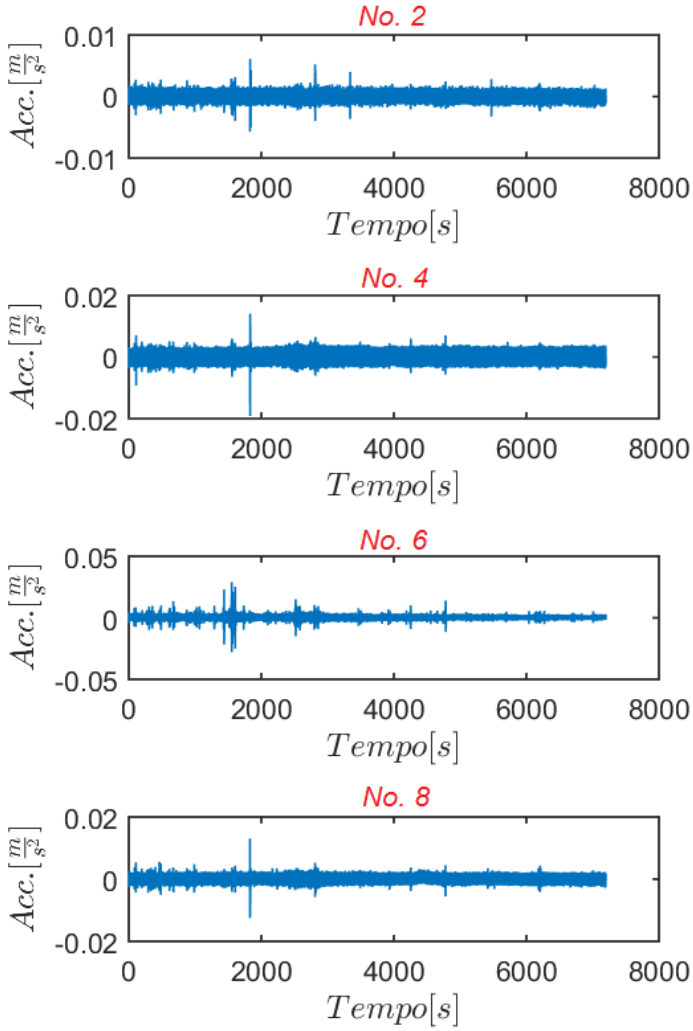

Figure 5.21: Acquisitions of accelerometers no. 2-4-6-8 with input environmental

By proceeding in the same way for all the other significant vibrational modes, the experimental frequencies were determined. The comparison is made by calculating the percentage error, variance, (5.8), tab. 5.3, from which the frequencies provided by the finite element model are close to those calculated experimentally.

$$\Delta f[\%] = \frac{f_{Theo} - f_{Exp}}{f_{Theo}} \cdot 100 \tag{5.8}$$

The comparison is also carried out by plotting the two estimates on a Cartesian plane, fig. 5.27, which shows a good correlation between the two groups of frequencies as close to the line passing through the origin of the axes and with a

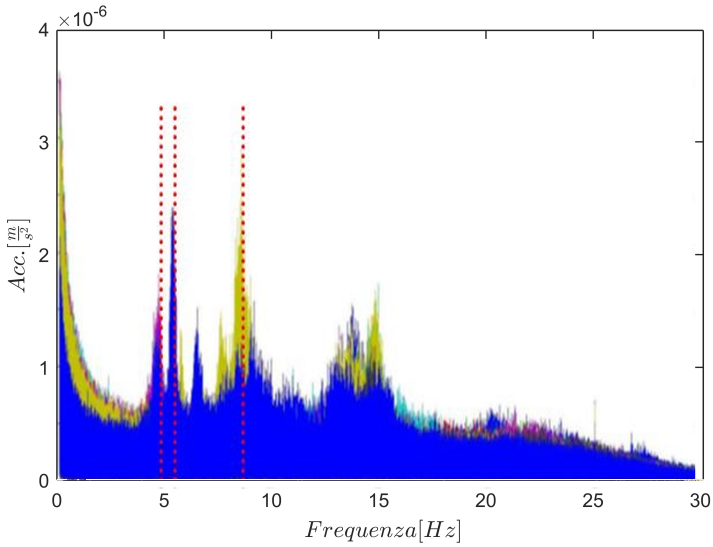

Figure 5.22: Overlap of spectra in terms of frequency (PSD)

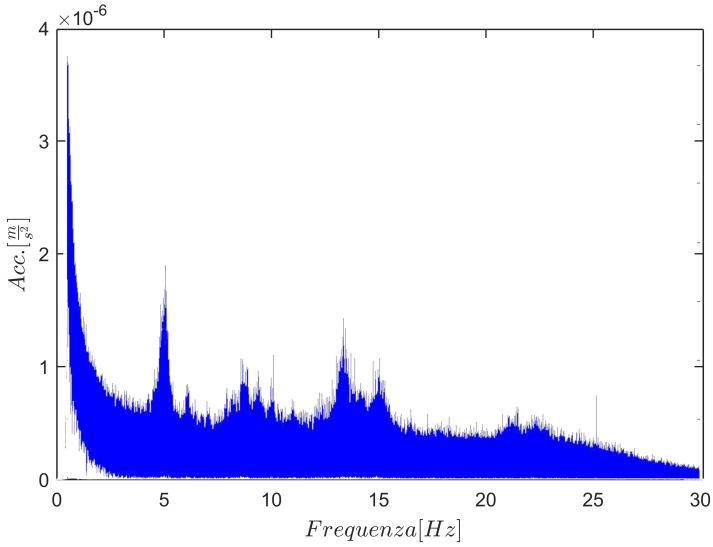

Figure 5.23: Indication of the first frequency (accelerometer no.6)

slope of 45°.

The investigations for the determination of the resonance frequency of the structure were conducted with experimental instrumentation, fig. 5.28; the acquisitions took place according to the indications of the SESAME project (European project, Site Effects Assessment Using Ambient Excitations) and the post-processing took place using Geopsy® software.

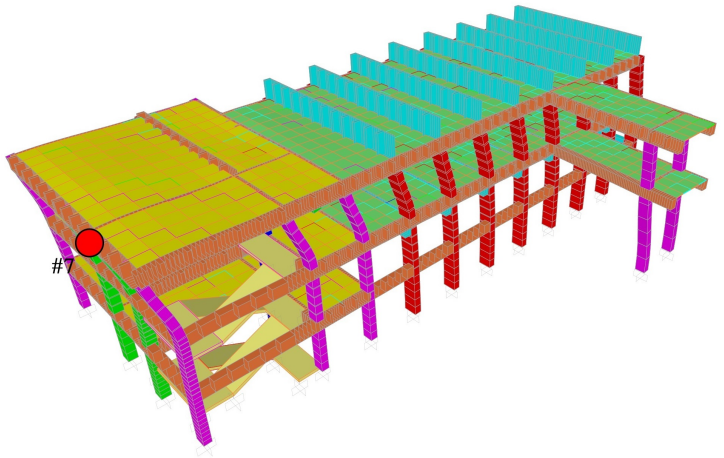

Figure 5.24: Accelerometer position number 7

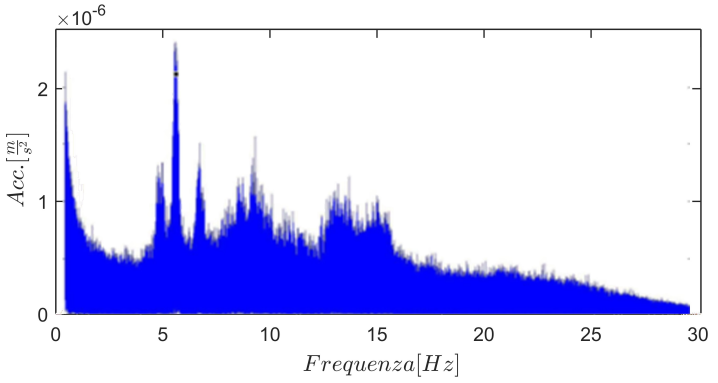

Figure 5.25: Indication of the second frequency: accelerometer no.7

Figure 5.26: DAQ, Data AcQuisition

The single-station microtremor measurements are carried out by means of sufficiently sensitive three-part seismometers in the frequency range of engineering interest 0.1 ÷ 20 Hz, corresponding to the frequencies of the vibrating modes of

Mode	$f_{Theo}[Hz]$	$f_{Exp}[Hz]$	$\Delta f[\%]$	Deviation Δf
1	4,9001	4,852	0,98	0.05
2	6,5951	6,067	8,01	0.53
3	9,1927	8,969	2,43	0.22
4	11,519	10,96	4,85	0.56
5	14,759	14,14	4,19	0.62
6	15,335	-	-	-
7	15,747	-	-	-
8	17,003	17,65	3,81	0.65

Table 5.3: Percent error: estimation of the degree of correlation between the data

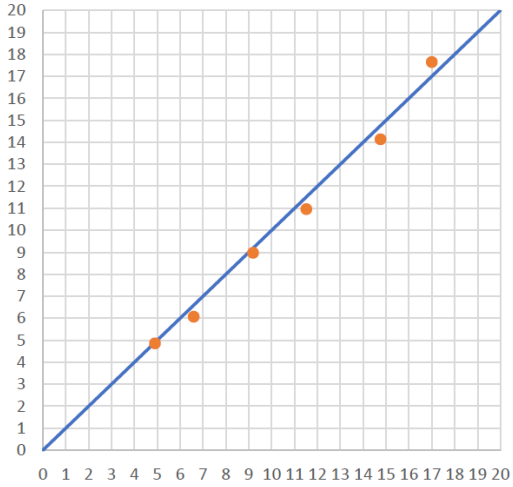

Figure 5.27: Plot of estimating the degree of correlation between the data: theoretical frequencies (x-axis) and experimental frequencies (y-axis)

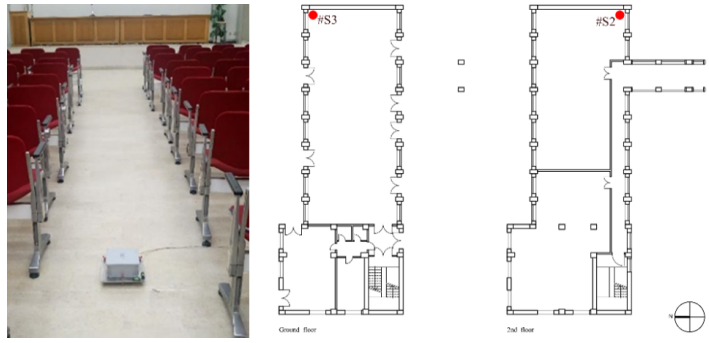

Figure 5.28: Tromograph: positions in the Auditorium

most structures.

In order to be sensitive enough, an instrument must be able to detect signal even in the most silent points of the earth's surface.

This technique is an experimental evaluation of the spectral amplitude ratios between the horizontal components (H) and the vertical component (V) of the environmental vibrations on the surface of the ground measured by specific three-component seismometers.

For this reason, the test is commonly called HVSR (Horizontal to Vertical Spectral Ratio) or Nakamura test.

The frequencies at which the H/V curve shows maximum peaks are linked to the resonant frequencies of the terrain considered below the measurement point or of the building in question. The main purpose of the HVSR test is to bring to evidence the presence of seismic resonance, for example between the investigated land and the structure, in order to allow an estimate of the frequencies at which the motion of the ground or of the structure can be amplified due to these phenomena.

In general, the estimation of the resonant frequency f is more precise as the greater the seismic impedance contrast responsible for this phenomenon is, that is, where the potentially dangerous effects are greater.

The measurements collected in the context of this work were carried out by means of a digital seismometer of the Experimental Tromograph type, already represented in chapter 2 in fig. 2.17.

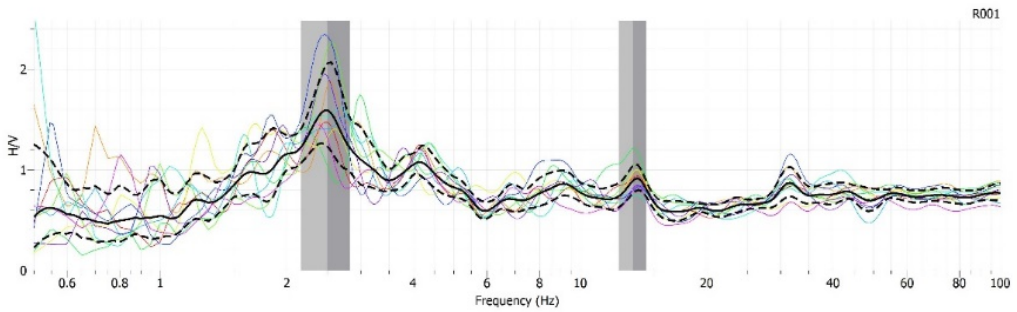

Figure 5.29: Tromograph's registrations: level of walking surface

The dynamic investigation was carried out by acquiring the recordings of seismic noise at the various interpolists and subsequently elaborating the traces of the horizontal components, depurated of the subsoil effect.

The registrations were made at level of walking surface, fig. 5.29, and in succession on the other interplans, up to level of laboratory, fig. 5.30, keeping the acquisition parameters with 500 Hz sampling frequency constant for each station, for a recording time of 20 minutes and with activation of only high-gain velocimetric channels for recording environmental micro-tremors.

Subsequently, the recorded traces were processed using the Geopsy software,

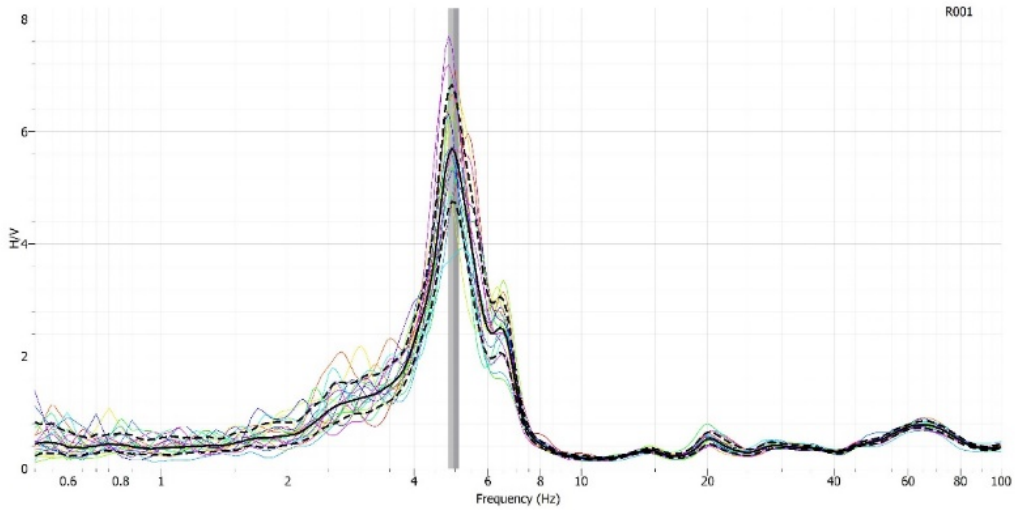

Figure 5.30: Tromograph's registrations: last level

thus obtaining the H/V spectrum so as to immediately verify possible soil-structure resonance effects and quickly identify the dominant frequency of the building.

The characteristic frequency of the site in question is 2.3 Hz, most likely linked to the lithological change due to the 20 meters of depth where there is the seismic bedrock corresponding to the passage to sand gravel.

Another seismic discontinuity, at 13 Hz, corresponds to the transition to poorly consolidated gravels.

The fundamental frequency of the building corresponds to 5.1 Hz.

In case of an earthquake, the building does not resonate with the ground since the fundamental frequency of the ground is 2.3 Hz.

5.9 Experimental data by EMA technique: activation of the vibration modes by sinusoidal forcing

The traditional EMA is normally conducted in a laboratory environment, but in the case of experimental tests conducted on the building of the institute Monaco has allowed to examine the effects of a forcing directly on the structure in question. Besides the accelerometers for recording the output, the realization of the test environment provided for the installation of a mechanical device capable of generating a harmonic forcing along an axis defined on the structure. This device is the vibrodina VIBRO 9001-S made by EnginLAB in collaboration with the DRC Srl and the SmartLab laboratory of the University of Calabria, already described in the section 2.8.

The accelerometric network remained positioned as in the initial configuration

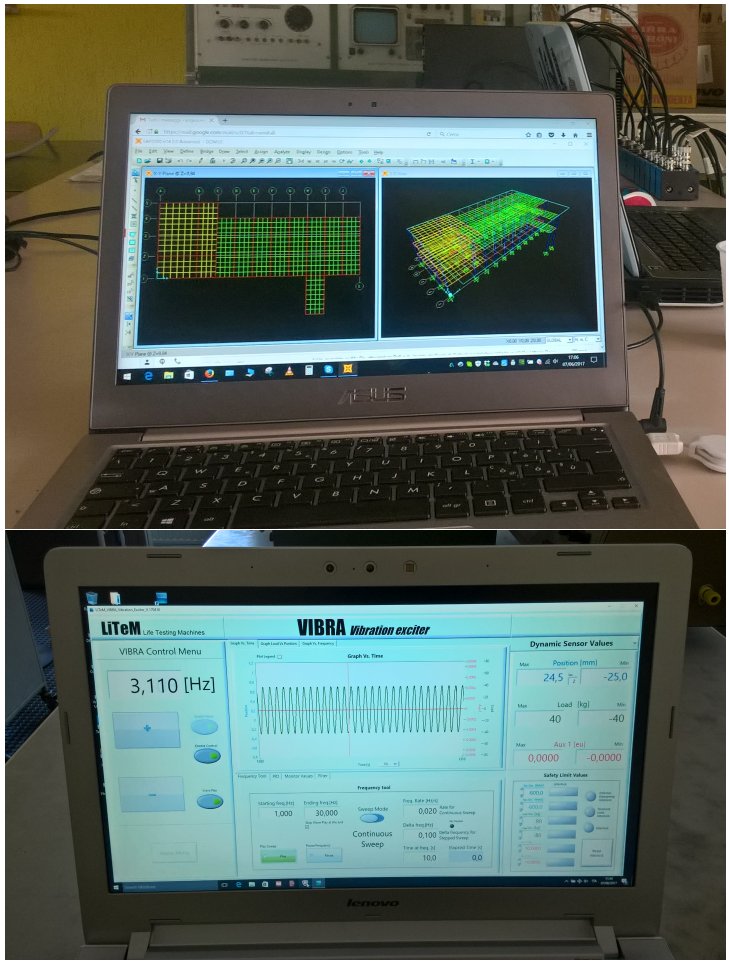

Figure 5.31: ITI A. Monaco: finite element modeling in SAP2000 and software screen for input data forcing

(case of environmental noise with OMA technique) except for the fact that, during the commissioning of the vibrodine, one of the eight monoaxial accelerometers was removed from the initial position in which it was in the configuration for the detection of white or environmental noise and was placed near the vibrodine.

The device, vibrodina, is composed of a mass of 40 kg that oscillates on a linear slide that allows a translational motion and with the management software it is defined the oscillation frequency and the relative load transmitted to the structure to which it is anchored. The vibrodina was located at the last accessible level of the structure (2nd floor) and two excitations were started, swept sine and stepped sine, in both cases the stroke of the vibrating mass was tested both parallel to the X axis and to the Y axis.

The swept sine is an excitation consisting of a sinusoidal signal, with a slow

and continuous frequency variation. The structure is excited at only one frequency and, given the slow increase in variation, it can be assumed that the response is stationary (continuos).

The stepped sine instead provides a discrete increase in frequency. In both cases the frequency range fluctuates between 1Hz and 25Hz, while the increment is different: in the swept sine the pitch is 0.02Hz and in the stepped sine it is 0.1Hz.

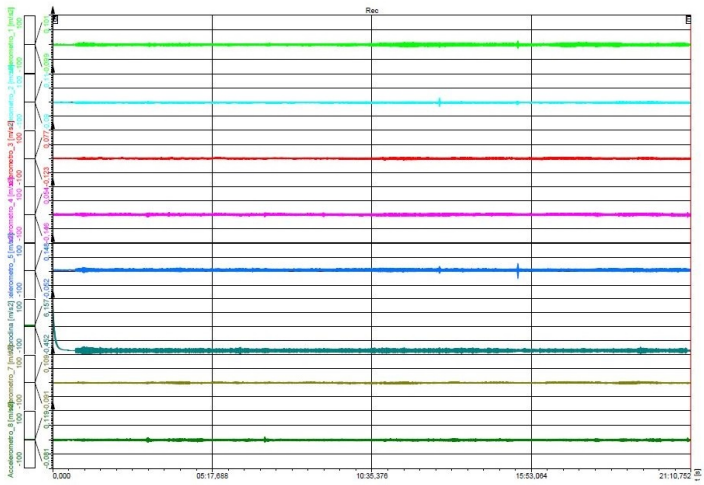

Figure 5.32: Acquisitions of the 8 accelerometers: forcing swept sine in X direction

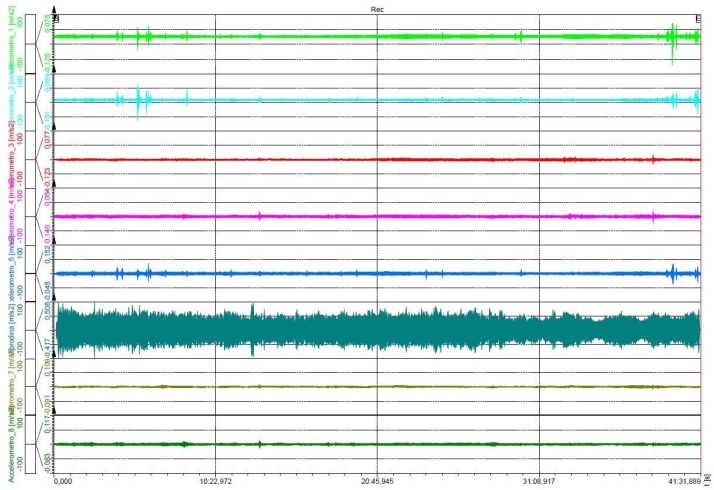

Figure 5.33: Acquisitions of the 8 accelerometers: forcing stepped sine in X direction

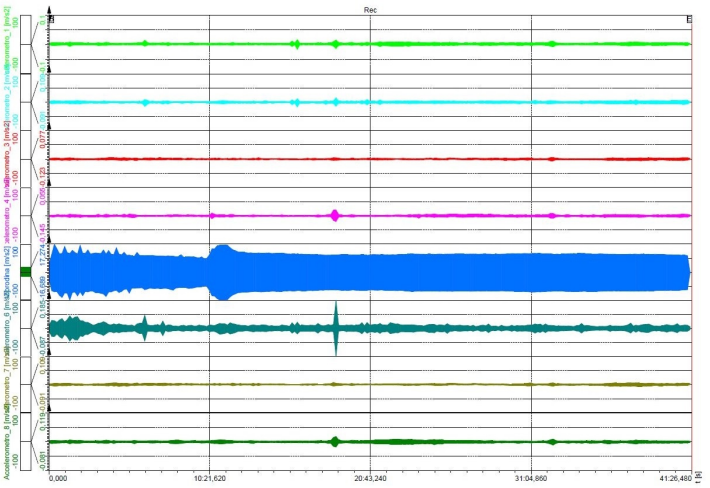

Figure 5.34: Acquisitions of the 8 accelerometers: forcing swept sine in Y direction

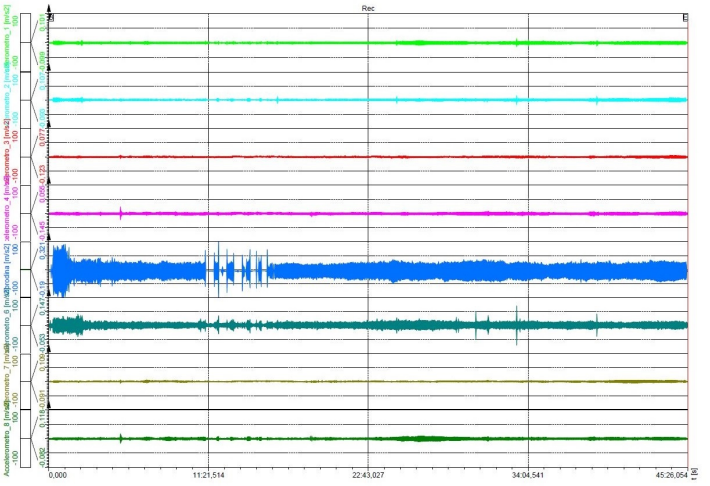

Figure 5.35: Acquisitions of the 8 accelerometers: forcing stepped sine in Y direction

Cases examined according to the type of excitation induced on the structure by vibrodina:

1. swept sine in X direction, 1÷25 Hz range, 0.02 Hz step;
2. swept sine in the Y direction, range 1÷25 Hz, 0.02 Hz step;
3. stepped sine in the X direction, 1÷25 Hz range, 0.1 Hz step;
4. stepped sine in Y direction, 1÷25 Hz range, 0.1 Hz step.

That is, based on the direction in the X,Y plane:

1. X-axis: swept sine (step = 0.02 Hz) and stepped sine (step = 0.1 Hz);
2. Y-axis: swept sine (step = 0.02 Hz) and stepped sine (step = 0.1 Hz).

During the tests with the vibrodine in the direction of the X axis the accelerometer no.6 was removed from the initial configuration and placed, on the floor, near the VIBRO 9001. Instead, during the tests with the vibrodine positioned according to the direction of the axis Y the accelerometer no.5 was placed on the floor near the machine, fig. 5.36.

Figure 5.36: Positioning of the VIBRO 9001: along the X axis with accelerometer no.6 near the vibrodine, along the Y axis with accelerometer no.5 near the vibrodine

- Acquisition of the hours 15:09:05,686

Forcing accelerometer on the mass of vibrodine

Forcing mode: stepped with 1 Hz÷25 Hz range; 0.1 Hz step updated 10 seconds

End of acquisition: 15:52:36,080

- Acquisition of 15:55:53,825

Forcing accelerometer on the floor near the vibrodine

Forcing mode: stepped with 1 Hz÷25 Hz range; 0.1 Hz step updated 10 seconds

End of acquisition: 16:37:25,714

- Acquisition of the hours 16:39:33,200

Forcing accelerometer on the mass of vibrodine

Force mode: continuous with 1 Hz÷25 Hz range; 0.02 Hz/s pitch

End of acquisition: 17:01:08.547

- Acquisition of the hours 17:02:28,100

Forcing accelerometer on the floor near the vibrodine

Force mode: continuous with 1 Hz÷25 Hz range; 0.02 Hz/s pitch

End of acquisition: 17:23:38.852

- Acquisition of the hours 17:47:32,178

Forcing accelerometer on the floor near the vibrodine

Forcing mode: stepped with 1 Hz÷25 Hz range; 0.1 Hz step updated 10 seconds

End of acquisition: 18:29:23.864

- Acquisition at 18:33:57.046

Forcing accelerometer on the floor near the vibrodine

Forcing mode: stepped with 1 Hz÷25 Hz range; 0.1 Hz step updated 10 seconds

End of acquisition: 19:19:23,100

All the acquisitions made are recorded 40 minutes recordings for each of the 8 available channels (no.7 accelerometers at the beam-pillar nodes and no.1 accelerometer near the vibrodine on the floor) in terms of acceleration (m/s^2), figg. 5.32, 5.33, 5.34, 5.35.

So, the acquisitions are mathematically filtered by Fourier Transform (Fast Fourier Transform, FFT) to have the accelerations (m/s^2) as a function of the frequencies (Hz), figg. 5.37, 5.38, 5.39, 5.40.

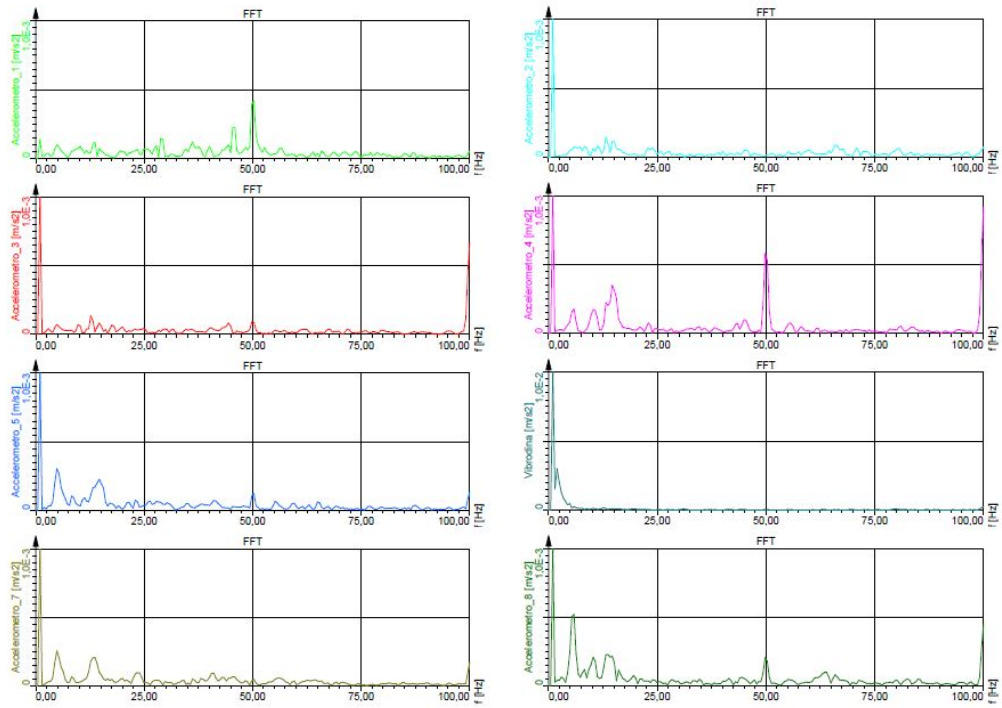

Figure 5.37: FFT of the accelerometers: forcing swept-sine in X direction

Once the recordings of the sinusoidal, stepped-sine and swept-sine forcing induced by the slide vibrodine have been transformed into accelerometric graphics as a function of time through the use of the Dewesoft software and depending on the frequency using the FFT, one has proceeded to identify the vibration modes activated by each individual test.

In the overlapping of the accelerometric readings as a function of time, that of the sensor placed near the vibrodine has always been omitted because it dominates all the others and does not allow the graphic identification of the peaks. For example, you can see in fig. 5.49 that the trend of the accelerometric readings does not change with or without that of the sensor near the VIBRO9001, so it is only for a more precise graphic identification with the Peak Picking method.

Especially in the modal analysis the modal parameters can be estimated directly from the processed data. The simplest and most immediate method is the so-called Peak Picking, PP, which consists in evaluating the natural frequencies from the simple observation of the peaks in the magnitude graph of the frequency response, FRF, the vibrational modes from the ratio between peaks at various points of the structure and dampings from peak widths. This method, although rudimentary, allows a valid estimation of the modal parameters.

One of the most advanced not parametric dynamic identification methods

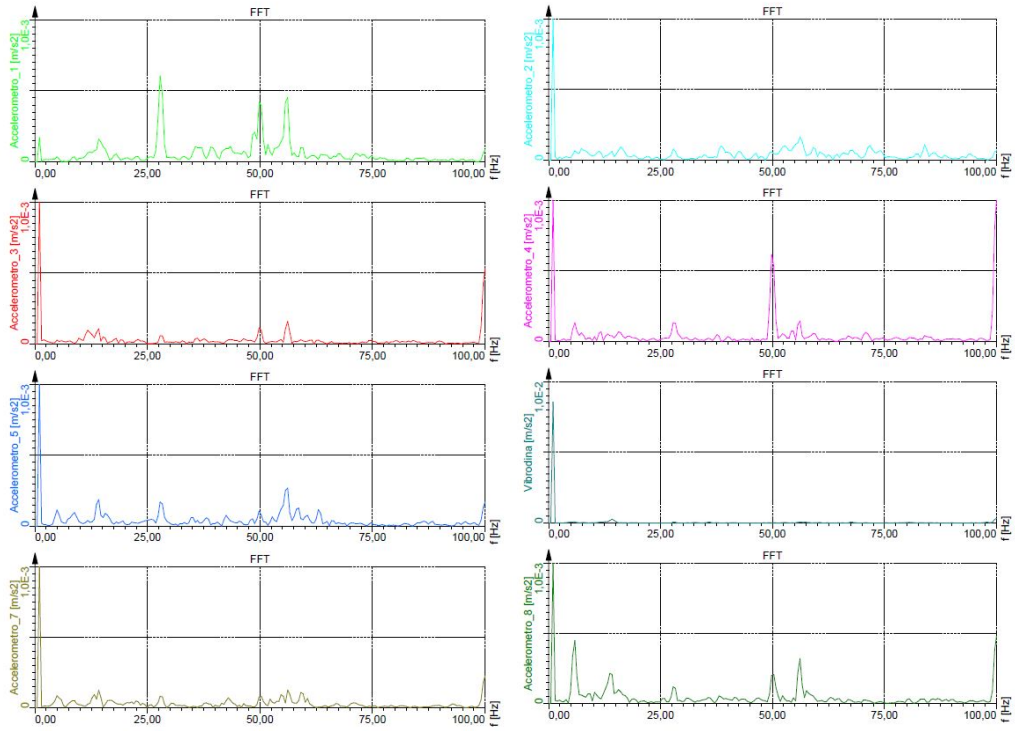

Figure 5.38: FFT of the accelerometers: forcing stepped-sine in X direction

is the Frequency Domain Decomposition, FDD. This method is based on the assertion that the eigenvectors, which represent the modes of vibration, constitute a base, being linearly independent, and therefore any movement of the system can be represented by their linear combination. It is therefore possible to decouple the components of the various modes. In analogy, this property can be applied, besides directly to the response x(t), also to the spectral density (PSD), through a decomposition to the singular values (SVD) of the matrix that represents it at each frequency value. The advantage of this method lies in the fact that it is possible to distinguish modes at nearby frequencies, which with the PP method would certainly be confused.

The following is the first type of test in which the vibrodine stresses the structure with a swept-sine-type sinusoidal forcing having a very small frequency increase (0.02 Hz) every 10 seconds and therefore of an almost continuous type, fig. 5.50.

Identification Results: recordings No.0000[2], VIBRO9001 on X-axis, swept sine

[2]Related mode shapes X-sweptsine-0000
Mode shape # 1:
-0.2479 - 0.0000i 0.1844 - 0.0025i -0.7268 + 0.0285i 0.6125 - 0.0184i
Mode shape # 2:

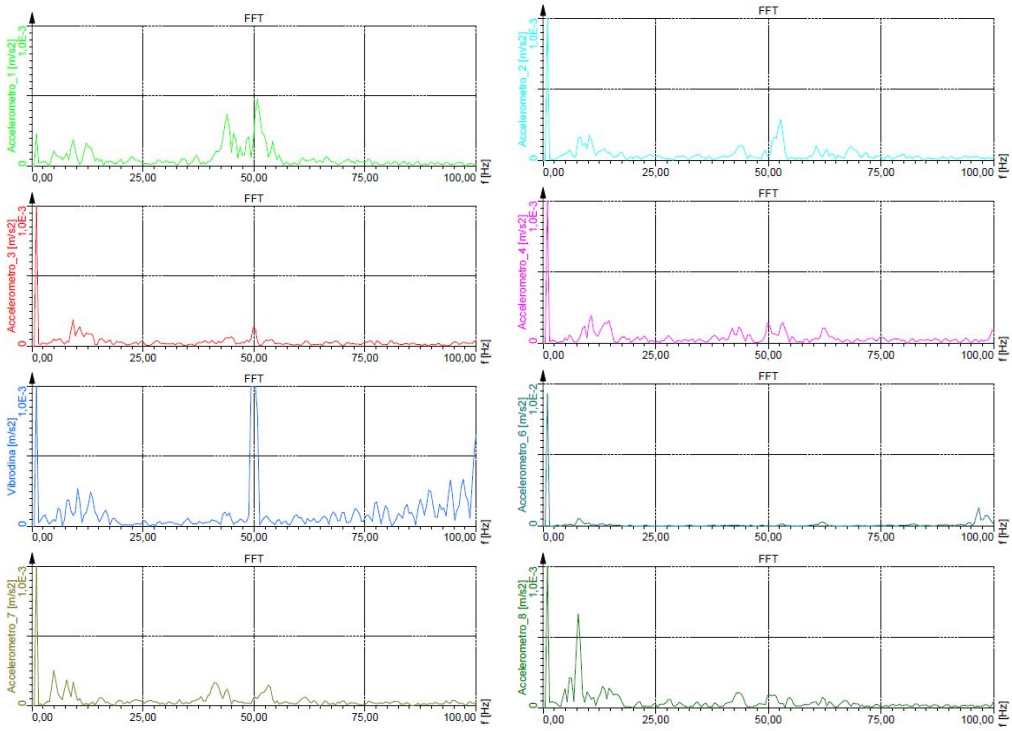

Figure 5.39: FFT of the accelerometers: forcing swept-sine in Y direction

with step 0.02 Hz every 10 seconds:

Mode: 1; Modal Frequency: 4.854 (Hz)
Mode: 2; Modal Frequency: 6.338 (Hz)
Mode: 3; Modal Frequency: 14.07 (Hz)

Identification Results: recordings No.0001[3], VIBRO9001 on X-axis, swept sine with step 0.02 Hz every 10 seconds:

Mode: 1; Modal Frequency: 4.923 (Hz)
Mode: 2; Modal Frequency: 6.279 (Hz)
Mode: 3; Modal Frequency: 13.95 (Hz)

-0.1834 + 0.0000i 0.1930 - 0.0150i -0.7034 + 0.1230i 0.6401 - 0.0967i
Mode shape # 3:
-0.7890 + 0.0000i 0.3934 - 0.0747i 0.3299 - 0.0916i -0.3140 - 0.0369i

[3]Related mode shapes X-sweptsine-0001

Mode shape # 1:
-0.2368 - 0.0000i 0.1795 + 0.0007i -0.7374 + 0.0013i 0.6066 - 0.0005i
Mode shape # 2:
-0.1941 + 0.0000i 0.2008 - 0.0127i -0.7147 + 0.0888i 0.6313 - 0.0671i
Mode shape # 3:
-0.7787 + 0.0000i 0.3917 - 0.1120i 0.3406 - 0.1154i -0.3124 - 0.0272i

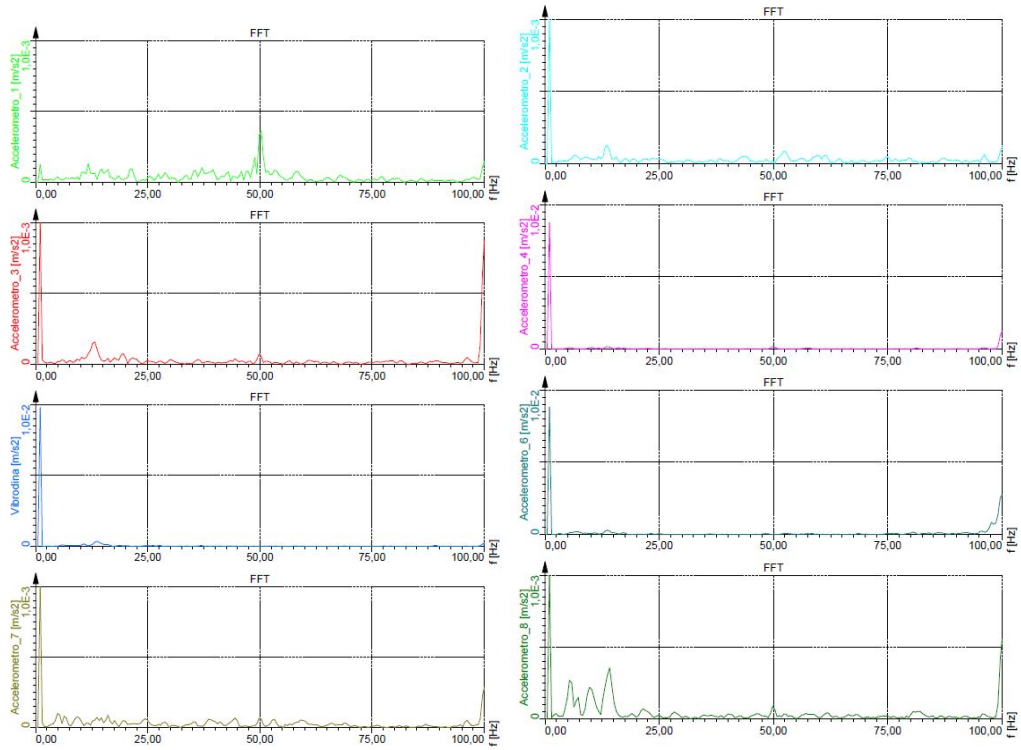

Figure 5.40: FFT of the accelerometers: forcing stepped sine in Y direction

From the comparison with the table, tab. 5.4, containing the contributions of the vibration modes extracted from the solver SAP2000 it is deduced that the continuous forcing (swept-sine) along the X-axis activates the first two modes of vibrating: rotational modal shape around the Z-axis having frequency equal to 4.9001 Hz and translational modal shape along the X-axis having frequency equal to 6.5951 Hz, fig. 5.51.

It is also reported the third graphically detected peak that corresponds to the activation of the fifth mode of vibration of the structure. In particular, it is a translational modal shape along the X-axis with a frequency of 14.759 Hz.

The following is the test in which the vibrodine stresses the structure with a stepped-sine-type sinusoidal forcing having a 0.1 Hz frequency increase every 10 seconds, fig. 5.52.

Identification Results: recordings No.0000[4], VIBRO9001 on X-axis, stepped

[4]Related mode shapes X-steppedsine-0000
Mode shape # 1:
-0.2430 - 0.0000i 0.1771 - 0.0063i -0.7323 + 0.0222i 0.6103 - 0.0184i
Mode shape # 2:
-0.1832 - 0.0000i 0.1962 - 0.0105i -0.7081 + 0.0455i 0.6485 - 0.0613i
Mode shape # 3:

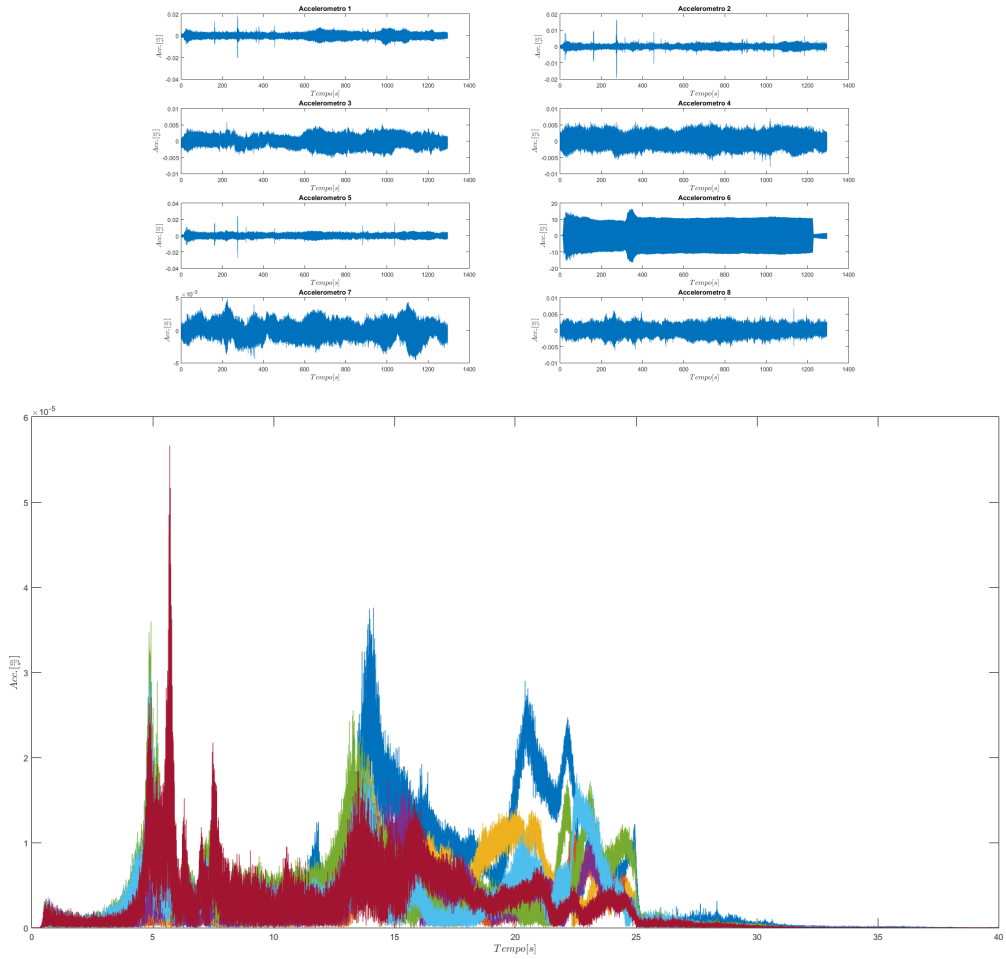

Figure 5.41: Swept-sine in X direction: recordings No.0000 and overlapping without the accelerometer near the vibrodine

sine with step 0.1 Hz every 10 seconds:

Mode: 1; Modal Frequency: 4.865 (Hz)
Mode: 2; Modal Frequency: 6.306 (Hz)
Mode: 3; Modal Frequency: 13.95 (Hz)

Identification Results: recordings No.0001[5], VIBRO9001 on X-axis, stepped

-0.8209 + 0.0000i 0.3827 - 0.0824i 0.2752 - 0.0796i -0.2979 - 0.0451i

[5]Related mode shapes X-steppedsine-0001
Mode shape # 1:
-0.2426 - 0.0000i 0.1790 - 0.0052i -0.7273 + 0.0136i 0.6163 - 0.0088i
Mode shape # 2:
-0.1940 + 0.0000i 0.1995 - 0.0044i -0.7179 + 0.0341i 0.6367 - 0.0257i

		Translation x		Translation y		Rotation z	
Mode	f_{theo} [Hz]	Mass [%]	Sum [%]	Mass [%]	Sum [%]	Mass [%]	Sum [%]
1	4,9001	1,58	1,58	50,00	50,00	87,00	87,00
2	6,5951	59,00	60,58	3,20	53,20	0,53	87,53
3	9,1927	0,24	60,81	19,00	72,20	1,06	88,59
4	11,519	0,43	61,24	5,13	77,33	0,10	88,69
5	14,759	21,00	82,24	0,03	77,36	1,52	90,22
6	15,335	0,00	82,24	7,00	84,35	0,46	90,68
7	15,747	0,87	83,11	0,39	84,74	2,55	93,23
8	17,003	2,35	**85,45**	2,65	**87,39**	1,03	**94,26**

Table 5.4: Contributions of the vibration modes

sine with step 0.1 Hz every 10 seconds:

Mode: 1; Modal Frequency: 4.905 (Hz)

Mode: 2; Modal Frequency: 6.302 (Hz)

Mode: 3; Modal Frequency: 14 (Hz)

From the comparison, tab. 5.4, with the contributions of the vibration modes extracted from the solver SAP2000 it is deduced that the stepped-sine forcing along the X-axis activates, also, the first two modes of vibrating: rotational modal shape around the Z-axis having frequency equal to 4.9001 Hz and translational modal shape along the X-axis having frequency equal to 6.5951 Hz, fig. 5.51, and also a little the subsequent translational mode along X which is the 5th theoretical modal shape.

The following tests, instead, consist of excitation of the structure with sinusoidal and continuous forcing (swept-sine with very small step) induced by the slide vibrodine positioned along the structure's Y-axis.

The results extrapolated with MATLAB show an unclear application of the graphical method of selection of the peaks. In particular, from the first registration, fig. 5.53, a series of very close peaks are obtained and therefore not identifiable with certainty.

From the second registration fig. 5.54, instead, we obtain a graphical trend with no obvious graphical peak. Therefore, in the case of excitation with pseudo-continuous sinusoidal forcing along the Y-axis it is not possible to identify with certainty which modes of vibration are activated.

Proceeding with the last tests, the excitations of the structure are reported by means of stepped non-continuous sinusoidal forcing with a frequency increase of 0.1 Hz every 10 seconds.

Even with these forcing it is not possible to extrapolate with certainty the peaks corresponding to modes of vibration as they are graphs where the frequency

Mode shape # 3:
-0.7916 + 0.0000i 0.3873 - 0.1005i 0.3183 - 0.1198i -0.3084 - 0.0487i

peaks are too close together.

The only peculiarity that all the graphs have in common, even those with the vibrodine acting along the Y-axis, is that the first peak of all the graphs, whether isolated and well defined with respect to the others or with successive peaks that are too close together, always corresponds to the first vibrating mode extrapolated from the SAP2000 solver and that is to the torsional mode with a frequency of 4.9001 Hz with a higher percentage of participating mass than the others.

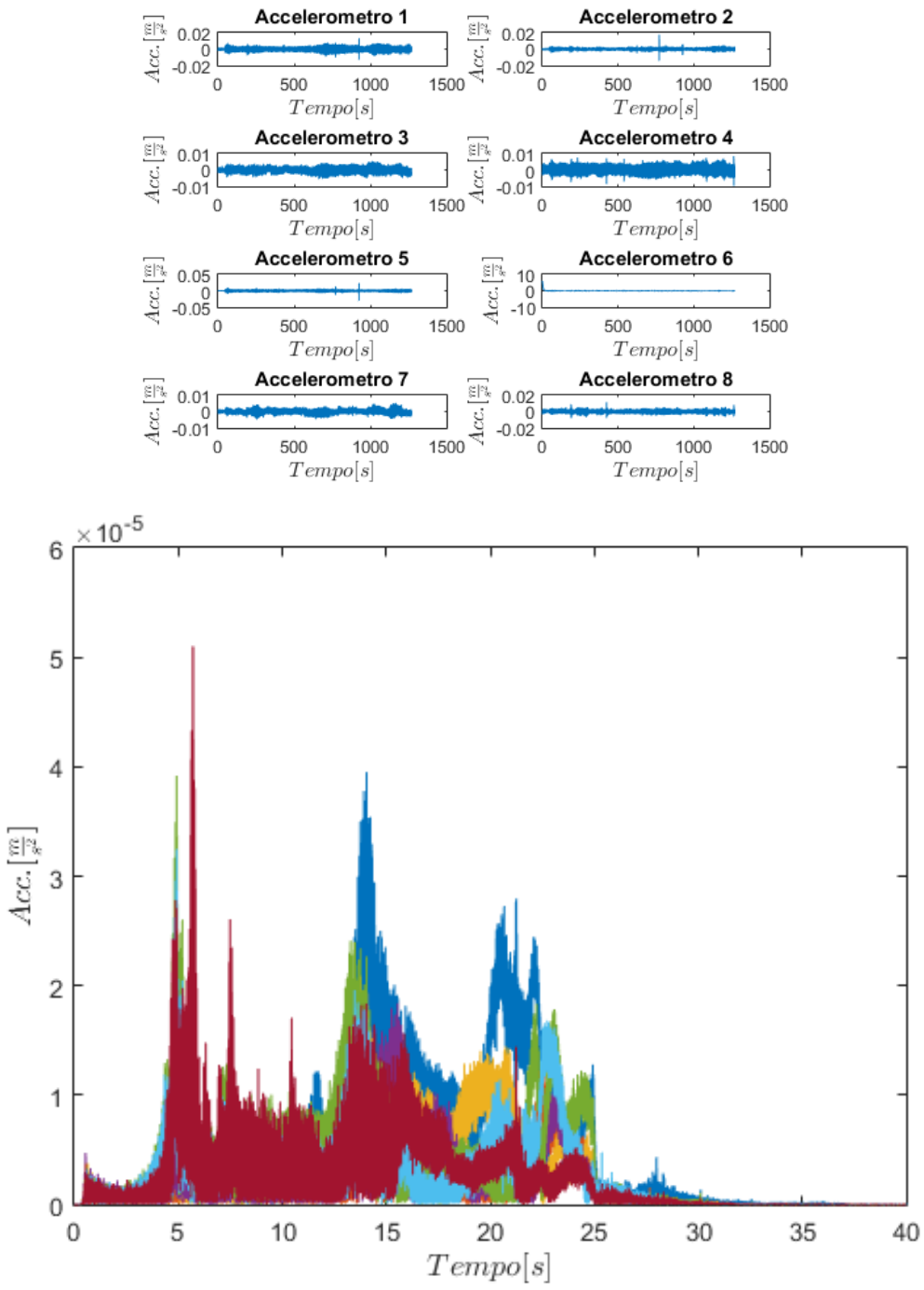

Figure 5.42: Swept-sine in X direction: recordings No.0001 and overlapping without the accelerometer near the vibrodine

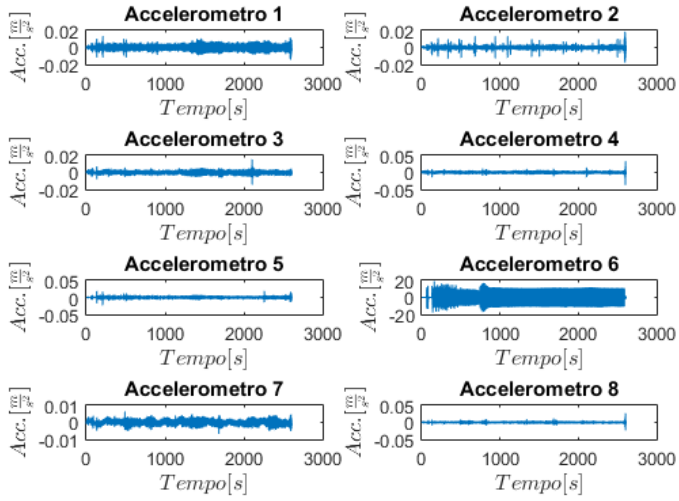

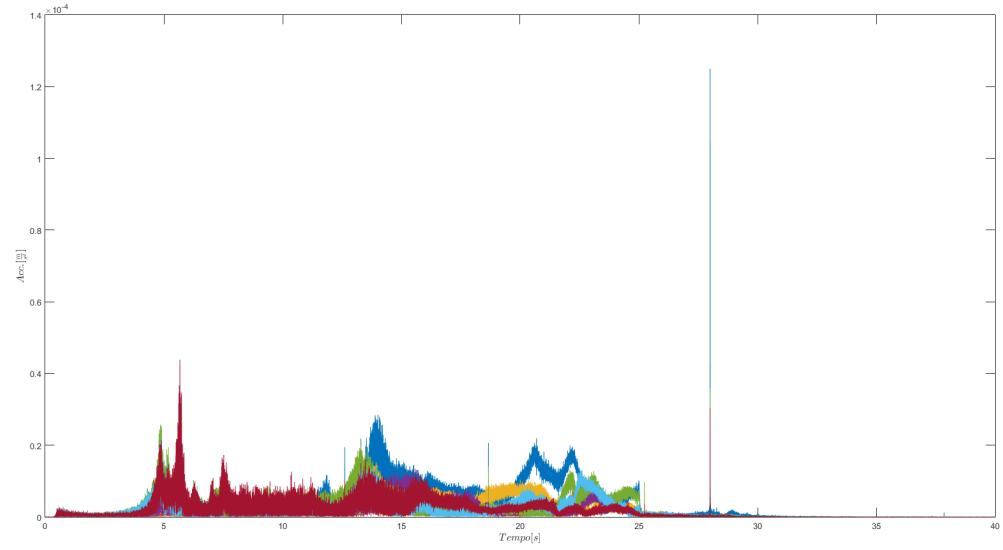

Figure 5.43: Stepped-sine in X direction: recordings No.0000 and overlapping without the accelerometer near the vibrodine

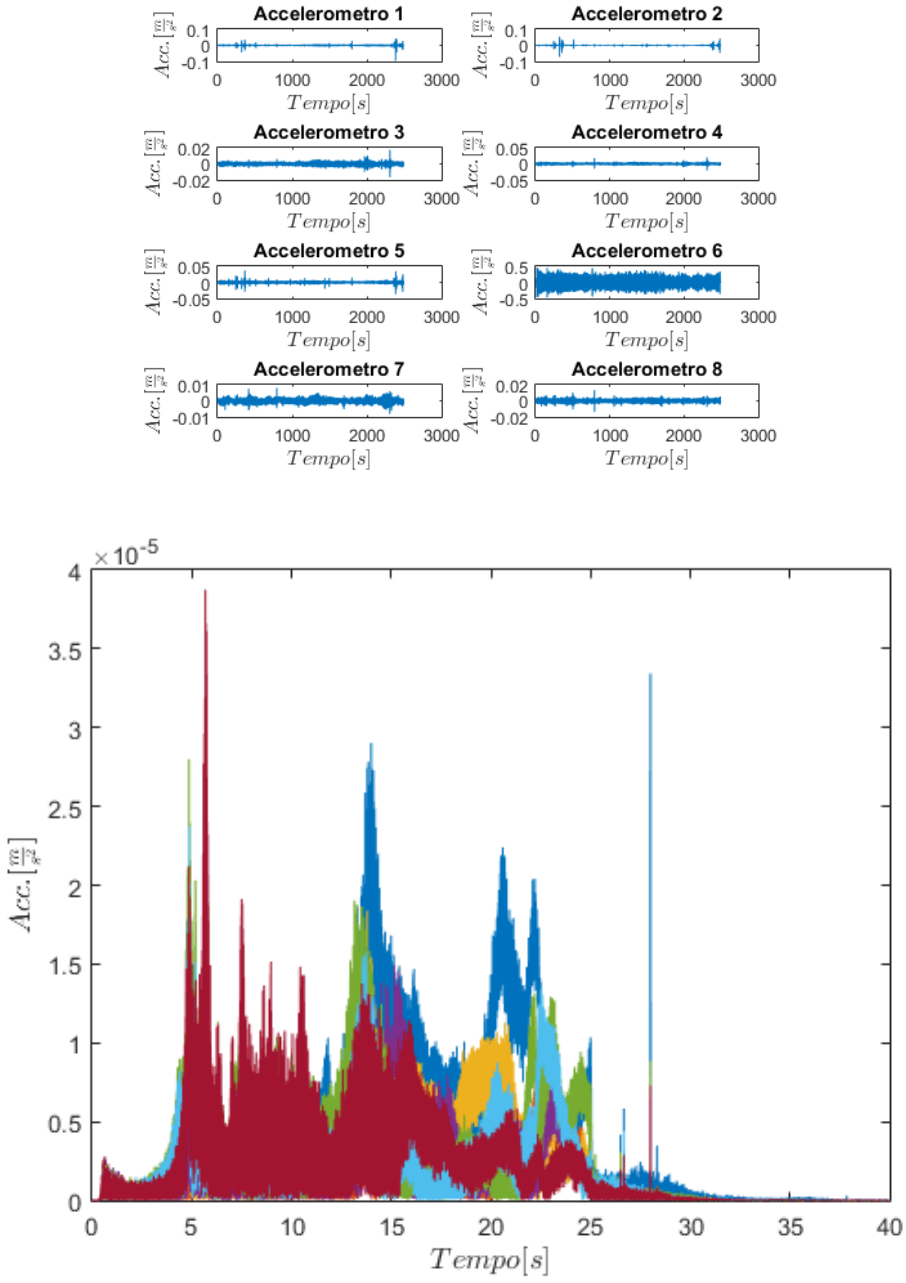

Figure 5.44: Stepped-sine in X direction: recordings No.0001 and overlapping without the accelerometer near the vibrodine

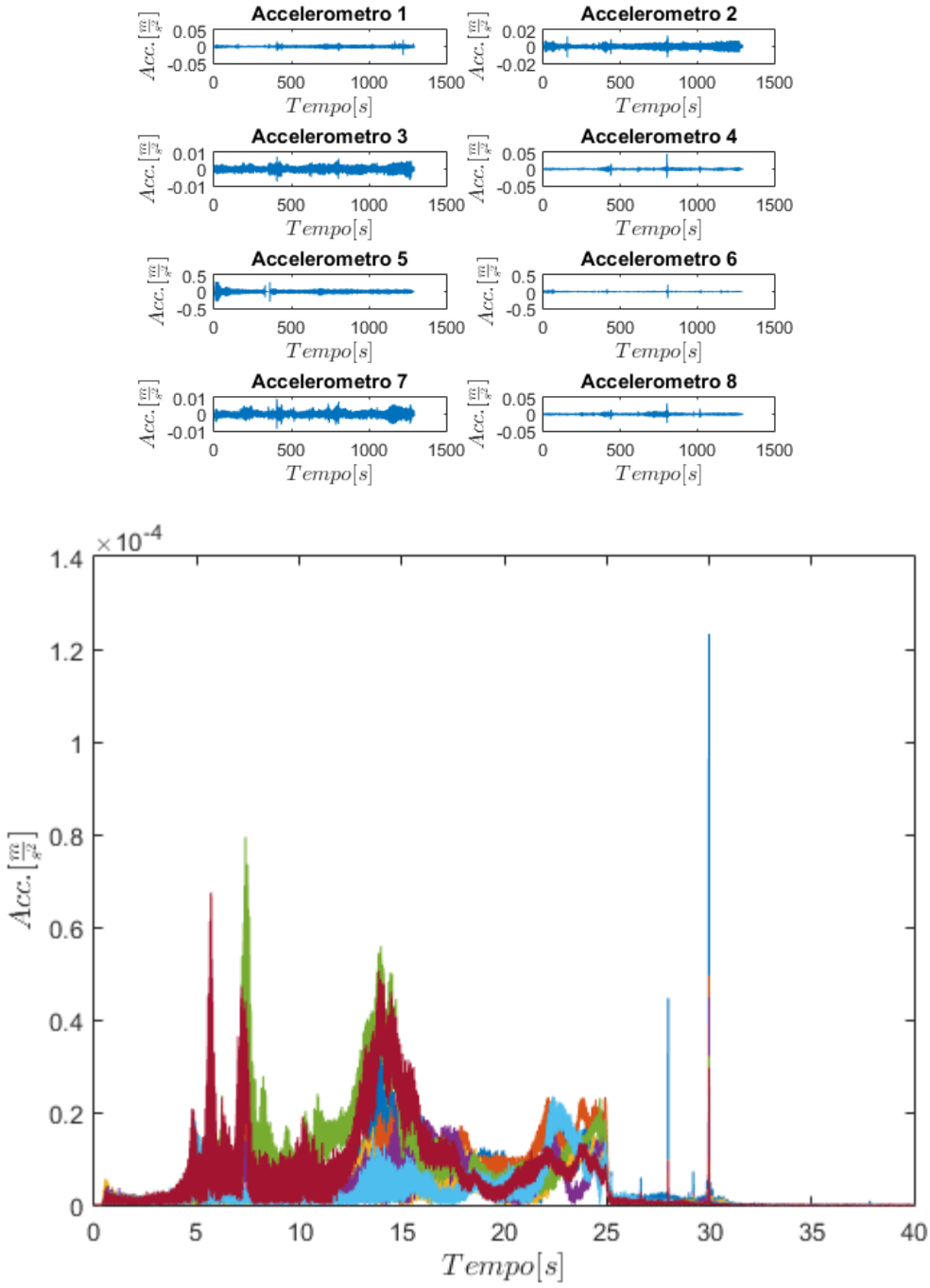

Figure 5.45: Swept-sine in Y direction: recordings No.0000 and overlapping without the accelerometer near the vibrodine

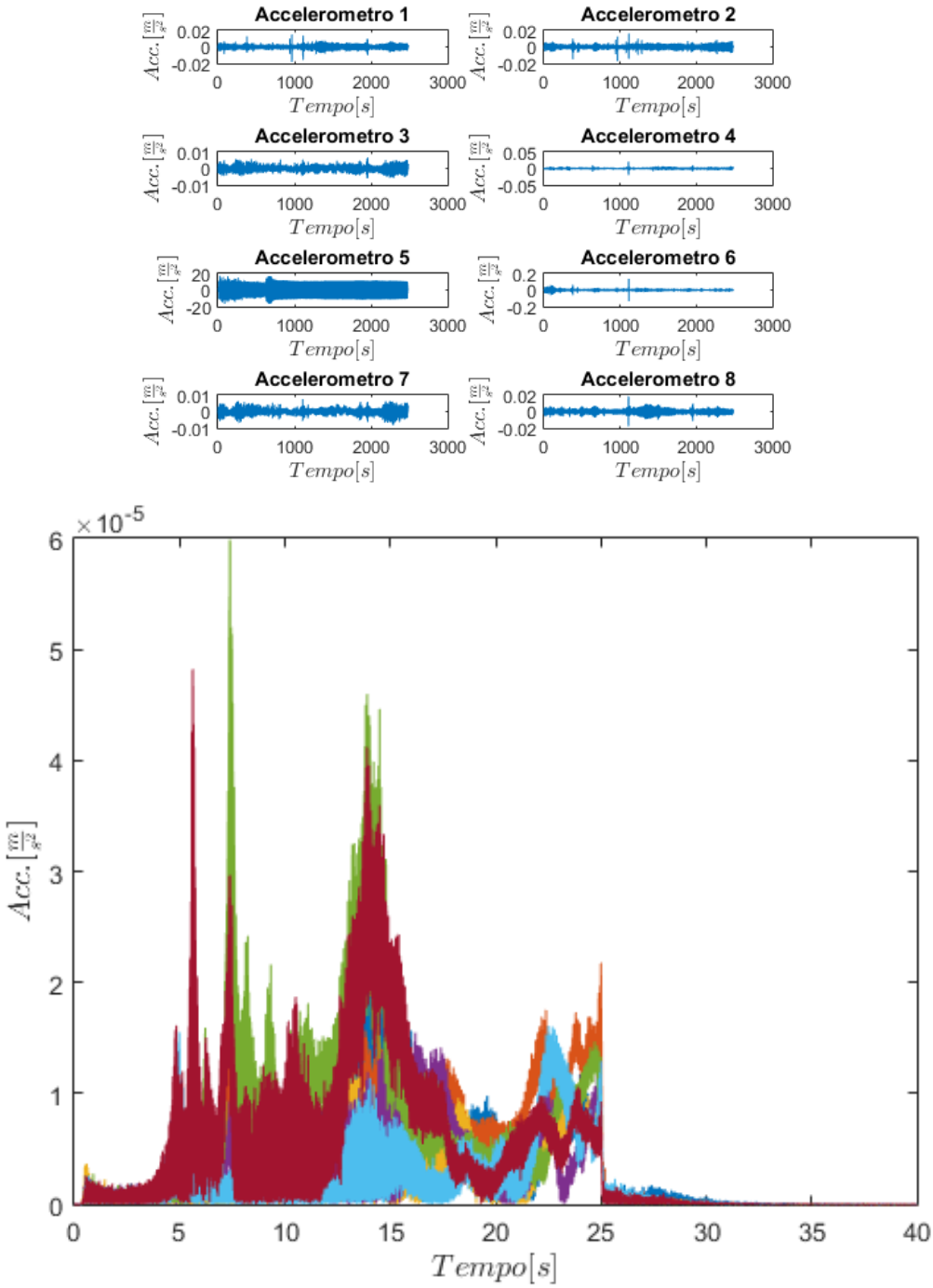

Figure 5.46: Swept-sine in Y direction: recordings No.0002 and overlapping without the accelerometer near the vibrodine

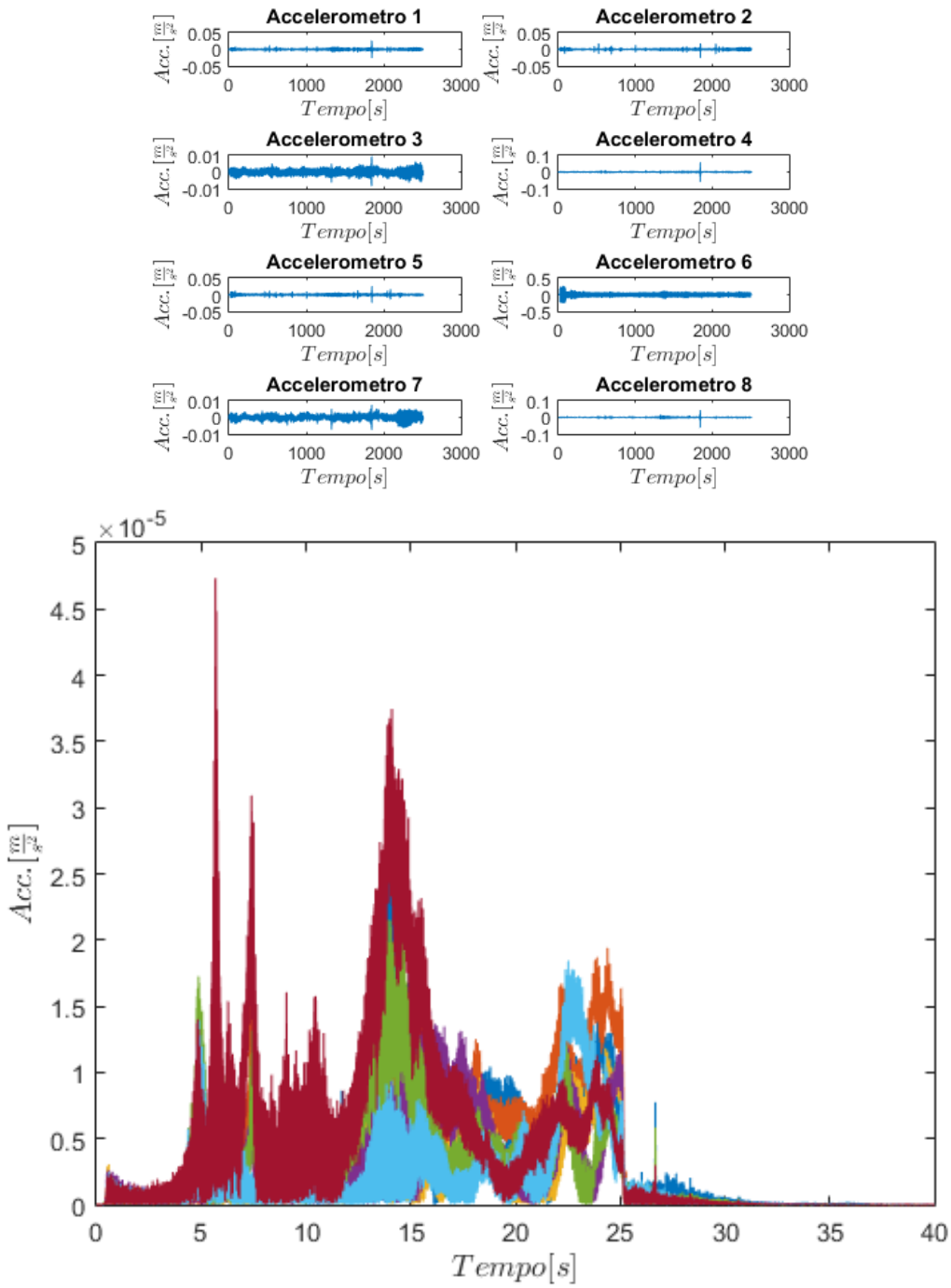

Figure 5.47: Stepped-sine in Y direction: recordings No.0000 and overlapping without the accelerometer near the vibrodine

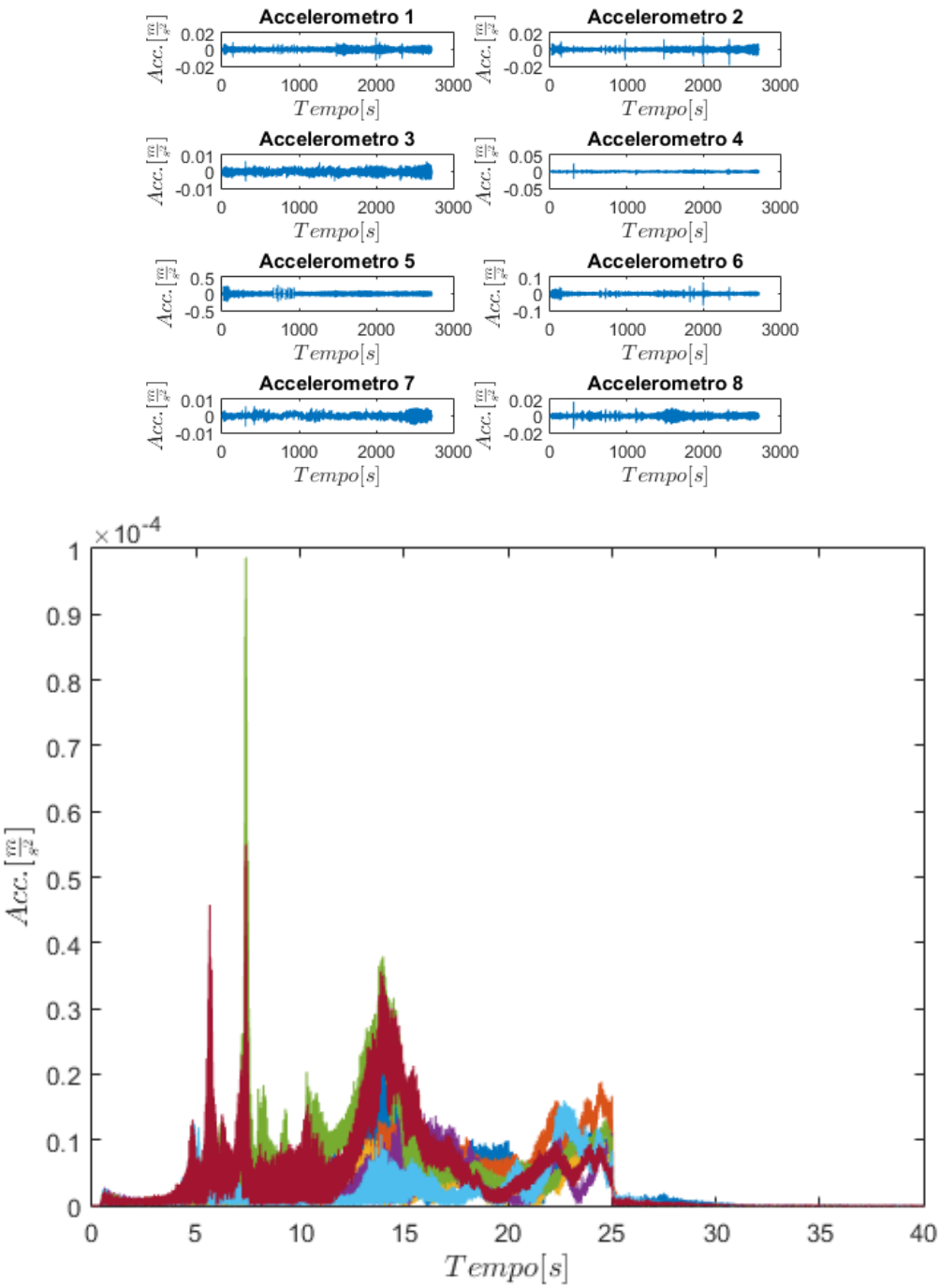

Figure 5.48: Stepped-sine in Y direction: recordings No.0001 and overlapping without the accelerometer near the vibrodine

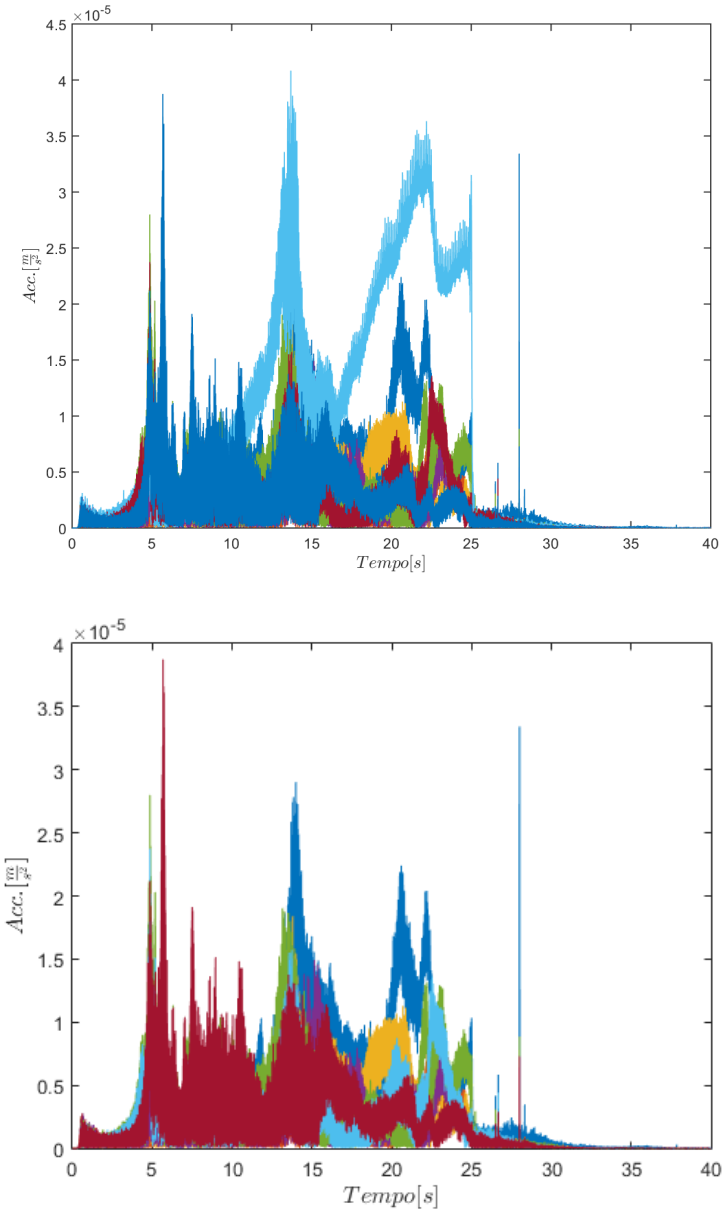

Figure 5.49: Overlap with and without sensor near VIBRO9001

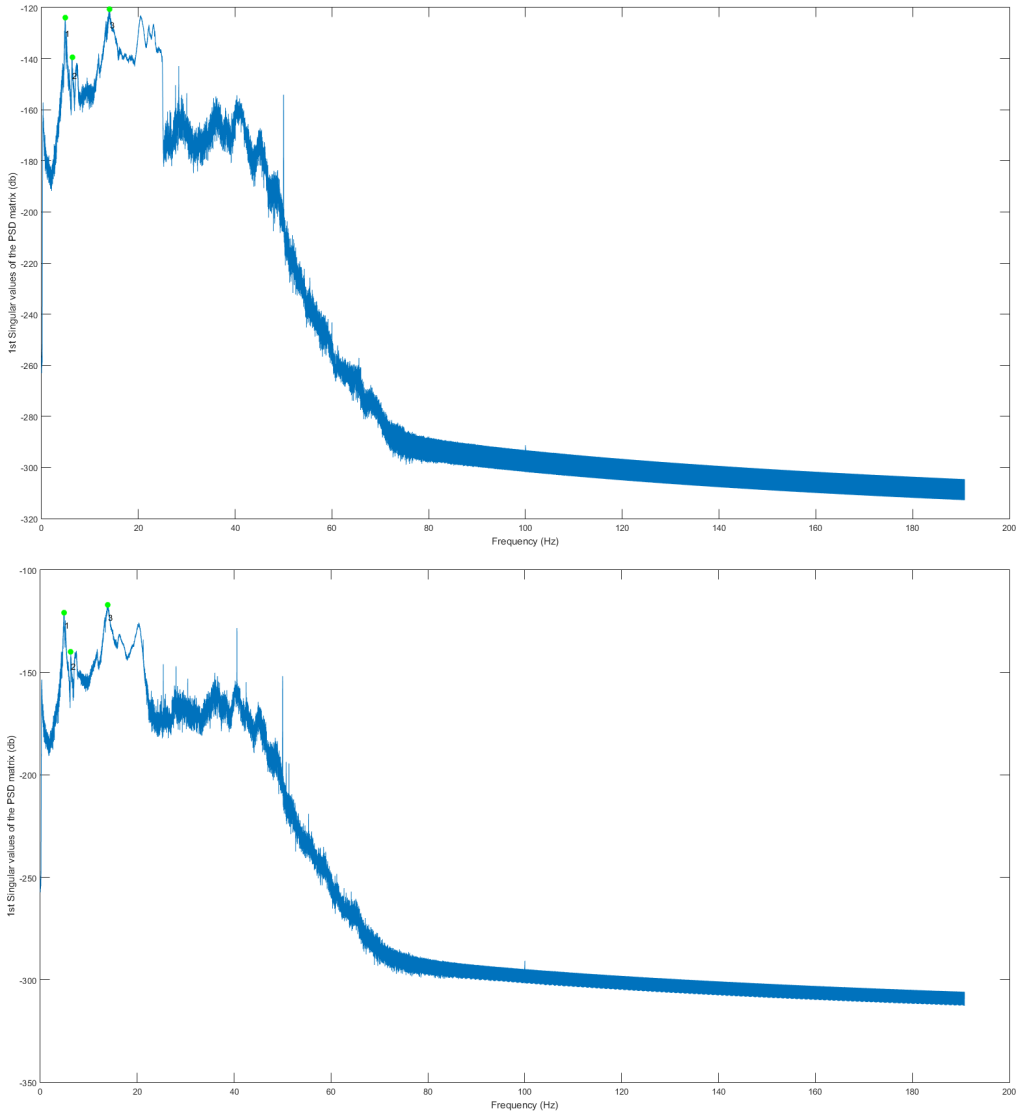

Figure 5.50: Swept-Sine along X-axis: recordings No.0000 and No.0001

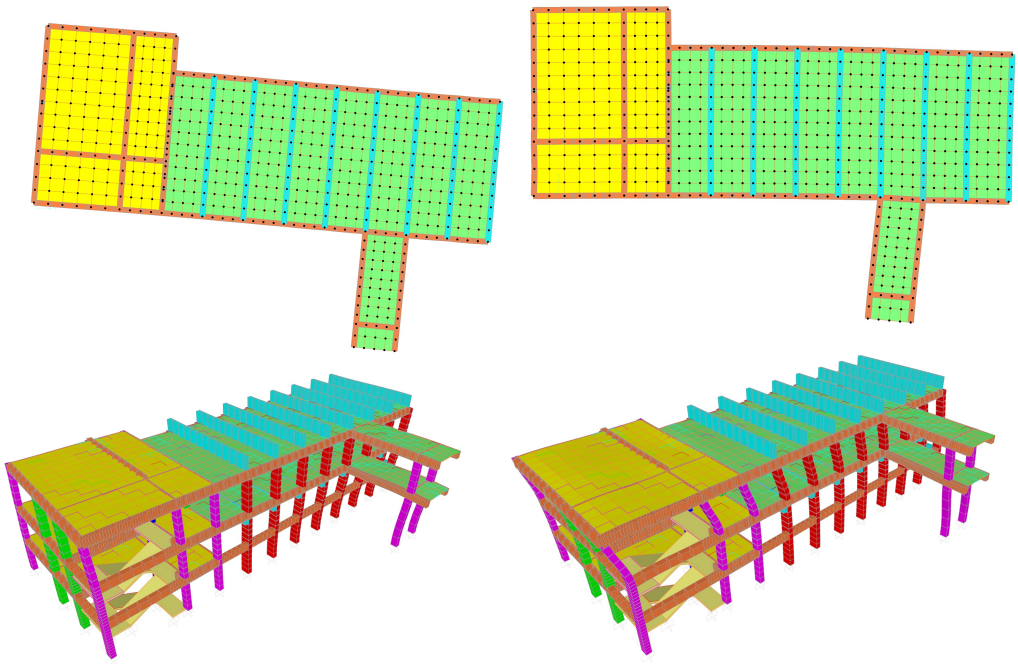

Figure 5.51: Deformed shapes of 1st and 2nd vibration mode

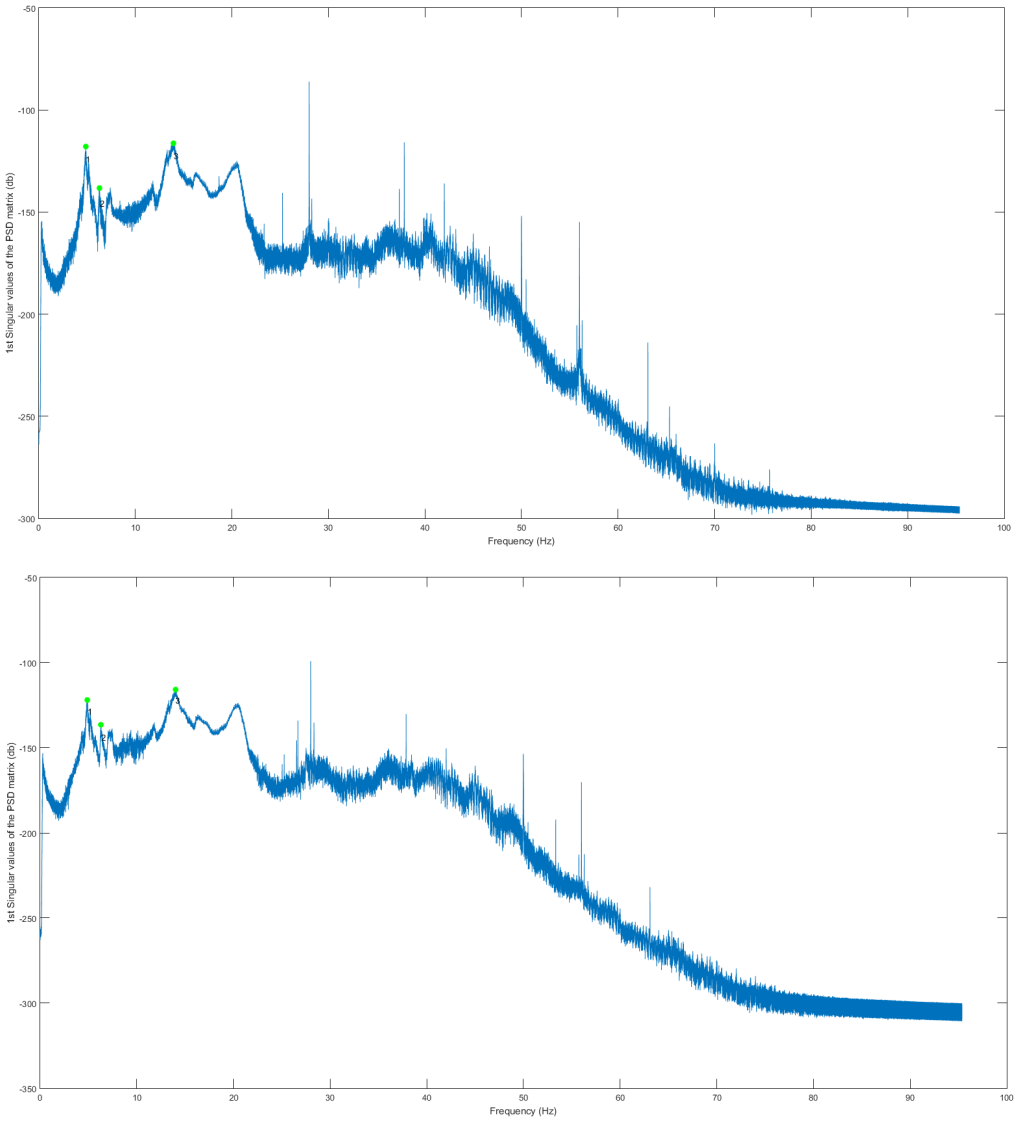

Figure 5.52: Stepped-Sine along X-axis: recordings No.0000 and No.0001

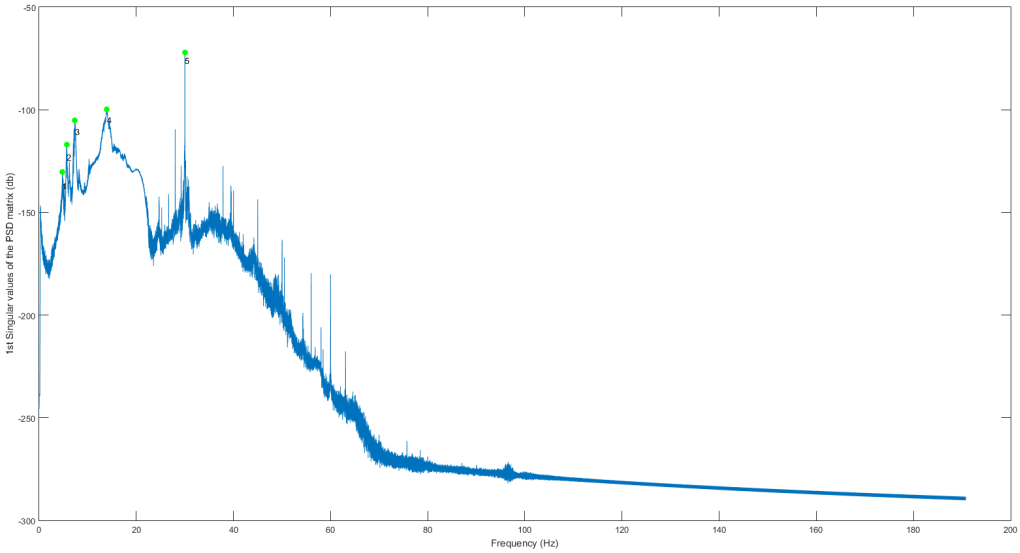

Figure 5.53: Swept-Sine along Y-axis: recordings No.0000

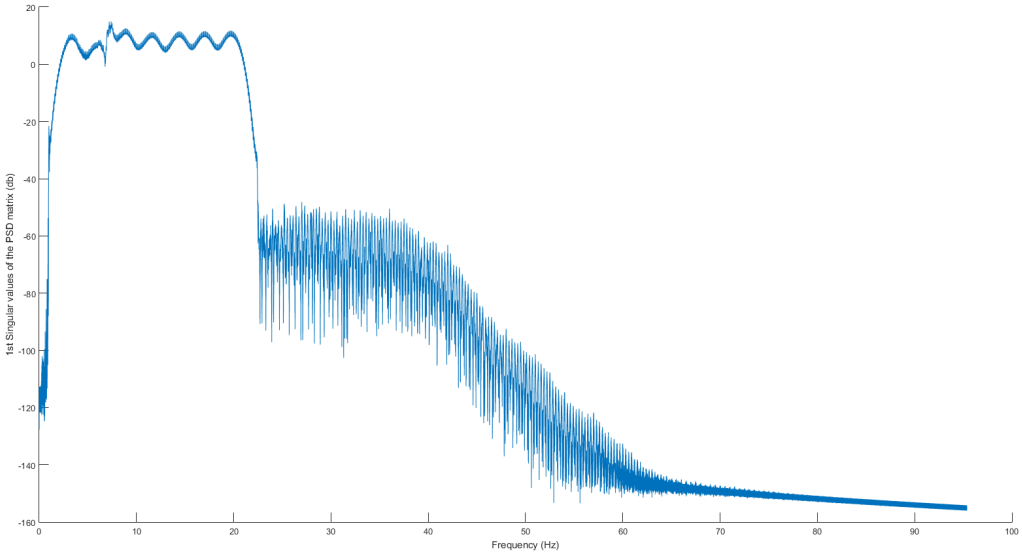

Figure 5.54: Swept-Sine along Y-axis: recordings No.0001

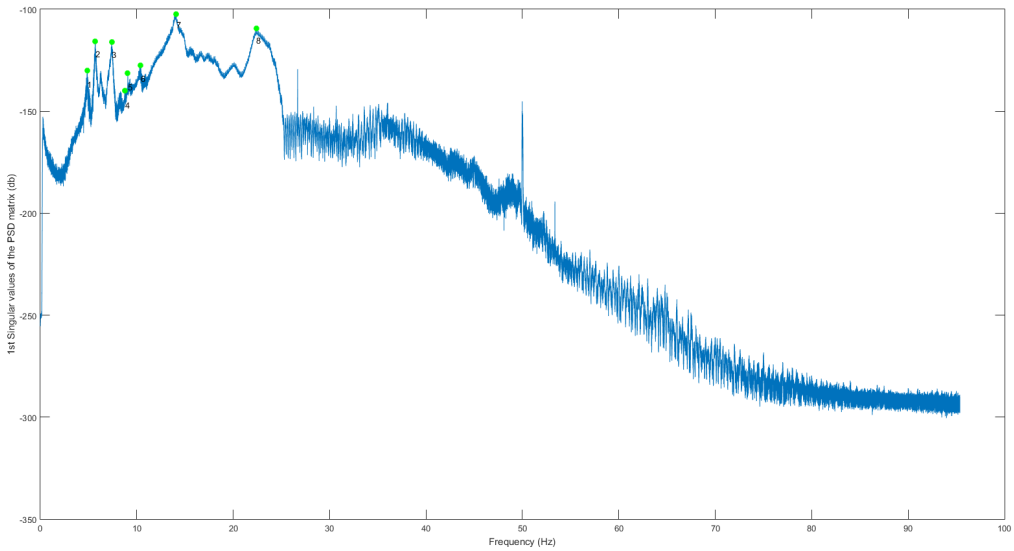

Figure 5.55: Stepped-Sine along Y-axis: recordings No.0000

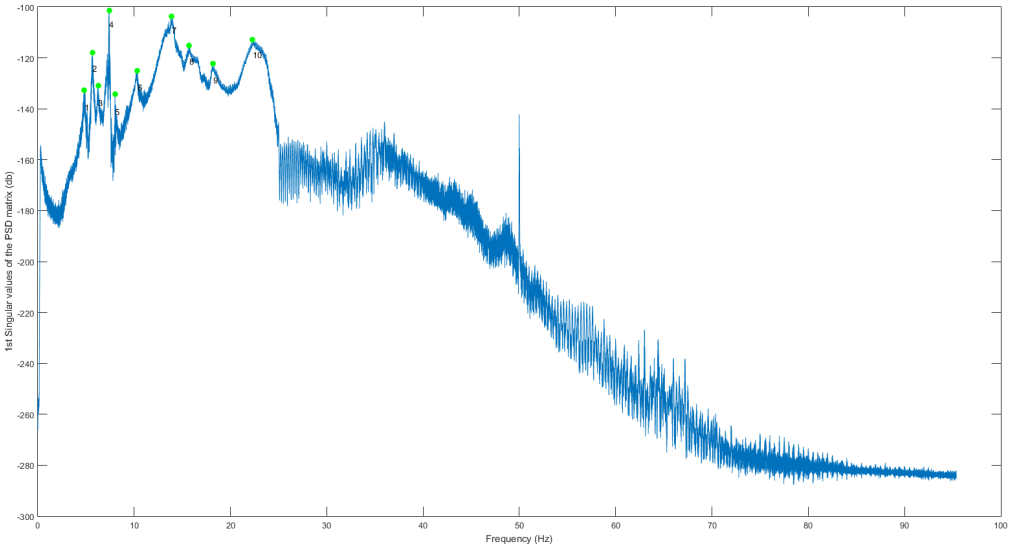

Figure 5.56: Stepped-Sine along Y-axis: recordings No.0001

Conclusions

In the present ph.D. thesis the main argument was the definition of a method and of a set of instrumentation capable of monitoring the Structural Health of a road or of a civil structure. To this aim were analysed the most useful dynamic methods to test and to monitor a structure. To fix the set of instrumentation three bridges and the Auditorium of a school building were studied and analysed by the SMART Lab research team during the development of same italian and european research project. During these research project not only software tools were developed but different accelerometric networks were tested. Moreover a particular new tool, a new vibrodina were designed in cooperation with the DRC factory, built and tested in the case of ITI Monaco Auditorium structural monitoring. A method to alert for a possible damage was at the end obtained, also demonstrating the useful connection between iot and structural analysis methods. In the following the peculiarity of each chapter are resumed.

This work is based on the concept that with the use of logical definitions it is possible to develop a simple procedure, so a procedure has been implemented for the activation of the main vibrating modes of a structure and in particular the identification of its fundamental modal shape. Several aspects have been considered in this thesis work: the implementation of a data-driven software tool for the identification of the modes of vibration and the relative frequencies of the dynamic structural behavior; the development of a kit for structural monitoring and dynamic identification composed of a mono-axial accelerometric piezoelectric network of 8 units, a portable vibrodine and a tomograph.

In the fourth chapter, which concerned a series of tests on road infrastructures, when the portable vibrodine had not yet been realized, the environmental noise readings were carried out only by means of an accelerometric network, at first, and then with the addition of vibratory readings of the soil and the structure itself by means of an experimental tomograph. Experiments on Calabrian bridges, following the OMA procedure, have shown that the kit of eight monoaxial accelerometers provides the same frequencies obtained from the modeling of road infrastructures using very refined solvers. And therefore it was possible with the stresses induced by environmental vibrations to read the modal forms of the structure to be tested.

Obviously the various configurations of the accelerometers arranged on the

drive-over plate of each bridge are not always suitable for capturing the vibration modes of the infrastructure but only for a pure fact of positioning limited to the accessible part so as not to run into dangers. The readings of the experimental vibrations using the 8 monoaxial accelerometers, suitably transformed in frequency, have provided, through the matlab code, the interpretation of the frequencies according to the PSD and the graphical interpretation of the peaks with PP, have allowed the identification of the ways of vibrating the structure in real time. The results of the experimental tests, white noise, conducted on the Fiume Trionto bridge, with the aid of the only accelerometric network of eight units, all mono-axial, highlighted the importance of the configuration of the sensors. Already visually, by the modal shapes it is immediate univocally associating to each mode of vibration experimental a corresponding analytical mode. The limited number of available accelerometers, made it possible to compare only few modes of vibration as the measuring points were placed only on the central span of the bridge. The result shows that the experimental frequencies calculated with the Matlab code (data-driven) are almost coincident with those calculated by the FEM solver.

In fact, there has been a deviation almost null for all modes and for both configurations. Thus showing a good correlation between the two models, theoretical and experimental: MIDAS GEN and ABAQUS finite element method codes oriented structural analysis *versus* DATA-DRIVEN in MATLAB code. In particular, in the experimentation on the second bridge, Fiume di Mare, it was seen that it was not possible to unequivocally read the second way of vibrating the structure itself since the readings of the sensors deduced from the Fourier transform provide two peaks, respectively, of 4 Hz and 4.5 Hz. The configuration of the tests carried out did not univocally activate this vibration mode. On the other hand, despite the non-uniqueness of the frequency peak in the second modal form, it is however evident that the difference between the experimental and the theoretical frequencies, for the first three modes of vibration of the bridge, is practically zero since the deviations between the same fluctuate between 0.05 and 0.36.

From the tests carried out on the road surface of the Caprovini bridge, it should be noted that with the B configuration the sensors do not lead to significant values of the frequencies and the dimensionless ratio of the damping. Even if it was right to test the positioning of the accelerometric sensors in this second so-called vertical (in the test configuration B, no.8 measurement stations were placed, no.6 accelerometers in the vertical direction, z-axis, at points 1-4-7-8-11-14, and no.2 in the horizontal directions, y-axis, transverse to the bridge, at points 2-6) mode.

The mean values of the frequencies determined experimentally on the Caprovini bridge, taken from the accelerometer readings of the sensors placed according to the configuration A, were compared with the so-called theoretical ones, taken from the modal analysis of the finite element model. In practice, with the second configuration it was not possible to activate the first mode of vibrating and therefore using configuration A, on the other hand, shows the activation of the first two

modes of vibrating with a deviation from the theoretical frequencies between zero (0.04) and the unit (0.99). Also in this case the experimental frequencies correspond perfectly to those extracted from the modal analysis of the FEM modeling.

The obvious deduction of these first tests is that it is not the set of environmental forcing naturally induced (white noise) not to activate the main vibrations of the road infrastructures but only concerns the fact that the eight monoaxial accelerometers were to be arranged according to the three directions coinciding with the axes x, y, z so as to read the translational modal forms (along axis x and along axis y) and the rotational ones (around axis z).

For the two bridges where it was possible to experiment with the tromograph a perfect coincidence was obtained between the fundamental frequencies of the road infrastructures, deduced from the readings of the microtremors, and those of the theoretical modes (FEM and Modal Analysis) and experimental (white noise, set accelerometer, data-driven). More precisely, the frequency intercepted by the tromograph corresponds to the fundamental frequency of the structure and in particular to the frequency which corresponds to the modal shape with a higher percentage of participating mass. For the Fiume di Mare bridge the fundamental frequency read by the tromograph is equal to 4.4 Hz and corresponds to the second mode of vibration of the infrastructure which is of the rotational type with a translational component along the y axis. For the Caprovini bridge, the fundamental frequency read by the tromograph is 2.4 Hz and corresponds to the first mode of vibration of the infrastructure which is purely translational along the y axis. Given the results of experiments on Calabrian bridges, it is therefore possible with the stresses induced by environmental vibrations to read the modal forms of the structures thanks to the matlab code validated precisely during these tests. To capture the vibration modes of the structures in general, the positioning of the accelerometric network must be improved. For this reason, as soon as we had an additional structure in which we were able to perform dynamic tests, we chose the positioning of the accelerometric network based on previous experiences.

In the fifth chapter the tests were also carried out with portable vibrodine and concerned both the study of white noise and that of artificial forcing.

After having carried out in situ the characterization of the structural concrete of the Auditorium of the ITI Monaco building complex, thanks to the results of the carbonation tests to evaluate the degradation process in concrete, the pacometric investigations for the verification and the identification of the position of the steel bars immersed in the concrete, of the sclerometric tests, of the pull-out tests and of the core samples extraction it was possible to qualify the concrete to today's date and insert the data in the finite element modeling performed with a simple solver, SAP2000. Always with the same solver the modal analysis was performed and the main ones (at least 85% participating mass) were obtained. From the values of the participating mass for each of these modes of vibration it was deduced that the first mode has a strong torsional component (around the z axis) but also a good translational contribution along the y axis. From the verification

carried out on the torsional stiffness, as prescribed by the NTC18 (paragraph 7.4.3.1), it is clear that it does not satisfy (unchecked) the condition imposed ($r^2/l_s^2 > 1$) and therefore the structure is torsionally deformable. On the basis of these considerations and by virtue of what has been experimented on the road infrastructures we have arranged the monoaxial accelerometers only along the two directions x and y but in such a way as to read not only the translations but also the rotations in the xy plane around the z axis.

Apart from a series of precautions in wiring the accelerometers in order to reduce signal acquisition problems, the first experiments concerned the acquisition of environmental noise or white noise. So anonymous forcing (unknown input) because difficult to measure but well defined output. The appropriately transformed acquisitions provided the graphs of the power spectral density function which shows the strength of the variations as a function of frequency. In other words, it shows at which frequencies variations are strong and which variations are weak. Once the PSD peaks have been identified and the corresponding frequency values have been read on the graph itself, a perfect similarity can be stated with the frequencies extrapolated from the solver modal analysis: the deviation is minimal indeed almost nil and does not exceed the 0.65 difference, also the percentage error is very low.

In conclusion, the OMA technique, always used to validate the modal analysis made with commercial software solver, in this case has allowed to demonstrate also the validation of the data-driven software for the identification of the peaks in frequency as well as the effectiveness of the positioning of the sensors according to the geometric conformation of the structure.

So these first experiments with white noise have clearly shown that the peaks of the spectral density represent the modal shapes of the structure in the exercise phase and that the progressive order of the peaks is equivalent to the progressive order of the modal shapes that mostly involve the participation of the masses. The subsequent experiments, on the other hand, concerned the activation of the structure's own vibration modes by means of an artificial sinusoidal-type forcing induced in situ by means of a portable vibrodine designed and built ad hoc.

The tests conducted with the experimental vibrodine, positioned right on the real structure, were divided into two groups according to the orientation of the vibrodine itself: along the x axis and along the y axis. Keeping in mind that the shorter side of the rectangle that circumscribes the building in plan view is parallel to the x axis while the longer side to the y axis and obviously the height of the building is parallel to the z axis of the classic Cartesian system. Both the two configurations, in short vibrodine along x and vibrodine along y, have activated the fundamental vibrating modes of the structure itself.

In particular, the vibration modes have been activated that have a participating mass greater than 19%.

And, in particular, with the configuration that provided the VIBRO9001 positioned parallel to the x axis, the vibrating modes have been activated that provide

Mode activated	X swept [Hz]	X swept [Hz]	X stepped [Hz]	X stepped [Hz]	average [Hz]	f_{Theo} [Hz]	deviation	f_{Exp} [Hz]	deviation
1	4.854	4.923	4.865	4.905	4.887	4.9001	0.013	4.852	0.035
2	6.338	6.279	6.306	6.302	6.306	6.5951	0.29	6.067	0.24
5	14.07	13.95	13.95	14.00	13.99	14.759	0.77	14.14	0.15

Table 5.5: Modes activated by artificial forcing

a translation of the structure along the same axis. In fact the peaks corresponding to the second and fifth mode of vibration of the translational structure parallel to the x axis are clearly evident.

The artificial forcing induced by the vibrodine on the active structure always, as the first way of vibrating intended as the first graphical peak, a modal form with a frequency, on average, equal to 4.887 Hz and corresponding to the mode with the most participating mass and which is mainly rotational around z with a good translational component along y as it is a torsional deformation.

In the vibrodine configuration along y we do not have clear and isolated graphic peaks or well spaced below 20Hz as the vibrating modes that can be activated with this configuration are all characterized by a very low percentage of participating mass and in any case not more than 19 (19% , 7%, 5.13%, 2.65%).

The only peculiarity that all the graphs of the spectral density have in common, even those with the vibrodine acting along the Y axis, is that the first peak of all the graphs, whether isolated or well defined with respect to the others or with successive peaks also close together, it always corresponds to the first vibratory mode extrapolated from the SAP2000 solver, that is to the torsional mode having a theoretical frequency of 4.9001 Hz but above all with a higher percentage of mass participating than the others. This peculiarity is also visible with the result of the experimental tromograph that provides a value of 5.1 Hz as the fundamental frequency of the structure. The previous results obtained from the geometrical and geomatic analyses, from the mechanical characterization, from the theoretical and experimental analyses for the definition of the vibrating modes and the principal frequencies of the structure that can be interpreted as undamaged structure, allow at any time a comparison between the latter data and those instantly detectable by the accelerometric network constantly present on the structure. A difference, over a predefined tolerance, between modes and frequencies in the case of an undamaged and damaged structure, will trigger the transmission of an alert and the consequent actions of maintenance or rescue intervention.

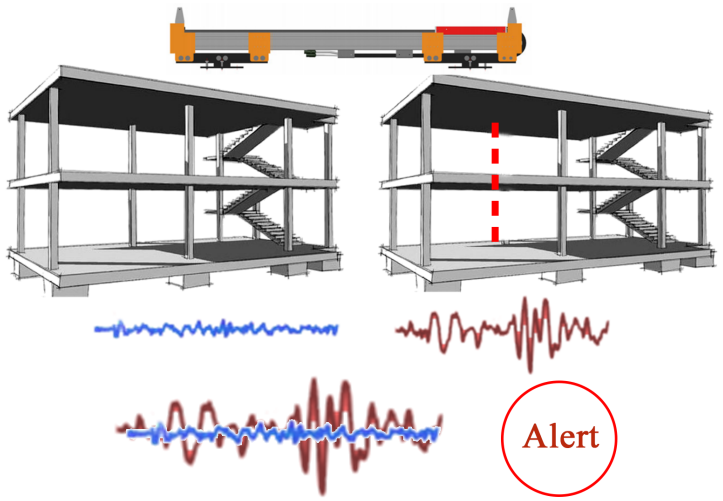

Figure 5.57: Alert

Bibliography

[1] S. W. Doebling, C. R. Farrar, M. B. Prime, D. W. Shevitz, Damage identification and health monitoring of structural and mechanical systems from changes in their vibration characteristics: a literature review.

[2] X. Jiang, S. Mahadevan, Bayesian probabilistic inference for nonparametric damage detection of structures, Journal of engineering mechanics 134 (10) (2008) 820 – 831.

[3] D. E. Hudson, Dynamic tests of full-scale structures, Journal of the Engineering Mechanics Division 103 (6) (1977) 1141–1157.

[4] A. P. Jeary, B. R. Ellis, Vibration test of structures at varied amplitudes, in: Dynamic Response of Structures: Experimentation, Observation, Prediction and Control, ASCE, 1981, pp. 281–294.

[5] W. A. Dalgliesh, J. Rainer, Measurements of wind induced displacements and accelerations of a 57 storey building in toronto, canada.

[6] J. Littler, B. Ellis, Interim findings from full-scale measurements at hume point, Journal of Wind Engineering and Industrial Aerodynamics 36 (1990) 1181–1190.

[7] S. J. Dyke, D. Bernal, J. Beck, C. Ventura, Experimental phase ii of the structural health monitoring benchmark problem, in: Proceedings of the 16th ASCE engineering mechanics conference, 2003.

[8] D. Ghosh, R. Sharman, H. R. Rao, S. Upadhyaya, Self-healing systems—survey and synthesis, Decision support systems 42 (4) (2007) 2164–2185.

[9] A. Mita, Emerging needs in japan for health monitoring technologies in civil and building structures, in: Proc. Second International Workshop on Structural Health Monitoring, 1999, pp. 56–67.

[10] J. M. Brownjohn, Structural health monitoring of civil infrastructure, Philosophical Transactions of the Royal Society A: Mathematical, Physical and Engineering Sciences 365 (1851) (2006) 589–622.

[11] A. Pandey, M. Biswas, M. Samman, Damage detection from changes in curvature mode shapes, Journal of sound and vibration 145 (2) (1991) 321–332.

[12] H. Hwang, C. Kim, Damage detection in structures using a few frequency response measurements, Journal of Sound and Vibration 270 (1-2) (2004) 1–14.

[13] W. Su, C. Huang, S. Hung, L. Chen, W. Lin, Locating damaged storeys in a shear building based on its sub-structural natural frequencies, Engineering Structures 39 (2012) 126–138.

[14] Q. Huang, Y. Xu, J. Li, Z. Su, H. Liu, Structural damage detection of controlled building structures using frequency response functions, Journal of Sound and Vibration 331 (15) (2012) 3476–3492.

[15] R. Y. Liang, J. Hu, F. Choy, Theoretical study of crack-induced eigenfrequency changes on beam structures, Journal of Engineering Mechanics 118 (2) (1992) 384–396.

[16] A. Morassi, Crack-induced changes in eigenparameters of beam structures, Journal of Engineering Mechanics 119 (9) (1993) 1798–1803.

[17] R. Adams, P. Cawley, C. Pye, B. Stone, A vibration technique for nondestructively assessing the integrity of structures, Journal of Mechanical Engineering Science 20 (2) (1978) 93–100.

[18] O. Salawu, Detection of structural damage through changes in frequency: a review, Engineering structures 19 (9) (1997) 718–723.

[19] J.-C. Chen, J. A. Garba, On-orbit damage assessment for large space structures, AIAA journal 26 (9) (1988) 1119–1126.

[20] K. Roy, S. Ray-Chaudhuri, Fundamental mode shape and its derivatives in structural damage localization, Journal of Sound and Vibration 332 (21) (2013) 5584–5593.

[21] H. Zhu, L. Li, X.-Q. He, Damage detection method for shear buildings using the changes in the first mode shape slopes, Computers & Structures 89 (9-10) (2011) 733–743.

[22] H. Li, Y. Huang, J. Ou, Y. Bao, Fractal dimension-based damage detection method for beams with a uniform cross-section, Computer-Aided Civil and Infrastructure Engineering 26 (3) (2011) 190–206.

[23] A. Messina, E. Williams, T. Contursi, Structural damage detection by a sensitivity and statistical-based method, Journal of sound and vibration 216 (5) (1998) 791–808.

[24] Z. Shi, S. Law, L. Zhang, Damage localization by directly using incomplete mode shapes, Journal of engineering mechanics 126 (6) (2000) 656–660.

[25] N. Stubbs, J.-T. Kim, C. Farrar, Field verification of a nondestructive damage localization and severity estimation algorithm, in: Proceedings-SPIE the international society for optical engineering, SPIE INTERNATIONAL SOCIETY FOR OPTICAL, 1995, pp. 210–210.

[26] N. Stubbs, J.-T. Kim, Damage localization in structures without baseline modal parameters, AIAA journal 34 (8) (1996) 1644–1649.

[27] H. W. Shih, D. P. Thambiratnam, T. H. Chan, Vibration based structural damage detection in flexural members using multi-criteria approach, Journal of sound and vibration 323 (3-5) (2009) 645–661.

[28] P. Cornwell, S. W. Doebling, C. R. Farrar, Application of the strain energy damage detection method to plate-like structures, Journal of sound and vibration 224 (2) (1999) 359–374.

[29] S. Das, P. Saha, S. Patro, Vibration-based damage detection techniques used for health monitoring of structures: a review, Journal of Civil Structural Health Monitoring 6 (3) (2016) 477–507.

[30] S. Artese, C. Altomare, J. Lerma, R. Zinno, Terrestrial laser scanning registration analysis and its effects on a masterpiece dome, in: 3D/4D Documentation in Cultural Heritage, International Conference On Cultural Heritage EuroMed, 2014, pp. 89–99.

[31] S. Artese, V. Achilli, R. Zinno, Monitoring of bridges by a laser pointer: Dynamic measurement of support rotations and elastic line displacements: Methodology and first test, Sensors 18 (2) (2018) 338.

[32] S. Artese, A. Miceli, P. Talarico, A. Venneri, G. Zagari, R. Zinno, Ponti antichi e moderni: utilizzo di tecniche geomatiche per il rilievo, la rappresentazione e la modellazione strutturale, GEOmedia 20 (4).

[33] U. GIS, Francesca ansioso1, serena artese1, floriana magarò1, angela miceli1, chiara miceli1, paolo talarico1, assunta venneri1, giuseppe zagari1 e raffaele zinno1.

[34] F. Ansioso, S. Artese, F. Magaro, A. Miceli, C. Miceli, P. Talarico, A. Venneri, G. Zagari, R. Zinno, A gis for the preservation and enhancement of the via annia-popilia, GEOMEDIA 21 (2) (2017) 14–21.

[35] R. Zinno, F. Magarò, On the monitoring of structures and soils by tomography, WIT Transactions on The Built Environment 152 (2015) 257–266.

[36] S. Artese, A. Miceli, P. Talarico, A. Venneri, G. Zagari, R. Zinno, Ancient and modern bridges: using geomatic techniques for relief, representation and structural modeling, GEOMEDIA 20 (4) (2016) 6–10.

[37] S. Artese, J. L. Lerma García, G. Zagari, R. Zinno, The survey, the representation and the structural modeling of a dated bridge, in: 8th International congress on archaeology, computer graphics, cultural heritage and innovation, Editorial Universitat Politècnica de València, 2016, pp. 162–168.

[38] G. Fortino, P. Trunfio, Internet of things based on smart objects: Technology, middleware and applications, Springer, 2014.

[39] A. Guerrieri, V. Loscri, A. Rovella, G. Fortino, Management of cyber physical objects in the future internet of things, Springer, 2016.

[40] F. Cicirelli, A. Guerrieri, G. Spezzano, A. Vinci, An edge-based platform for dynamic smart city applications, Future Generation Computer Systems 76 (2017) 106–118.

[41] R. Zinno, S. Artese, G. Clausi, F. Magarò, S. Meduri, A. Miceli, A. Venneri, Structural health monitoring (shm), in: The Internet of Things for Smart Urban Ecosystems, Springer, 2019, pp. 225–249.

[42] Non destructive testing: Determination of rebound number.

[43] Determination of pullout force.

[44] Standard Test Method for Pullout Strength of Hardened Concrete.

[45] Cored specimens – Taking, examining and testing in compression.

[46] O. C. Zienkiewicz, R. L. Taylor, R. L. Taylor, The finite element method: solid mechanics, Vol. 2, Butterworth-heinemann, 2000.

[47] D. J. Ewins, H. Saunders, Modal testing: theory and practice (1986).

[48] R. J. Allemang, Experimental modal analysis.[for vibrating structures].

[49] R. Potter, M. Richardson, Mass, stiffness and damping matrices from measured modal parameters, in: ISA International Instrumentation-Automation Conference, New York, New York, 1974.

[50] M. delle Infrastrutture, Norme tecniche per le costruzioni, Min. Inf 14.

[51] N. T. per le Costruzioni, Norme tecniche per le costruzioni. ministerial decree 14/01/2008/, official (2008).